Ulm University

International Graduate School in Molecular Medicine



Characterization of neural networks in rodents using functional ultrasound imaging

Dissertation submitted in partial fulfilment of the requirements for the degree of "Doctor rerum naturalium" (Dr. rer. nat.) of the International Graduate School in Molecular Medicine Ulm

Gillian Grohs-Metz

Los Angeles, California, USA

Institute of Anatomy and Cell Biology

Director: Prof. Dr. Tobias M. Böckers

2022

Current chairman of the Graduate School: **Prof. Dr. Bernd Knöll**
Current dean of the Medical Faculty: **Prof. Dr. Thomas Wirth**

Thesis Advisory Committee:

- First supervisor: **Prof. Dr. Tobias M. Böckers**
  Institute of Anatomy and Cell Biology
  University of Ulm

- Second supervisor: **Prof. Dr. Dr. Francesco Roselli**
  Laboratory for Systems Neurology
  Department of Neurology
  University of Ulm

- Third supervisor: **Prof. Dr. Bastian Hengerer**
  CNS Diseases Research Department
  Boehringer Ingelheim Pharma GmbH & Co. KG
  Biberach an der Riß

- External Reviewer: **Prof. Dr. Kristina Herfert**
  Functional and Metabolic Brain Imaging Group
  Department of Preclinical Imaging and Radiopharmacy
  University Hospital Tübingen

Day doctorate awarded: October 28th, 2022

Results gained in my thesis have been previously published in the following publication:

Grohs-Metz, G., Smausz, R., Gigg, J., Boeckers, T., Hengerer, B., 2022. *Functional ultrasound imaging of recent and remote memory recall in the associative fear neural network in mice.* Behav Brain Res 428, 113862. https://doi.org/10.1016/j.bbr.2022.113862.

I. Table of Contents

I. Table of Contents III
II. List of abbreviations V
1. INTRODUCTION 1
1.1. Psychiatric disease 1
1.2. Neural circuitry and networks 3
1.2.1. Associative fear neural network 4
1.2.2. Mesocorticolimbic pathway 6
1.3. Neurovascular coupling 8
1.4. Functional connectivity and neuroimaging 9
1.5. Thesis objectives 12
2. MATERIALS AND METHODS 13
2.1. Animals and license 13
2.2. Experimental timelines 15
2.3. Fear conditioning and behavioral expression protocol and analysis 18
2.4. Expression of DREADDs in PV+ interneurons in the vCA1 19
2.4.1. Surgical procedures 20
2.4.2. mCherry expression in satellite animals 21
2.5. Sedation protocol 21
2.6. Functional ultrasound imaging 22
2.6.1. Region of interest selection and imaging plane design 23
2.6.2. Acquisition parameters 26
2.6.3. fUS data pre-processing 27
2.7. Data processing and statistical analysis 28
2.7.1. Analysis of functional connectivity 28
2.7.2. Graph theory, principal component analysis, and machine learning 29
3. RESULTS 31
3.1. Study I: Functional ultrasound imaging of recent and remote memory recall in the associative fear neural network in mice 31
3.1.1. Recent and remote behavioral responses to cued fear expression test 31
3.1.2. Cue-evoked functional connectivity across memory recall imaging sessions 32
3.1.3. Recent and remote fear associated functional connectivity networks 35
3.1.4. Correlation of freezing behavior with functional connectivity 36
3.2. Study II: Deviations in network development in the 15q13.3 mouse model: a functional ultrasound study 37
3.2.1. Developmental trajectory of functional connectivity in 15q13.3 mice 37

3.2.2. Identification of a large-scale hyper-connected network in 15q13.3 mice 40
3.2.3. Genotype prediction based on functional connectivity 42
3.3. Study III: The influence of activation or inhibition of the parvalbumin positive interneuron network in the ventral CA1 on brain-wide networks measured with functional ultrasound 44
3.3.1. CBV changes resulting from pharmacological modulation of PV+ interneurons in the vCA1 44
3.3.2. Pharmacologically induced changes in connectivity resulting from modulation of PV+ interneurons in the vCA1 48
4. DISCUSSION 54
4.1. Study I: Functional ultrasound imaging of recent and remote memory recall in the associative fear neural network in mice 56
4.1.1. A single CS-US pairing generated robust and specific freezing behavior 57
4.1.2. Intra-amygdalar connectivity was prominent during both recent and remote memory retrieval 58
4.1.3. The hippocampus is active in cued memory retrieval 59
4.1.4. Activity in auditory processing regions during cue-evoked memory 60
4.1.5. Refinement of PFC connectivity during remote fear memory recall 61
4.1.6. Shock intensity, frequency, and robustness of memory 61
4.1.7. Major conclusions of study I 62
4.2. Study II: Deviations in network development in the 15q13.3 mouse model: a functional ultrasound study 63
4.2.1. Delays and deviations in connectivity patterns in 15q13.3 mice through development 63
4.2.2. The hyperconnectivity network of 15q13.3 mice 65
4.2.3. Genotype prediction from developmental network signatures 66
4.2.4. Major Conclusions of study II 67
4.3. Study III: The influence of activation or inhibition of the parvalbumin positive interneuron network in the ventral CA1 on brain-wide networks measured with functional ultrasound 68
4.3.1. CBV alterations after chemogenetic vCA1 PV+ interneuron modulation 68
4.3.2. Influence of vCA1 PV+ activity on functional connectivity in the mesocorticolimbic pathway 69
4.3.3. Major Conclusions of study III 71
4.4. Limitations 72
4.5. General Conclusions 74
5. SUMMARY 75
6. LIST OF REFERENCES 77
7. ACKNOWLEDGEMENTS 101
STATUTORY DECLARATION 103

II. List of abbreviations

3R	Replace, reduce, and refine
A1	Primary auditory cortex
BLA	Basolateral amygdala
BMA	Basomedial amygdala
BOLD	Blood-oxygen-level-dependent
CA1	Cornu Ammonis 1
CA3	Cornu Ammonis 3
cAMP	Cyclic adenosine monophosphate
CBV	Cerebral blood volume
CeA	Central amygdalar nucleus
Cg	Cingulate cortex
Cl	Cluster
CNO	Clozapine *N*-oxide
CNV	Copy number variant
CPu	Caudate putamen
CS	Conditioned stimulus
DG	Dentate gyrus
DREADD	Designer receptors exclusively activated by designer drugs
E/I	Excitatory/Inhibitory
Ent	Entorhinal cortex
FC	Fear conditioning
fMRI	Functional magnetic resonance imaging
fUS	Functional ultrasound
GPe	Globus pallidus, external segment
GPi	Globus pallidus, internal segment
Hb	Habenula
(v)HC	(ventral)Hippocampus
i.p.	Intraperitoneal
IL	Infralimbic cortex
L(a)A	Lateral amygdala
LaHypo & LH	Lateral hypothalamic area
LP(n)	Lateral posterior nucleus of the thalamus

M1	Primary motor cortex
M2	Secondary motor cortex
MD(n)	Mediodorsal nucleus of the thalamus
MeA	Medial amygdalar nucleus
mHypo	Hypothalamic medial zone
NAc	Nucleus Accumbens
NBS	Network-based statistics
OrA	Orbitofrontal area
p(35)	Post-natal day (35)
PCA	Principal component analysis
pCoA	Posterior cortical amygdalar area
PFC	Prefrontal cortex
PirT	Piriform transition area
PL	Prelimbic cortex
Po	Posterior complex of the thalamus
postA	Posterior amygdala
PV	Parvalbumin
pvHypo & PVH	Periventricular region of the hypothalamus
PVn	Paraventricular nucleus of the thalamus
ROI	Region of interest
RSC	Retrosplenial cortex
Rt	Reticular nucleus of the thalamus
S1BF	Primary somatosensory cortex, barrel field
S1FL	Primary somatosensory cortex, forelimb region
S1Tr	Primary somatosensory cortex, trunk region
S2	Secondary somatosensory cortex
SEM	Standard error of the mean
Sub	Subiculum
SVM	Support vector machine
TeA	Temporal association area
US	Unconditioned stimulus
UT	Unconditioned tone
VCtx	Visual cortex
VM(n)	Ventral medial nucleus of the thalamus
VPL	Ventral posterolateral nucleus of the thalamus

VPM	Ventral posteromedial nucleus of the thalamus
VPMC	Ventral pallidum, magnocellular nucleus
VPSI	Ventral pallidum, substantia innominata
VTA	Ventral tegmental area
ZI	Zona incerta

1. INTRODUCTION

1.1. Psychiatric disease

Psychiatric diseases are considerably widespread and are major causes of disability which generate substantial burdens of social, economic, and health. It is estimated that close to 1 billion people worldwide suffer from mental disorders of which only 15-25% are treated (James et al., 2018; Wang et al., 2007). Those affected frequently present with abnormal thoughts, perceptions, cognition, altered mood and emotions, along with disparities in behavioral and social interactions. Psychiatric diseases are made up of a heterogenous group of disorders which include schizophrenia, bipolar disorder, major depression, anxiety disorders, post-traumatic stress disorder, dementia, and autism along with numerous other illnesses.

Schizophrenia, in particular, affects 0.28% of the population worldwide although this is likely a conservative estimate due to sparse reporting from low-income countries. In actuality, a 1% prevalence is more likely. Although the prevalence of schizophrenia in children younger than 14 is very low, the reported cases increase exponentially between the ages of 15 and 19 and continue to rise sharply to the late 20s (Charlson et al., 2018). Given these figures, it is clear to see why schizophrenia is starting to be recognized as a neurodevelopmental disorder. The underlying neurobiological mechanisms may explain why the onset of symptoms present in late adolescence and early adulthood.

Brain maturation is considered a process of circuit refinement and is thought to be accomplished through three main mechanisms: the pruning of excess excitatory synapses, increased myelination, and the proliferation of inhibitory interneuron circuits (Figure 1.1) (Insel, 2010). Together, these processes effectively increase the ratio of white to gray matter at the systems level and shift the excitatory/inhibitory (E/I) balance of neurotransmission at the circuit level. Patients with schizophrenia have in fact been shown to display increased gray matter reduction and decreased white matter volume compared to healthy controls (Pol et al., 2004; Vita et al., 2012). These characteristics are pronounced in diagnosed patients, however, it is very likely that these processes are starting much earlier in development prior to the presentation of symptoms during the risk and prodromal stages of schizophrenia.

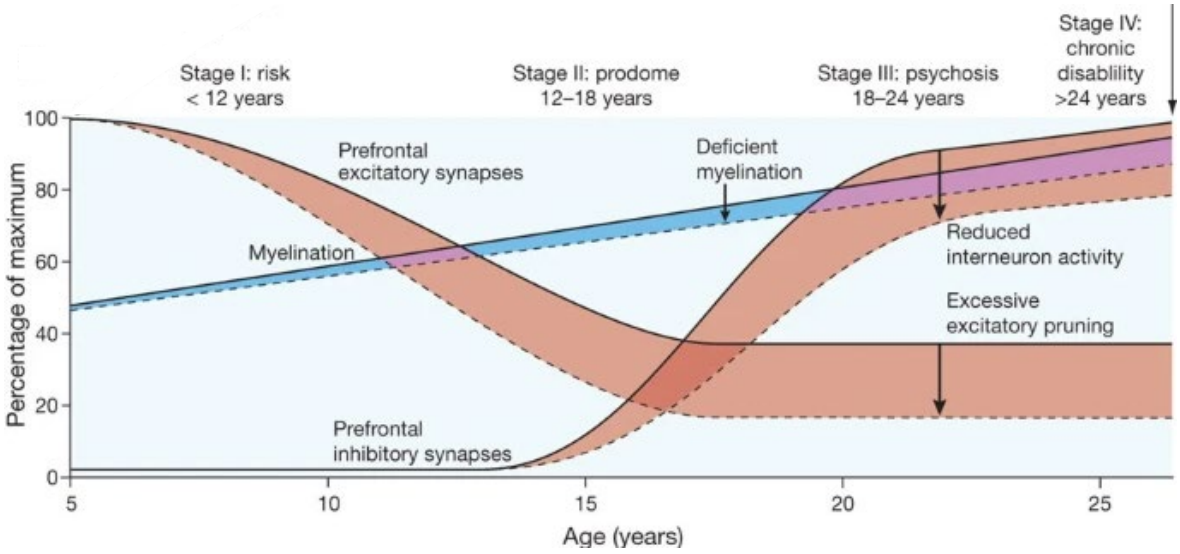

Figure 1.1 Neurobiological changes through development thought to promote circuit refinement and their alterations in schizophrenia. Redundant excitatory synapses are pruned followed by increased proliferation and arborization of inhibitory interneurons during the risk and prodromal stages. Myelination increases the efficiency of transmission in circuits that have been reinforced through learning and memory retrieval. Figure adopted from (Insel, 2010).

High heritability is another feature of note in schizophrenia. It is estimated that schizophrenia has around an 80% -point estimate of heredity. The risk of developing schizophrenia for those with a diagnosed first degree relative is 5- to 10- fold over the general population (Cardno et al., 1999; Sullivan et al., 2003). It is, however, quite surprising that even with this very evident heritability factor, the genetic association of schizophrenia is multifactorial and mostly ambiguous. Genome-wide studies have found large variability in single candidate gene discrimination and environmental influences, factors that make studying schizophrenia in the research setting increasingly complex.

An alternative approach to studying single gene mutations with relatively low penetrance, is to find a genetic variant that has a high likelihood of developing a given disease. Disorders that have chromosomal abnormalities which encompass several genes, such as copy number variants (CNVs), are prime candidates for disease modeling. While these variants are relatively rare in the general population, they confer a very high risk of developing psychiatric disorders such as schizophrenia (Odds ratio = 2 - 57) (Rees et al., 2014), an attribute that enables the study of the developmental processes leading to schizophrenia. Furthermore, recent advances in gene editing technology have made animal models of these syndromes easier to generate.

One such CNV consisting of a microdeletion in the 15q13.3 locus of chromosome 15, has been shown to confer a high risk of developing schizophrenia (Odds ratio = ~7.5), as well as

autism, intellectual disability, and epilepsy (Rees et al., 2014). A mouse model of this syndrome has been previously developed and expresses many of the features of the human 13q13.3 microdeletion syndrome. Similar to schizophrenia patients, these animals display auditory processing deficits, an increase in gamma oscillations at rest but a decrease after an auditory stimulus, aggressive behaviors after stress, impaired spatial reference memory, and also develop increased body weight (Fejgin et al., 2014). Furthermore, these mice exhibit hyperconnectivity throughout multiple brain regions (Gass et al., 2016), which is frequently correlated with multiple aspects of schizophrenia (Klingner et al., 2014; Krishnadas et al., 2014). It should be noted, however, that these preclinical studies were conducted in adult mice. As alluded to previously, understanding and detecting the subtle changes throughout development that lead to this phenotype, are crucial in not only developing more effective therapies, but in finding biomarkers to help identify patients at risk for developing schizophrenia.

1.2. Neural circuitry and networks

A major aspect of preclinical research is the translation of results and concepts into a clinical setting. Investigating neural circuitry and network are very useful tools in bridging this gap, especially in exploratory studies. A neural circuit is a group of interconnected components that respond together and coordinate signals for a specific function. At a larger scale, circuits converge into networks that are capable of integrating multiple inputs and are central to the execution of complicated cognitive functions. Changes in circuitry or networks may result from the convergence of multiple genes, behaviors or symptoms, and stimuli into a single read out, which can be especially useful in exploring the underlying mechanisms and heterogenous nature of psychiatric disease.

Fortunately, many examples of network architecture, along with the processes involved in circuit refinement, are conserved through species which make undertaking this type of research with animals more rational (Jung and Dasen, 2015; Reichert, 2009; Tosches, 2017). The ability to recapitulate elements of human circuitry, as well as the capability to modulate networks in an invasive way that is not possible in humans, make animal models useful for both guiding future research and provide a translatable screening tool for drug development.

As neural networks are considered to be one of the foundations of brain function, it is not surprising that virtually all psychiatric disorders are associated with at least some degree of

circuit abnormalities (McTeague et al., 2020, 2017). The following sections describe 2 networks that are highly involved in psychiatric disease in detail: the associative fear network and the mesocorticolimbic pathway.

1.2.1. Associative fear neural network

The associative fear network is one of the best described networks in neuroscience due to the ease and speed in which it can be instilled as well as the high reproducibility of experiments. During classical Pavlovian fear conditioning (FC) animals are trained to associate a neutral stimulus, the so-called conditioned stimulus (CS), with a paired aversive event, the unconditioned stimulus (US). This memory is then thought to be physically encoded into a distributed neuronal ensemble, collectively referred to as an engram (Bergstrom et al., 2011). During the next few hours, the engram is strengthened through consolidation, a process involving *de novo* protein synthesis (Jarome and Helmstetter, 2014). If the CS is then presented later it will elicit a fear response, namely freezing behavior in rodents, even in the absence of the US. During this re-presentation of the CS, the engram undergoes reconsolidation. The memory is particularly liable during reconsolidation, in that it can either strengthen then memory or lead to its decline (Nader et al., 2000). In fact, multiple presentations of the unpaired CS results in the deterioration of the behavior response through a new learning process termed fear extinction. In rodents, fear conditioning has been shown to be particularly effective, as animals can show signs of memory retrieval up to 1 year after training (Lux et al., 2016). Fear memory is most often associated with post-traumatic stress disorder. However, schizophrenic patients have also been shown to display abnormalities in the perception and processing of fear (Das et al., 2007; Holt et al., 2009; Tuominen et al., 2022).

The neurocircuitry of cued associative fear memory (Figure 1.2.1) has been extensively studied. The precise initiation locus of a fear memory is unknown, and most likely arises from numerous brain regions simultaneously. However, the amygdala has been consistently shown as a key mediator in fear circuitry. The amygdala can be subdivided into the lateral amygdala (LA), basolateral amygdala (BLA), basomedial amygdala (BMA), and the central nucleus of the amygdala (CeA). The LA is the main input nucleus of the amygdala and integrates signals from auditory, visual, and somatosensory inputs, among others (Linke et al., 2000). The BLA and BMA are then thought to interpret, process, and regulate fear-related neurotransmission from the LA. These areas then send relays to the CeA, the major

output nucleus of the amygdala that is responsible for the autonomic and motor responses to fear, reviewed in Lee et al., (2013).

Although the prefrontal cortex (PFC) shares many reciprocal connections with the amygdala, its role in fear conditioning has only emerged in the last decade. The PFC can be subdivided into the prelimbic (PL) and infralimbic (IL) cortices; areas that are in close proximity structurally but elicit contrasting roles in fear conditioning. PL activity is positively associated with freezing behavior and lesioning this region has been shown to reduce CS-evoked freezing behavior. The PL has also been shown to be involved in the consolidation of memory (Burgos-Robles et al., 2007). Lesions of the IL, however, attenuate extinction learning (Chang and Maren, 2010). Concurrently, stimulation of either region during reconsolidation sessions produces bidirectional effects on freezing (Vidal-Gonzalez et al., 2006). In the clinic, schizophrenia patients have been shown to display reduced activity between the amygdala and the PFC during the perception of fear (Das et al., 2007), a characteristic that can impede normal social interaction.

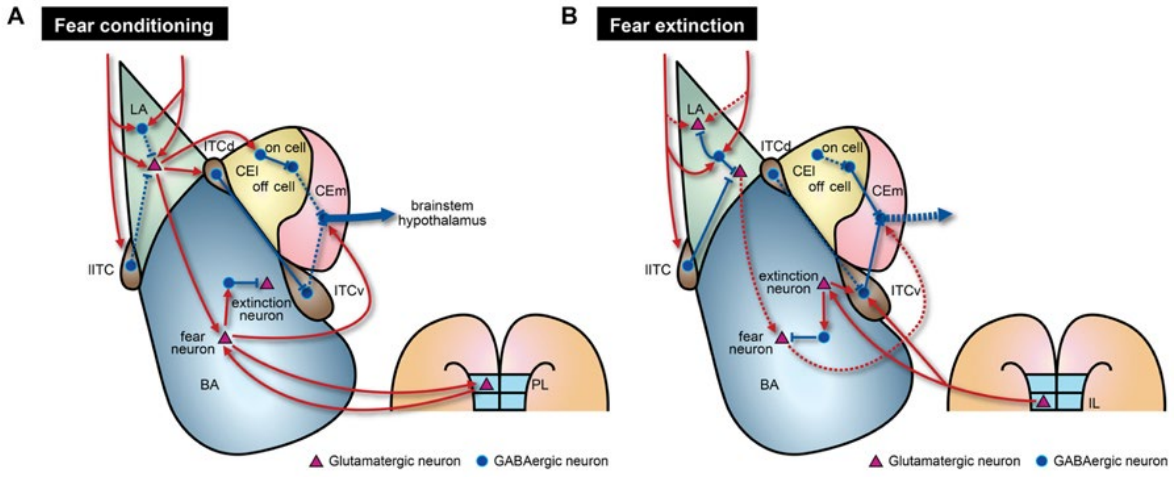

Figure 1.2.1 Proposed model of the associative fear neural circuitry of the amygdala and PFC. (A) During fear conditioning, increased input to the LA disinhibits intra-amygdalar circuits. Concurrently, reciprocal connections between the PL and basal amygdala (most likely BLA subdivision), reinforce the signal and results in increased output from the CeA, culminating in fear behavior. (B) During extinction learning, inhibitory circuits in the LA reduce activity in the basal amygdala (most likely both the BLA and BMA), augmented by novel input from the IL, effectively reducing output from the CeA and therein fear behavior. Figure adopted from (Lee et al., 2013).

The cortical sensory regions involved in contextualizing auditory cues are also of relevance in associative fear memory. Incoming auditory signals are relayed from the thalamus to the auditory cortex. There, signals are integrated between both the primary auditory cortex (A1) and temporal association areas (TeA) (Foxe et al., 2002). While the thalamus relays some incoming sensory signals directly to the amygdala, direct functional connections between

auditory/association cortices and the amygdala have also been detected (Kwon et al., 2012). In addition, the TeA has also shown a function in remote memory recall (Cho et al., 2016). Interestingly, there is evidence of reduced activity in the association cortices after extinction training (Barrett et al., 2003; Wheeler et al., 2013). Interplay between these regions and the amygdala and their role in modulating the fear response remains to be studied in depth.

Finally, while the hippocampus (HC) has a well-defined role in forming context-associated fear memories, its role is somewhat controversial in cued fear, where it is thought that fear retrieval occurs independently of the HC (Kim and Jung, 2006; Sanders et al., 2003). In a seminal study, Maren et al., (1997) showed that lesions of the HC after cued FC do not diminish freezing responses while they have a significant effect on fear responses that are associated with a context. It is thought that after consolidation of a memory, the engram moves to cortical structures, where it has been shown that late, rather than early lesions of cortical structures effect behavioral expression and therein memory retrieval (Kwon et al., 2012; Sacco and Sacchetti, 2010). Others, however, have shown that the HC is involved in both contextual and cue associative fear memory during both early and late retrieval (Bast et al., 2003; Oh and Han, 2020; Quinn et al., 2008). These disparities might be explained by competitive trace theory (Yassa and Reagh, 2013). Here it is theorized that the HC is actually performing a function in recontextualization during remote memory retrieval by using overlapping memory traces to reconstruct a memory. These disparities and gaps in knowledge warrant further study, especially in the context of defining global functional connectivity impairments in association with the symptoms of schizophrenia.

1.2.2. Mesocorticolimbic pathway

The dopamine hypothesis of schizophrenia theorizes that hyperactivity in dopaminergic neurotransmission underly some of the symptoms of schizophrenia, mainly the positive symptoms of hallucinations, delusions, and hyperactivity. This is supported by the finding that pharmacological inhibition of D2 dopamine receptors by conventional antipsychotics are normally effective in reducing these positive symptoms (Gardner et al., 2005). This hypothesis, however, does not fully explain the negative and cognitive symptom domains that are also prevalent in schizophrenia, which have been associated with deficits, rather than excessive dopamine signaling (Collo et al., 2020; Slifstein et al., 2015). The idea that aberrations in dopamine signaling are likely influenced by structures outside the classical dopamine pathways, namely in glutamatergic signaling, is becoming more prevalent and can

account for some of the positive and cognitive schizophrenic symptoms (Moghaddam and Javitt, 2012). As these ideas develop, it is becoming more apparent that the dopamine and glutamate hypotheses likely complement each other, and both contribute to the overall pathophysiology of schizophrenia. In light of the prevalence of treatment resistant schizophrenia, further investigation of potential pathophysiological mechanisms is crucial for developing effective therapies for all 3 major symptom domains.

The ventral hippocampus (vHC) has emerged as a potential intermediary structure that can address both the glutamatergic and dopaminergic transmission abnormalities associated with schizophrenia (Grace, 2010; Kätzel et al., 2020). In fact, decreased HC volume has been registered during neuroimaging studies of patients with schizophrenia (Erp et al., 2016). A functional circuit describing the potential influence of the vHC in dopaminergic signaling in the mesocorticolimbic network has been proposed by Kätzel, et al. (Figure 1.2.2). They proposed that the ventral subiculum (vSub), the region responsible for major output of the vHC, promotes dopamine release in the nucleus accumbens (NAc), which in turn indirectly activates the dopaminergic neurons in the ventral tegmental area (VTA). In addition, they suggest that the prefrontal cortex (PFC) and anterior cingulate cortex (Cg) are also targeted by dopaminergic signaling. These anterior cortical regions are intimately involved in feedback and feedforward mechanisms in the network with numerous reciprocal connections with the amygdala and vHC (Kätzel et al., 2020).

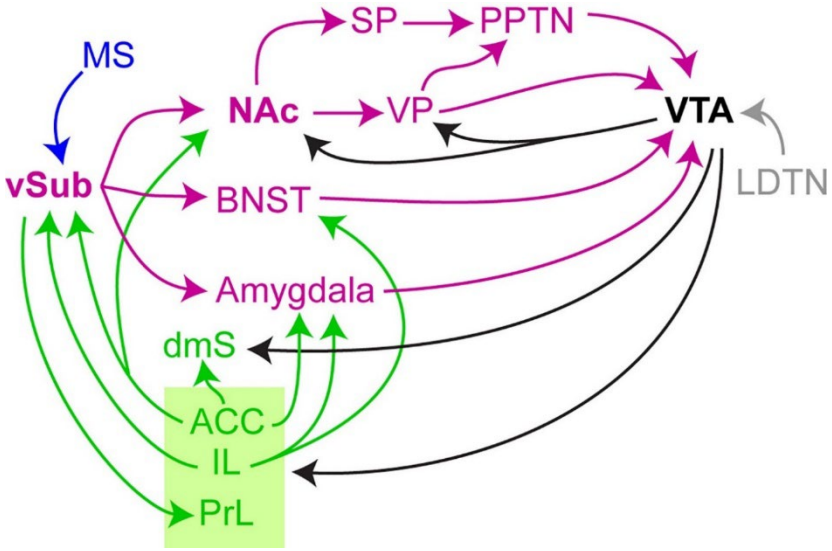

Figure 1.2.2 Projections to and from the ventral hippocampus and their functional connections with mesocorticolimbic associated regions. The ventral HC, NAc, VTA, and PFC/cingulate act as major hubs to influence dopamine signaling in the wider mesocorticolimbic network. MS= medial septal, vSub= ventral subiculum, ACC= anterior cinculate cortex, IL= infralimbic cortex, PrL= prelimbic cortex, dmS= dorsomedial (associative) striatum, BNST= bed nucleus of the stria terminalis, NAc= nucleus accumbens, VP= ventral pallidum, SP= subpallidal region, PPTN= pedunculo-pontine tegmental nucleus, VTA= ventral tegmental area, LDTN= latero-dorsal tegmental nucleus. Figure adopted from (Kätzel et al., 2020).

Interestingly, though many studies have shown HC *hyperactivity* in both schizophrenic patients and in unaffected first-degree relatives (Malaspina et al., 1999; McHugo et al., 2019), other studies have shown decreased *functional connectivity* of the HC with other structures (Dugré et al., 2021; Edmiston et al., 2020). The disparity could be caused by abnormal regulation from the inhibitory interneuron network which regulates not only the neural activity within the HC, but also coordinates its output to downstream targets. Indeed, an extensive and pivotal study by Marissal et al., (2018) showed that chemogenetic modulation of a subpopulation of inhibitory interneurons which express parvalbumin (PV+) in the ventral CA1 (vCA1) region of the HC with chemogenetics effectively reversed abnormal neural function and behavioral deficits in a 22q11 CNV mouse model of schizophrenia. Crucially, animal models with PV+ interneuron modulations recapitulate many of the features of schizophrenia (Lodge et al., 2009; Metzner et al., 2019; Shen et al., 2021). More research in this area is necessary to further elucidate the role of the vHC and PV+ interneurons in the pathophysiology of schizophrenia. The ability to separate up and downstream processes in dopaminergic signaling abnormalities could undeniably assist in the development of therapeutics that not only alleviate symptoms but could prevent both disease onset and progression.

1.3. Neurovascular coupling

While it is possible to monitor the electrophysiological properties of cortical and subcortical neural circuits invasively in animals, the feasibility of this approach is very limited in humans. Fortunately, there are non-invasive readouts of brain function that allow indirect measurement of whole brain neural activity, which can either be replicated or more easily translated to human studies. Various properties of cerebral hemodynamics have proven invaluable in research as a method of indirectly measuring neural activity. Increases and decreases in the brain activity correlate with changes in metabolic demand which must be compensated with blood flow to deliver nutrients and remove waste (Sanganahalli et al., 2016), a concept referred to as neurovascular coupling. This concept is the basis of the blood-oxygen-level-dependent (BOLD) method of measuring neural activity with functional magnetic resonance imaging (fMRI). Numerous studies have shown that various measures of neural activity, such as EEG and local field potentials from microelectrodes, temporally correlate with hemodynamic responses detected via laser Doppler or BOLD MRI imaging in both conscious and anesthetized animals (Liu et al., 2019; Lui et al., 2015; Menon et al.,

1997). More recently, the novel imaging modality functional ultrasound (fUS), which measures blood flow directly, has also shown a correlation of cerebral blood volume (CBV) with EEG as well as with the next generation Neuropixel electrode array (Figure 1.3) (Nunez-Elizalde et al., 2022; Sieu et al., 2015). Interestingly, (Sieu et al., 2015) deduced that the fUS signal was found to temporally match most closely with the firing rate of regional inhibitory neurons, a feature that is of great importance for measurements of functional connectivity.

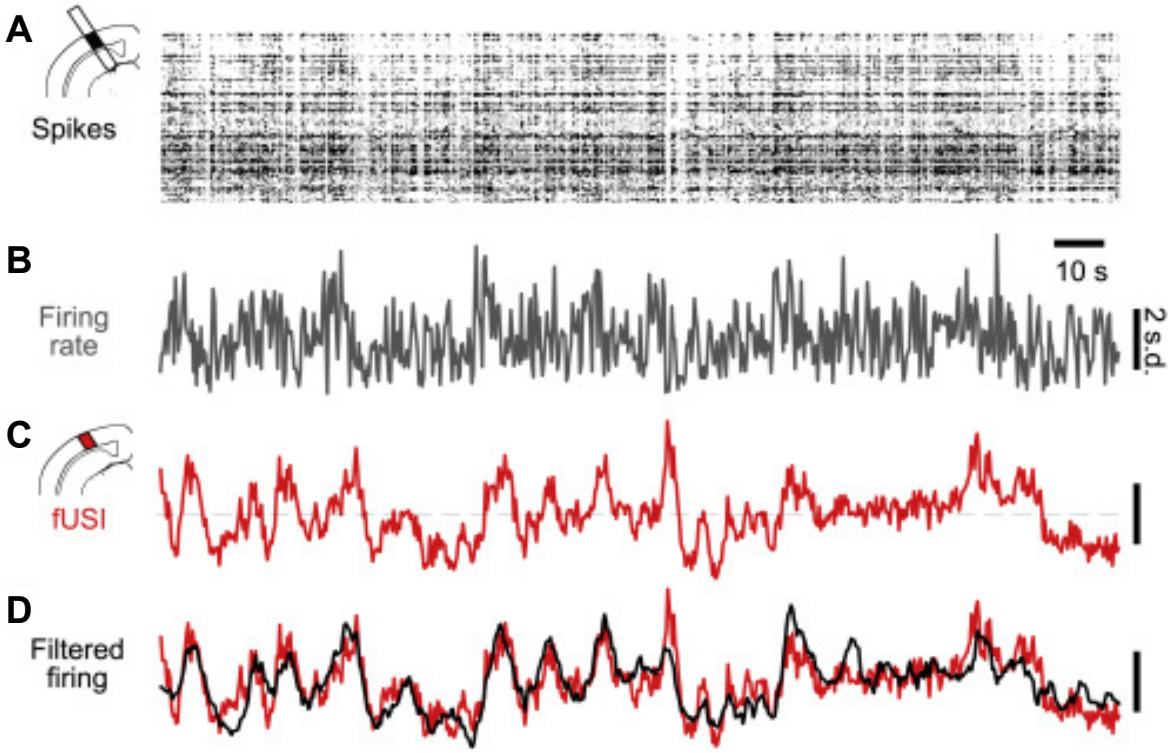

Figure 1.3 Temporal correlation of fUS signal with electrophysiological recordings from Neuropixel electrode arrays. (A) Raw spike recordings and (B) mean firing rates from the visual cortex measured with a Neuropixel array. (C) Average fUS measured power Doppler signal detected in parallel to Neuropixel recording. (D) Data smoothing of electrophysiological recordings closely mirror CBV recordings by fUS. Figure adopted from (Nunez-Elizalde et al., 2022).

1.4. Functional connectivity and neuroimaging

Functional connectivity, a measure of network integration through the temporal correlation of regional neural activity, has emerged as a highly informative approach to understanding the basis of cognition, behavior, and mood. Changes in functional connectivity range from hypo- to hyperconnectivity and generally associate with symptom severity in psychiatric disease (McTeague et al., 2020, 2017). Opportunely, functional connectivity can be measured non-invasively via indirect blood flow measurements using techniques such as

fUS and BOLD imaging and is well conserved across mammals (Assaf et al., 2020). Functional connectivity reflects the combined effects of neural and vascular activity. In most current detection and analytical approaches, this measured connection is non-directional (Zhan and Yu, 2015). Connectivity is calculated through the correlation of a time series of spontaneous hemodynamic fluctuations normally from two different regions of interest (ROIs) (Figure 1.4). Though functional connectivity can measure indirect connectivity between 2 disparate regions, it is influenced by direct structural connections (Honey et al., 2010), therefore high degrees of connectivity are detected between bilateral homotopic regions.

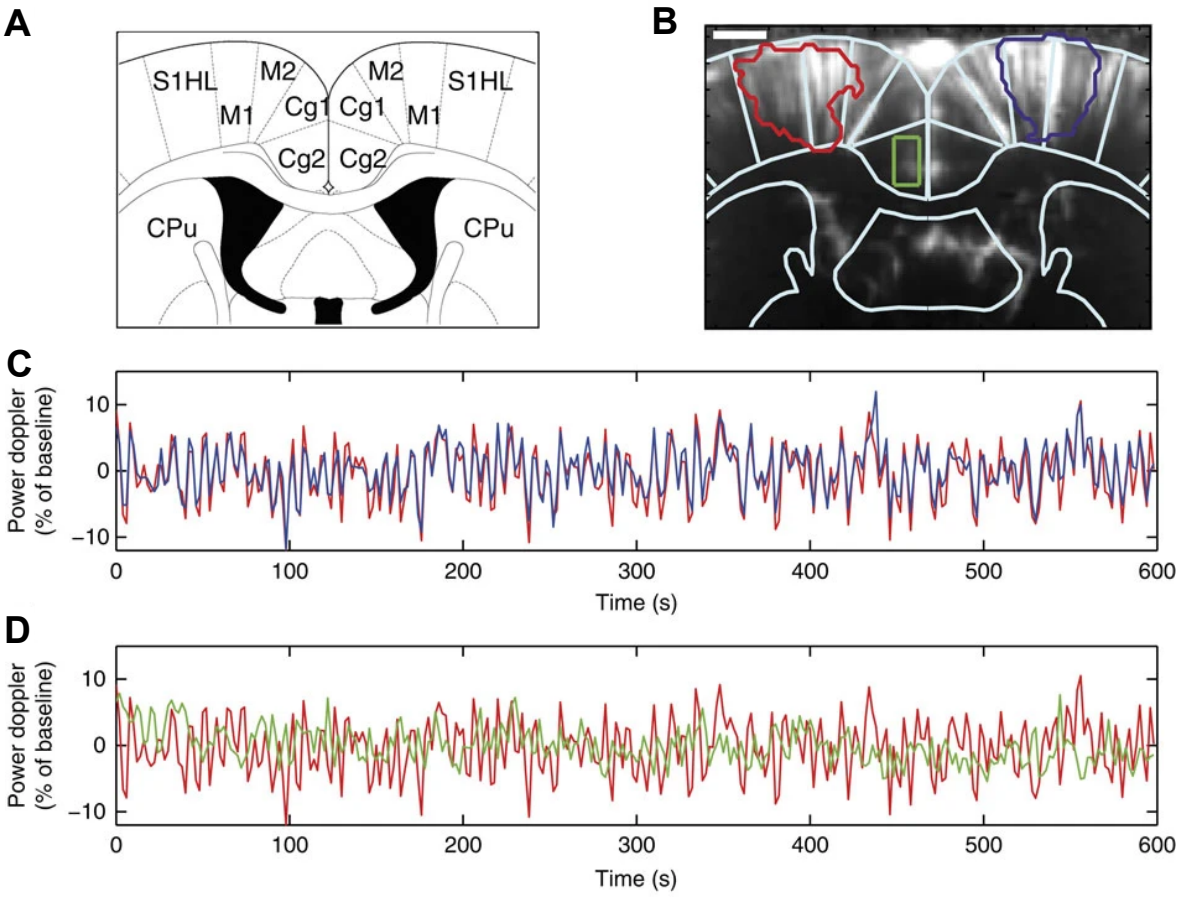

Figure 1.4 Visualization of functional connectivity measures of fUS signal. (A) Neuroanatomical delineations from Paxino stereotactic atlas, (B) overlaid onto fUS signal with left (red) and right (blue) hind limb primary somatosensory regions combined with the primary motor cortex, as well as cingulate (green) ROIs. (C) Bilateral homotopic regions show high temporal correlation while (D) regions with less direct functional connectivity show weaker correlation. Figure adopted from (Osmanski et al., 2014).

Even though CBV closely follows neural activity, as mentioned in Section 1.3, functional connectivity is paradoxically detected through relatively low frequency oscillations (Yuen et al., 2019). Though gamma rhythms, which are considered to be the basis of neural connectivity, oscillate between 40 and 100 Hz, they have been found to correlate most

closely with hemodynamics and the BOLD response. which is typically < 0.25 Hz (Goense et al., 2016; Lima et al., 2014; Logothetis et al., 2001; Ma et al., 2016). It should again be noted that gamma oscillations have been shown to be highly correlated with interneuron activity (Chen et al., 2017). It is important, however, to keep in mind that the low frequencies measured in functionally connectivity, likely reflect the release of vasodilatory modulators rather than electrical signals themselves (Jiang et al., 2018).

Functional connectivity can be measured under different experimental conditions. Changes can be measured in response to a cue, such as that used in fear conditioning, in response to a pharmacological challenge, or at rest in the absence of any stimuli (resting state networks). It might be somewhat surprising that task associated functional connectivity closely mirrors resting state networks (Cole et al., 2014; Smith et al., 2009). Some theorize, that the spontaneous oscillations observed at rest are indicative of neural pathways that have been used repeatedly during various tasks (Fair et al., 2009). The incorporation of such a varied array of elements that coalesce to comprise functional connectivity, make it an extremely useful tool in both preclinical and clinical research.

The relatively novel fUS imaging modality provides a valuable tool to investigate neural circuitry at the whole brain scale. The non-invasive nature of fUS imaging enables longitudinal, network wide coverage with an exceptionally high signal-to-noise ratio (Gesnik et al., 2017; Macé et al., 2011; Osmanski et al., 2014). fUS employs ultrafast, plane wave technology to measure Doppler signal from blood flow. It has a higher resolution than many other imaging modalities such as positron emission tomography and many MRI machines, and is less restraining in terms of magnetic objects, noise, mechanical ventilation, and physical access to animals (Catana, 2019; Deffieux et al., 2021; Mandino et al., 2020). These combined attributes render fUS imaging an ideal technique for studying neural networks in mice in the context of psychiatric disease.

1.5. Thesis objectives

Given the need for treatment options that can alleviate all 3 symptom domains (positive, negative, and cognitive) and the relevance of whole brain connectivity patterns in schizophrenia, the present project centered on characterizing disease-related aberrations in neural networks associated with psychiatric disease using fUS imaging technology. We applied 3 experimental approaches to assess the applicability of fUS imaging in preclinical psychiatric disease research.

First, we designed a study associated with fear behavior, a commonly reported abnormality in patients with schizophrenia. We used fear conditioning to encode an auditory cued associative fear memory to investigate if we could detect and monitor the evolution of a memory trace over time. We also sought to correlate cue-evoked functional connectivity with expressed behavior. This objective was addressed in **study I**:

- *Functional ultrasound imaging of recent and remote memory recall in the associative fear neural network in mice*

Next, we used a transgenic copy number variant animal model to recapitulate the post pubescent onset of schizophrenic symptoms. We measured functional connectivity at 4 developmental milestones from pubescence to adulthood, aiming to define network alterations and to identify a critical transition in network connectivity that can predict the conversion to an adult neural signature. This objective was investigated in **study II**:

- *Deviations in network development in the 15q13.3 mouse model: a functional ultrasound study*

Finally, we used designer receptors exclusively activated by designer drugs (DREADD)-based chemogenetics to investigate a proposed model of circuit aberrations in schizophrenia using a pharmacological fUS approach. This approach was important to determine if subtle differences in circuitry would reflect an overall change in regional recruitment and functional network organization. This objective was explored in **study III**:

- *The influence of activation or inhibition of the parvalbumin positive interneuron network in the ventral CA1 on brain-wide networks measured with functional ultrasound*

Here, we present functional ultrasound imaging as an approach to identify and characterize neural networks and activity in the context of psychiatric disease.

2. MATERIALS AND METHODS

As described in section 1.5, the three studies that make up this thesis are:

Study I: *Functional ultrasound imaging of recent and remote memory recall in the associative fear neural network in mice*

Study II: *Deviations in network development in the 15q13.3 mouse model: a functional ultrasound study*

Study III: *The influence of activation or inhibition of the parvalbumin positive interneuron network in the ventral CA1 on brain-wide networks measured with functional ultrasound*

Similar sedation, imaging, and data pre-processing procedures were used for all three studies. Differences in individual study procedures are detailed in the respective paragraphs.

2.1. Animals and license

All experiments were approved by the Regierungspräsidium (Tübingen, Germany) under VVH 17-007G and performed in an AAALAC (Association for Assessment and Accreditation of Laboratory Animal Care International) accredited facility in accordance with the European Convention for Animal Care and Use of Laboratory Animals. Animals were habituated for 7 days after delivery from their respective vendors before any experiments were performed and maintained on a normal 12:12 light-dark cycle (lights on at 6am) in standard temperature (22 ± 2ºC) and humidity (55 ± 10%) controlled rooms with *ad-libitum* access to normal chow and water. The following animals were used for the studies described in this work:

Study I: Male C57/BL6, 7-8 weeks old, 21-23 g weight at study onset, were purchased from Charles River Research Models and Services (Germany). Animals were singly housed to reduce aggression and variability in behavior. Animals were 7-8 weeks old at study onset, n=12 per group.

Study II: Hemizygous male Df(h15q13)$^{-/+}$ mice and Df(h15q13)$^{+/+}$ littermates, hereafter referred to as 15q13.3 and WT, were generated as previously described (Fejgin et al., 2014) by TaconicArtemis (Köln, Germany) and bred and shipped by Lundbeck (Valby, Denmark).

Animals were housed in mixed genotype groups of 4, n=16 for each group. Animals were 27 days old (p27) at delivery and experiments started at p35.

Study III: Heterozygous B6;129P2-Pvalbtm1(cre)Arbr/J(HE) male mice, hereafter referred to as PV-Cre mice were purchased from Charles River Research Models and Services (Germany). Mice were 19-22 days old at delivery and surgery was performed when mice were 31-41 days old, n=12 with an additional satellite n=1 per group for interim examination of viral expression. Imaging was performed 30 to 31 days after surgery.

2.2. *Experimental timelines*

Study I: Here we wanted to instill and measure an associative fear memory to investigate the evolution of the memory trace from recent to remote memory recall (Figure 2.2 :1). We took special precautions to reduce the development of contextual fear by handling the mice for 3 consecutive days in both the behavioral testing and imaging laboratories. Animals were habituated to the conditioning cages for 15 minutes on the day prior to the first imaging session (Day -2). Imaging sessions were completed from 7am to 1pm with no more than 3 mice per day. During baseline imaging sessions, animals were exposed to the tone that would be subsequently used for fear conditioning (FC) (Day -1). After 24 hours (Day 0), FC was performed in "context A" (described in Section 2.3) and animals were then allowed 24 hours in their home cages without contact. The following day (Day 1), a new context (context B) was used to test behavioral expression during recent fear recall to the tone in the afternoon. Then, after 4 hours in their home cages, animals were re-exposed to the original conditioning context (context A) to measure any potential contextual fear expression. On Day 2, recent recall was tested during imaging (imaging protocol outlined in Figure 2.6 :2 top). Finally, remote recall was tested during imaging on Day 31 and behaviorally on Day 32. Control animals were only exposed to the unconditioned tone (UT) and never to a foot shock.

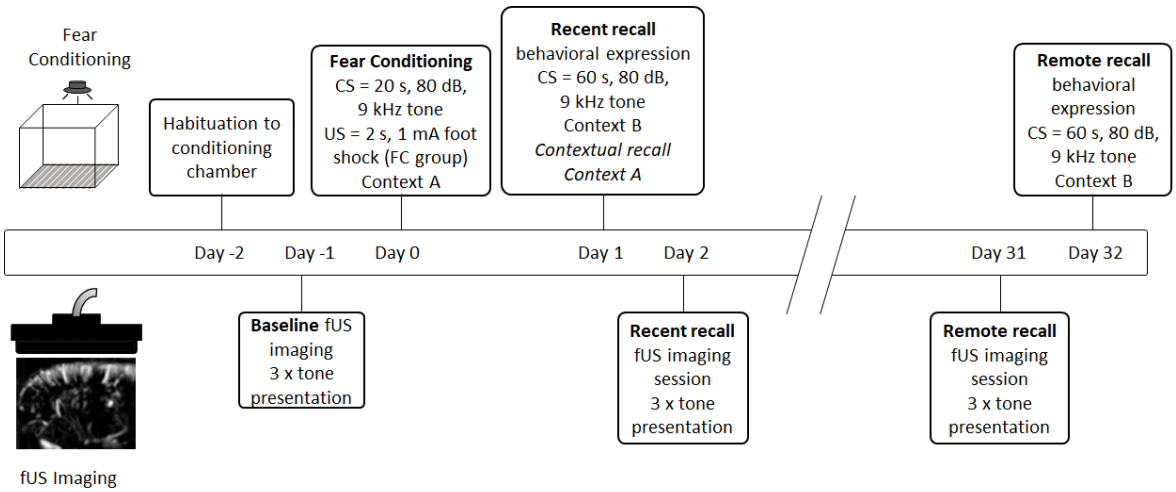

Figure 2.2 :1 Study I experimental timeline. Animals were handled extensively and habituated to the FC chamber prior to the start of experiments. After a baseline imaging session, animals were exposed to an auditory tone (CS) paired with a single foot shock (US) during FC. Recent and remote recall imaging and behavioral expression tests were performed after 24 hours or 31 days, respectively. Experiments with UT control animals were performed in the exact same manner except that they were not exposed to the US. (Reprinted with permission from Grohs-Metz et al., 2022 Behav Brain Res.)

Study II: Since the purpose of this study was to monitor changes in functional connectivity throughout development, animals were imaged on post-natal day 35 (p35), p42, p60 and p90 (Figure 2.2 :2). These timepoints were chosen to reflect transitions in neural network development in humans. In humans, maximum volumes of white and gray matter are measured during pre-pubescence and begin to refine during pubescence. In addition, the appearance of segregated pre-frontal networks occurs during this same time period (Bansal et al., 2008; Durston et al., 2001). During the transition from pre-pubescence to pubescence, a reduction in synaptic density, increases in myelination, and the refinement of circuitry associated with cognition is thought to occur (Giedd et al., 1999; Huttenlocher, 1979), which has been mirrored in mice (Baloch et al., 2009; Chahboune et al., 2007). Though changes in myelination occur throughout life, after adolescence, humans and mice alike are considered to express mature neurotransmission and synaptic density (Lebel and Beaulieu, 2011; Nabel et al., 2020). Since there is evidence of post-adolescent maturation of associative tracts in humans (Lebel and Beaulieu, 2011), we also imaged at p90.

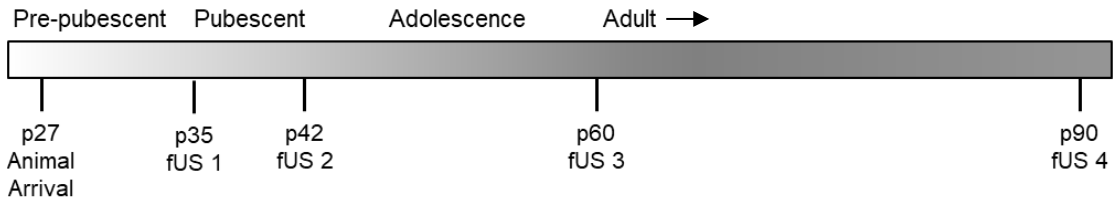

Figure 2.2 :2 Study II experimental timeline. After 7 days of habituation, hemizygous 15q13.3 mice underwent fUS imaging throughout development. Timepoints were designed to correspond with major milestones in pubescence, early and late adolescence, and adulthood.

Study III: In this study we wanted to investigate the role of inhibitory PV+ interneurons in vHC connectivity in the mesocorticolimbic pathway, specifically if modulating PV+ activity would lead to both focal and distal network modulation. Since the subiculum has been described as a major output region of the HC (Amaral et al., 1991; Cenquizca and Swanson, 2007; Witter et al., 1989), we decided to target the vCA1 as many studies pointed to this particular region as an origin of hippocampal dysfunction (Krieckhaus et al., 1992; Wolff et al., 2018), in slight amendment to the network proposed in Figure 1.2.2. Specifically, we sought to alter the transmission behavior of a subpopulation of PV+ interneurons in the vHC and investigate if this would affect connectivity in mesocorticolimbic structures as measured with fUS. Since amphetamine induced dopamine release is thought to recapitulate the features of psychosis in otherwise healthy humans and animals (Breier et al., 1997; Wang et al., 2010), we used phenotypically normal mice. We therefore performed stereotactic surgery on heterozygous PV-Cre mice to bilaterally inject the vCA1 with DREADD expressing adeno-associated viruses (AAVs) (described in Section 2.4). We then allowed 4 weeks to ensure significant viral expression which was then tested in satellite animals, followed by pharmacological fUS imaging (Figure 2.2 :3).

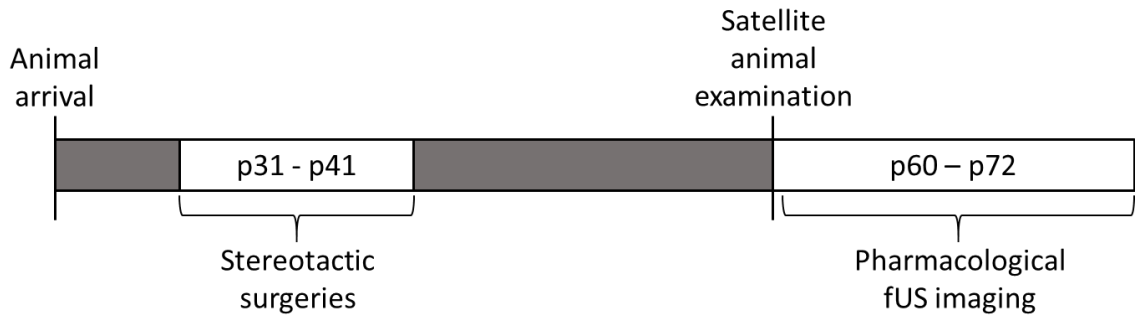

Figure 2.2 :3 Study III experimental timeline. After 1 week of acclimation, heterozygous PV-Cre mice were stereotactically injected with DREADD expressing AAV viruses bilaterally into the vCA1. Satellite animals were examined after 4 weeks to determine the presence and specificity of viral expression. Following this confirmation, the remaining study animals underwent pharmacological fUS imaging.

2.3. Fear conditioning and behavioral expression protocol and analysis

"Study II behavioral experiments were carried out in four identical chambers (VFC-008, Med Associates, Vermont, USA), each enclosed in a sound attenuating box (NIR-022SD, Med Associates, Vermont, USA). VideoFreeze SOF-843 software (MedAssociates, Vermont, USA) was used to create protocols, run experiments and extract freezing data (detailed in (Anagnostaras et al., 2010)). In brief, each chamber consisted of a stainless-steel grid floor through which the electric shock (US) was delivered, a speaker in the side wall for tone (CS) delivery, and a fan for air circulation and constant background noise (65 dB) generation. An overhead LED-based light source provided white and near-infrared light, the latter being used by a VID-CAM-MONO-5 USB video camera to detect motion and freezing. Freezing was defined as the absence of all movement apart from that related to breathing. The minimum freezing duration was taken as 1 second in which the detected motion fell below the threshold (Motion Index Threshold = 18) (Anagnostaras et al., 2010). Sessions were recorded at 30 frames per second. Mice were habituated to the chamber and grid floor for 15 minutes on the day prior to beginning the study (Day -2, Fig. 2.2 :1) and were transferred in their home cages to the testing room 30 minutes prior to experiments. The FC and FE protocols were adapted from published literature (Kamprath and Wotjak, 2004; Lux et al., 2016) as follows: during FC, each mouse was placed in a separate chamber, which was lightly wiped with 75 % ethanol prior to start. The house light was set to 35 lux, referred to as 'context A'. After three minutes of free exploration, a 20-second continuous tone (80 dB, 9 kHz, 10 ms rising and falling time) was played and co-terminated with a 2-second, 1 mA electric shock delivered through the grids, followed by one minute of free exploration before returning to the home cage. Mice were then left undisturbed in their home cages for 24 hours, after which FE to the CS was carried out in a novel context, referred to as 'context B'. This consisted of completely covering the grids with a smooth flat white acrylic sheet, on top of which bedding was added to stimulate motility. One black and one grey acrylic sheet covered the left and right walls, respectively, and the house-light was increased to 50 lux. Mice freely explored the novel context for 3 min, then the same 80 dB, 9 kHz tone was played for 1 min (3 x 20 s bouts with 1 s in between), but without a shock, and again animals were returned to their home cages 1 min after the tone ended. The specificity of the freezing response to tone was tested on the same afternoon by re-exposing

the animals for 5 min to context A without delivering the tone or the shock, to evaluate the contextual freezing response. Control animals were only exposed to the unconditioned tone (UT) without shock (n = 12), all other handling and experimental conditions were identical to the fear conditioned (FC) group (n = 12).” (Grohs-Metz et al., 2022)

“Automatic scoring of total freezing and % freezing for each time point were performed by VideoFreeze software. After 3 minutes of free exploration, pre-tone, post-tone, and freezing measurements were calculated from the 20 s prior to and post tone and compared to the first 20 s of the tone presentation during each recall session. Contextual freezing was calculated using a 20 s time bin after 3 minutes of free exploration.” (Grohs-Metz et al., 2022)

2.4. Expression of DREADDs in PV+ interneurons in the vCA1

We sought to investigate the influence of PV+ interneuron modulation in the vCA1 region on neural activity throughout the mesolimbic cortex. Since it has been shown that both positively and negatively modulating the vHC can affect network connectivity (Călin et al., 2018; Marek et al., 2018; Pati et al., 2019), we decided to test both inhibition and excitation of vCA1 PV+ interneurons to investigate any potential contrasting effects. We chose a chemogenetic pharmacological model in order to prompt acute changes without affecting overall network development and thereby reduced the likelihood of compensation from alternative networks. Therein, we chose to utilize 3 expression transgenes originally created by the Bryan Roth laboratory and supplied by UZH-VVF, Zurich:

• inhibitory DREADD (hM4Di): ssAAV-DJ/2-hSyn1-dlox-hM4D(Gi)_mCherry(rev)-dlox-WPRE-hGHp(A)

• excitatory DREADD (hM3Dq): ssAAV-DJ/2-hSyn1-dlox-hM3D(Gq)_mCherry(rev)-dlox-WPRE-hGHp(A)

• mCherry control (mCherry): ssAAV-DJ/2-hSyn1-dlox-mCherry(rev)-dlox-WPRE-hGHp(A)

Upon activation by the synthetic agonist, clozapine-N-oxide (CNO), hM4Di initiates a signaling cascade that primarily reduces intracellular cyclic adenosine monophosphate (cAMP), thereby reducing the excitability of the cell via hyperpolarization and inhibition of presynaptic vesicle release (Roth, 2016). Activation of the hM3Dq DREADD on the other

hand, stimulate the release of intracellular calcium, priming interneurons to generate post-synaptic inhibitory currents (Călin et al., 2018).

2.4.1. Surgical procedures

PV-Cre mice were administered 0.5 mg/kg s.c. Meloxicam (Metacam, Boehringer Ingelheim Vetmedica, Germany, 10 mg/ml injection volume in physiological saline solution) thirty minutes before any procedures. Mice were then anesthetized with a mixture of 4% isoflurane in O_2. The skull was closely shaved, and animals were fixed in a 3-D stereotactic alignment system (Model 1900, David Kopf Instruments, USA) and isoflurane was adjusted to 1.5 – 2.0% depending on animal breathing depth and paw withdrawal reflex. Temperature was maintained at 37ºC with a homeothermic heating system and 0.25% Bupivacaine was injected under the scalp (~0.05 – 0.10 mL). A sagittal incision was created slightly to the right of midline to reduce the likelihood of the scar interfering with the fUS signal during imaging of the left hemisphere. A planar head position was ensured by aligning bregma, lambda, and parietal bones to 0º. Small burr holes were drilled in the appropriate location and the following coordinates were used for a single viral injection:

AP -3.10, ML ± 3.15, DV -4.55

Needles were inserted 0.05 µm past injection point and left in place for 5 minutes to make an injection pocket. Needles were retracted to the target coordinates and viruses were injected in a 300 nL volume at a 200 nL/min flow rate and left in place for 5 minutes after injection completion. Viral titres were:

hM4Di 5.0 x 10^{12} vg/mL
hM3Dq 2.7 x 10^{12} vg/mL
mCherry 3.0 x 10^{12} vg/mL

Needles were then retracted 0.05 µm and kept in place for another 5 minutes to minimize viral withdraw upon full needle retraction. Burr holes were left unfilled, and the incision was sutured. Animals were given softened food and a high calorie diet supplement to aid in recovery.

2.4.2. mCherry expression in satellite animals

We allowed 4 weeks of recovery to allow ample time for viral expression. One mouse from each group was then designated as a satellite animal to ensure viral mCherry reporter expression prior to fUS imaging experiments. As the viruses were constructed with dlox sites on either side of the DREADD expression cassettes (Section 2.4.1), and we used mice that expressed Cre recombinase in PV+ interneurons, we expected and inevitably detected fairly specific expression in the vCA1 (Figure 2.4.2). To extract the brains from the satellite animals, mice were deeply anesthetized with sodium pentobarbital and transcardially perfused with 4% paraformaldehyde. Fixed brains were cut using a cryostat into 50µm sections and mounted onto glass coverslips for examination.

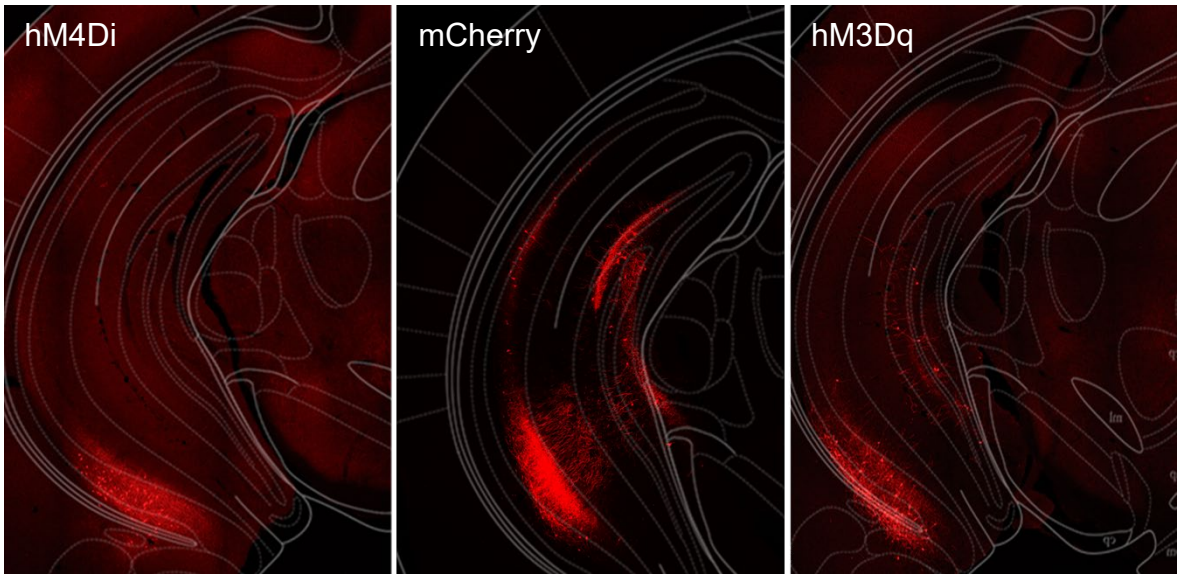

Figure 2.4.2 Expression of the viral mCherry reporter in satellite animals. Fluorescence was detected in all 3 groups and localized to the vCA1 region, though the individual from the mCherry group did show some evidence of unintended viral spreading.

2.5. Sedation protocol

Animals were lightly sedated with dexmedetomidine, a potent α2-adrenergic receptor agonist, during fUS imaging sessions. It is said to exert its hypnotic effects in the locus coeruleus, where it induces a state of unconsciousness that is similar to natural sleep (Weerink et al., 2017). It is frequently used in neurosurgeries that requires patient feedback as patients are easily roused and exhibit minimal respiratory depression (Yu, 2012). Animals sedated with dexmedetomidine have been shown to exhibit stable BOLD responses as well as respiratory and cardiac function (Nasrallah et al., 2014; Reinwald et al., 2020). Also, a

recent study using fUS in conscious animals showed that at low doses, medetomidine did not significantly alter functional connectivity (Ferrier et al., 2020). Furthermore, dexmedetomidine is readily antagonized with atipamezole, with animals typically regaining the righting reflex within several minutes (Baker et al., 2011).

We developed a dexmedetomidine sedation protocol based on that of Boido et al., (2019). A dexmedetomidine solution was prepared daily by diluting 1 mg/mL aliquots (Tocris, USA) with physiological saline solution which was then filtered through a sterile 0.1 µm syringe filter (Watman, Germany). Sedation was induced in a plexiglass chamber with 5% isoflurane. Hair over the scalp was very closely shaved with an electric razor and 0.05 mg/kg Metacam s.c. was administered as analgesia for any potential discomfort from stereotactic fixation. Animals were then fixed in a 3-D stereotactic alignment system (Model 1900, David Kopf Instruments, USA) positioned on top of an anti-vibration table (CleanBench™, TMC, Germany). Skulls were fixed with non-rupture ear bars and isoflurane was reduced to 1%. Temperature was maintained at 37ºC with a homeothermic warming system (PhysioSuite, Kent Scientific, USA). A flexible s.c. catheter (Surflo i.v. catheter, Terumo Europe) was placed over the shoulders and a bolus of dexmedetomidine hydrochloride delivered (0.067 mg/kg study I and II, 0.05 study III). A 5 mL/kg hr^{-1} infusion was then initiated with 0.20 mg/kg hr^{-1} dexmedetomidine (study I & II) or 0.15 mg/kg hr^{-1} dexmedetomidine (study III) using a programmable syringe pump (PHD Ultra, Harvard Apparatus, USA). Isoflurane was reduced in 0.1% increments after 10 minutes with total isoflurane cessation within 20 minutes of bolus administration. Structural imaging was performed during and shortly after isoflurane turn down, however, functional imaging was initiated no earlier than 10 minutes after isoflurane cessation. After acquisition completion, dexmedetomidine was antagonized with atipamezole (Alzane, Zoetis, Germany) at 5 times the total administered dexmedetomidine dose.

2.6. Functional ultrasound imaging

“Dedicated small animal fUS hardware and software (Iconeus, Paris, France) were used for all imaging sessions. A linear ultrasonic probe (15 MHz central frequency, Iconeus, Paris, France) with 128 piezoelectric transducers connected to an ultrafast ultrasound scanner (Iconeus One - 128 channels, Iconeus, Paris, France) was used to emit ultrasonic plane waves and to receive and process backscattered Power Doppler signal. Spatiotemporal singular value decomposition clutter filtering for blood signal isolation and fUS image compilation

has been described in depth previously (Demené et al., 2015; Ferrier et al., 2020; Gesnik et al., 2017; Macé et al., 2011; Osmanski et al., 2014), and results in an image compiled from 200 compounded ultrafast frames acquired at a 500 Hz frame rate, each of those being the sum of ultrasonic echoes acquired from a set of 11 tilted plane waves (-10 to 10°, separated by 2°) emitted at a 5500 Hz pulse repetition frequency. The final sequence of functional images yielded a 2.5 Hz frame rate (1 power Doppler image acquired every 400 ms) with a spatial resolution of 100 x 100 x 400 µm." (Grohs-Metz et al., 2022)

2.6.1. Region of interest selection and imaging plane design

Since the probe used for acquisition in the current studies was linear, it was necessary to strategically design imaging planes that could acquire data from the highest priority regions of interest (ROIs) (ROI abbreviations denoted in Table 2.6.1). For study I, we aimed to create an imaging plane that encompassed regions that were expected to have the most influence over an auditory cued fear associated memory trace (Grewe et al., 2017; Tovote et al., 2015) (Figure 2.6.1 A & B), namely the basal amygdalar complex and output nuclei, the PFC, and regions involved in auditory sensation. For study II, a coronal plane encompassing regions of the somatosensory cortex, dorsal hippocampus, thalamus, amygdala, and hypothalamus was designed to image 15q13.3 mice (Figure 2.6.1 C & D). Finally, for study III we composed a plane covering the ventral hippocampus, nucleus accumbens, PFC, and cingulate cortex (Figure 2.6.1 E & F). We assigned the highest priority to imaging the vCA1 in study III. Therefore, although the VTA has been shown to play a pivotal role in the mesolimbic pathway, an imaging plane with the vCA1 and VTA would have excluded most of the other ROIs in the mesocorticolimbic network. We therefore chose a plane for study III that included the regions listed previously.

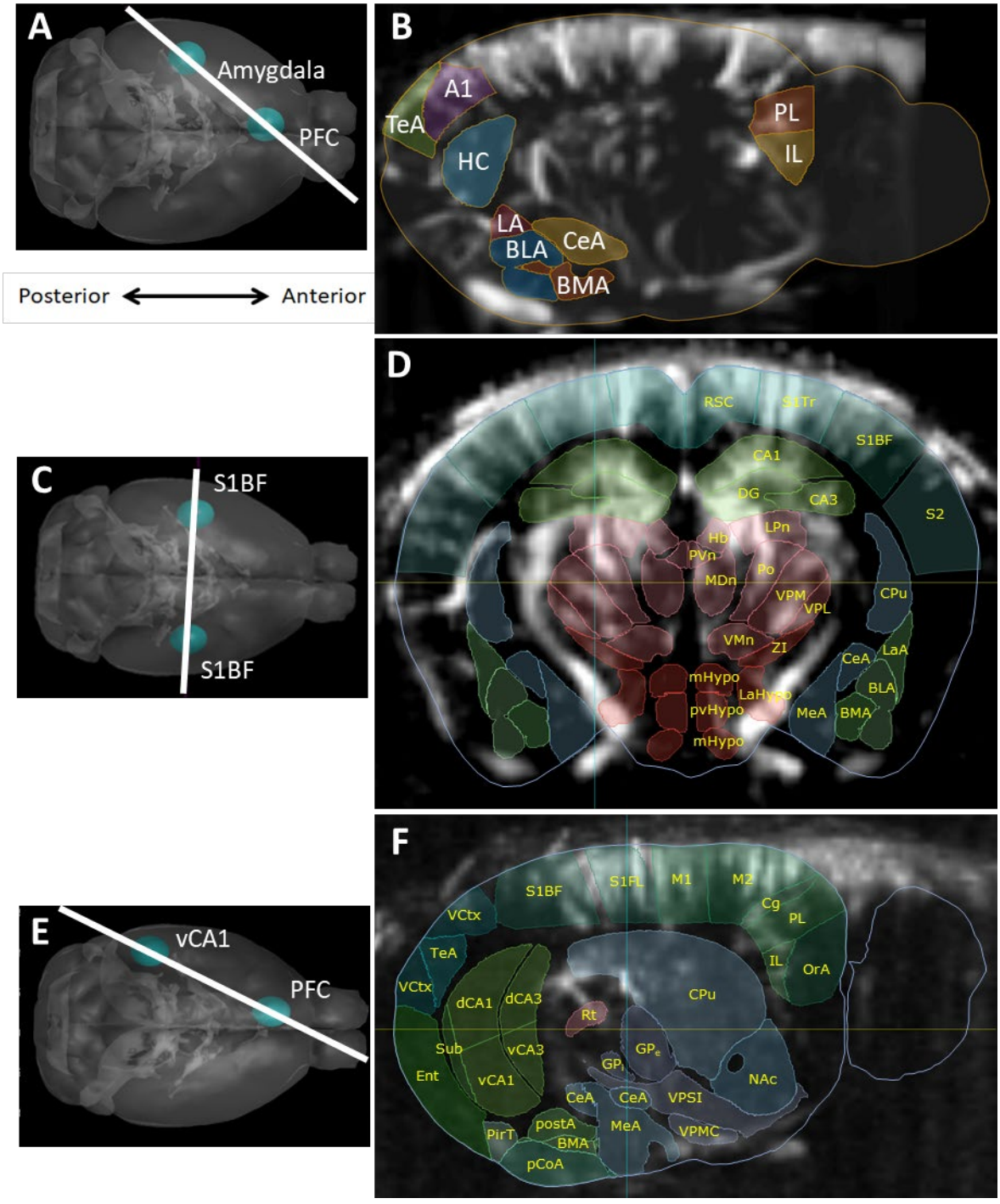

Figure 2.6.1 Linear imaging planes used in each study. The brain of each mouse was registered in 3D to the Allen common coordinate framework (CCFv3) at the beginning of each imaging session in order to calculate the coordinates for probe positioning. Anatomical ROI delineations are overlaid on a representative fUS Doppler image for each study. (A) Oblique probe position and (B) ROI designation for study I (Reprinted with permission from Grohs-Metz et al., 2022 Behav Brain Res.). (C) Coronal probe position and (D) ROI designation for study II. Data was extracted from both left and right hemispheres. (E) Oblique probe position and (F) ROI delineation used in study III. Data from regions which were present in 2 different areas for the same plane was averaged during pre-processing ((D) mHypo and (F) VCtx and CeA). ROI abbreviations are defined in Table 2.6.1.

Table 2.6.1 ROI description for all studies. Full description according to Allen mouse brain common coordinate framework v3 (Wang et al., 2020).

Full Description	Abbrev.	Study		Full Description	Abbrev.	Study
Auditory cortex	A1	I		Orbital cortex	OrA	III
Basolateral amygdalar nucleus	BLA	I/II		Posterior cortical amygdalar area	pCoA	III
Basomedial amygdalar nucleus	BMA	I/II/III		Piriform transition area	PirT	III
Field CA1	(d/v)CA1	II/III		Prelimbic cortex	PL	I/III
Field CA3	(d/v)CA3	II/III		Posterior complex of the thalamus	Po	II
Central amygdalar nucleus	CeA	I/II/III		Posterior amygdalar nucleus	postA	III
Cingulate cortex	Cg	III		Hypothalamic periventricular region	pvHypo	II
Caudoputamen	CPu	II/III		Paraventricular nucleus of the thalamus	PVn	II
Dentate Gyrus	DG	II		Retrosplenial area	RSC	II
Entorhinal area	Ent	III		Reticular nucleus of the thalamus	Rt	III
Globus pallidus, external segment	GPe	III		Primary somatosensory area, Barrel Field	S1BF	II/III
Globus pallidus, internal segment	GPi	III		Primary somatosensory area, forelimb	S1FL	III
Habenula (Epithalamus)	HB	II		Primary somatosensory area, Trunk	S1Tr	II
Hippocampus (not delineated)	HC	I		Supplementary somatosensory area	S2	II
Infralimbic cortex	IL	I/III		Subiculum	Sub	III
Lateral amygdalar nucleus	LA/LaA	I/II		Temporal association areas	TeA	I/III
Lateral hypothalamic area	LaHypo	II		Visual cortex	VCtx	III
Lateral posterior nucleus of the thalamus	LPn	II		Ventral medial nucleus of the thalamus	VMn	II
Primary motor area	M1	III		Ventral posterolateral nucleus of the thalamus	VPL	II
Secondary motor area	M2	III		Ventral posteromedial nucleus of the thalamus	VPM	II
Mediodorsal nucleus of thalamus	MDn	II		Ventral pallidum, magnocellular nucleus	VPMC	III
Medial amygdalar nucleus	MeA	II/III		Ventral pallidum, substantia innominata	VPSI	III
Hypothalamic medial zone	mHypo	II		Zona incerta	ZI	II
Nucleus Accumbens	NAc	III				

2.6.2. Acquisition parameters

Once animals were sedated and fixed in the stereotactic frame (Section 2.5), the scalp was thoroughly saturated with saline solution to reduce the occurrence of air bubbles around hair shafts. The scalp was then covered generously with a degassed, isotonic, ultrasound coupling gel (Aquasonic Clear Ultrasound Transmission Gel, Parker Laboratories Inc., USA) and the fUS probe was lowered to approximately 1mm from the scalp. At the beginning of every imaging session, a series of 2D images covering the whole anterior to posterior range of the brain was acquired and these images were used to register the brain to a reference in 3D. This reference, provided by Iconeus (Paris, France), is comprised of vascular scans from multiple mice that were registered to an angiography template acquired with MRI as well as the Allen two-photon template. The software and mathematical procedures used to register the brains has been described in detail in (Nouhoum et al., 2021). Once the brain was registered, the pre-designed imaging planes were used to calculate respective probe coordinates.

For study I, we presented the auditory tone with a mini loudspeaker placed near the animal's head which we programmed for precise timing and output with an Arduino Uno microcontroller. Between 10 minutes of rest (baseline), we presented 3 blocks which consisted of 3 x 20 s rounds of tone (80 dB, 9kHz) with one second of pause between (Figure 2.6.2 top) for both recent and remote memory retrieval sessions.

Resting state data was acquired for 10 minutes at p35, p42, p60, and again at p90 for study II (Figure 2.6.2 middle).

During pharmacological fUS imaging for study III, 6 mg/kg CNO was delivered intraperitoneally via a pre-placed catheter so as not to disturb the animals during the acquisition (Figure 2.6.2 bottom). We chose the dose and timing of CNO administration based on the in-depth pharmacological profile described in (Jendryka et al., 2019). The images from all studies were then processed as described in the subsequent sections.

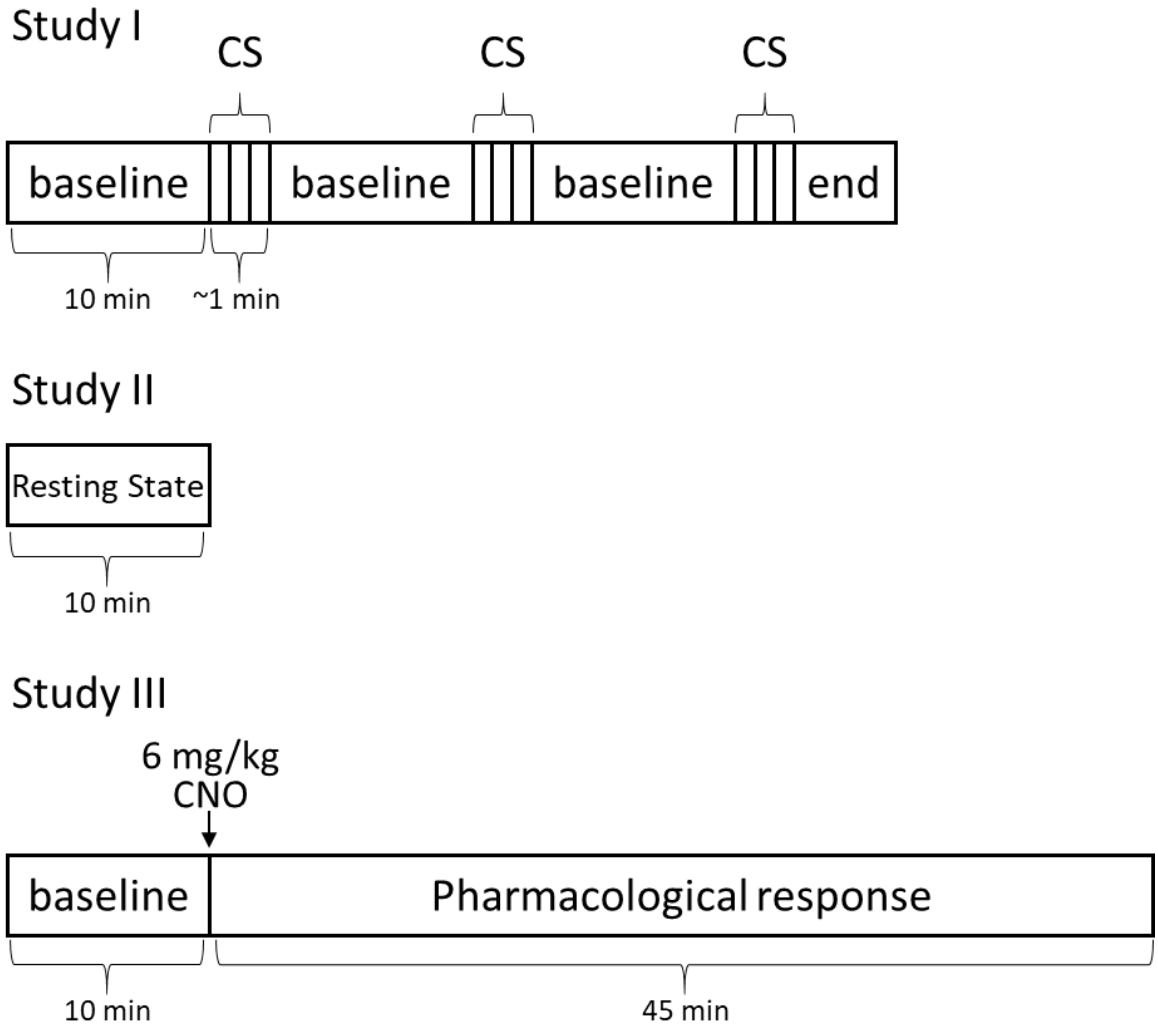

Figure 2.6.2 fUS acquisition parameters for individual studies. During study I, a tone of the same parameters used during FC training was presented to the mice during 3 different CS blocks between 10 minutes of rest (baseline). During the CS blocks the tone (80dB, 9kHz) was presented 3 times for 20 s with 1 second pause between. 5 minutes of rest was acquired at the end of the acquisition. Study II consisted of 10 minutes of resting state acquisition. After 10 minutes of baseline, 6 mg/kg CNO was delivered via i.p. and the pharmacological response was recorded for 45 minutes during fUS acquisitions for study III.

2.6.3. fUS data pre-processing

During imaging, a singular value decomposition filter that is integrated into the acquisition sequence, effectively denoises the images by isolating blood Doppler signal from the non-specific signals reflected from tissue. This process requires a complex algorithm that is described in (Demené et al., 2015). Due to this pre-processing and the stability afforded by firm fixation in the metal stereotactic frame, we were also able to avoid the influence of small, physiological motion artifacts without using complicated processing steps. Motion from ear or whisker twitches indicating loss of sedation, for example, created large, obvious artifacts in the data which could be manually identified and scrubbed, though we did have

to exclude several animals from connectivity analysis in study II and III due to larger blocks of data removal (>30 seconds) (described in sections 3.2.1 and 3.3.2).

To initiate analysis of neural activity, the temporal power Doppler signal was extracted from all voxels within the individual ROIs delineated via the Allen mouse brain common coordinate framework (Wang et al., 2020). Changes and CBV measured in study III, could be calculated directly from this data by normalizing the data to the baseline acquired prior to CNO administration, emphasizing the importance of a stable baseline outside any potential residual effects of the isoflurane used to induce sedation (section 2.5).

2.7. Data processing and statistical analysis

2.7.1. Analysis of functional connectivity

We employed a seed-based approach to assess connectivity between *a priori* ROIs. This approach assigns a mathematical value to connectivity by calculating the correlation, or similarity, between two temporal signals through a series of normalization and processing steps. "First, the signal accumulated from all voxels within a given ROI was normalized and detrended with a 4th-order polynomial fit to remove potential low frequency drift. A 0.2 Hz low pass filter was then applied to isolate resting state functional connectivity frequencies (Osmanski et al., 2014; Rabut et al., 2020). Finally, Pearson product moment correlation coefficients were calculated for each ROI-ROI pair and normalized using Fisher's *z* transformation to create a connectivity matrix." (Grohs-Metz et al., 2022). Additional calculations for each study were accomplished as follows:

Study I: "To compare cue-evoked functional connectivity, Δz values were calculated for each ROI-ROI pair by subtracting the connectivity value from the 60 seconds prior to the tone from that measured during the 60 second tone and averaged for the 3 tone blocks presented during each imaging session. Finally, those changes were compared across imaging sessions by calculating $\Delta\Delta z$ values via the difference in these Δz values. Node weight was calculated from the combination of all normalized correlation coefficients between a specific ROI and all other ROIs." (Grohs-Metz et al., 2022)

Study II: To analyze developmental changes in functional connectivity, we calculated the effect size (Cohens' *d*) using the *z* transformed correlation values as detailed in (Zerbi et al., 2019). Briefly, a standard effect size is calculated between a reference

measurement, in this case WT connectivity at p35, and the data of interest. In this way, effects can be normalized and classified as small to large. Fisher's *z* transformed matrices and Cohen's *d* matrices were further analyzed as described in the following section (2.7.2).

Study III: We employed a sliding window approach to measure the pharmacological connectivity response. Correlation matrices of 5-minute time bins representing window size were advanced in 1-minute increments. Snapshots at 15-, 30-, and 45-minutes post CNO administration were used for statistical analysis.

All statistical analysis tests were calculated with GraphPad Prism software (ver. 9, GraphPad Software, California, USA) using $p < 0.05$ as the standard for significance, expect for network-based statistics used in study II which was completed in MATLAB (ver. R2019b, MathWorks Inc., Massachusetts, USA). Data is presented as mean ± standard error of the mean (SEM) unless otherwise noted. The statistical test used for each set of data is denoted in the applicable figure or associated text.

2.7.2. Graph theory, principal component analysis, and machine learning

Graph theory, principal component analysis (PCA), and support vector machine (SVM) pattern classification for study II were performed in collaboration with Dr. Hugo Cruces-Solis, at the department of Central Nervous System Diseases Research, Boehringer Ingelheim Pharma GmbH & Co. KG.

First, to identify changes in functional connectivity between genotypes, we used the network-based statistics toolbox (NBS) in MATLAB, a validated method to perform statistical analysis on large networks (Zalesky et al., 2010) in combination with graph theory. For the input data, we used the z-transformed correlation values of the entire dataset and used a repeated measures design with a primary threshold of 3 and an arrangement parameter of 5000 permutations. The resulting t-values (edges) and numbers of significant connections of a particular ROI (node degree) were used to construct and visualize a distinct network of hyperconnectivity in the 15q13.3 mice.

Next, we used correlation matrix-based hierarchical clustering to group brain regions with similar connectivity patterns (Figure 2.7.2). Cohen's *d* matrices were ordered using this clustering organization.

A

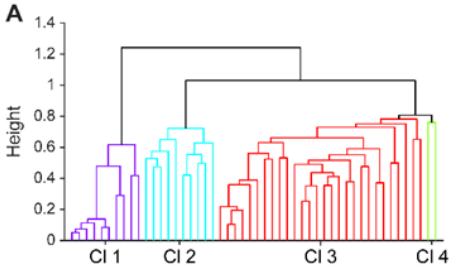

B

ROI	Cluster	ROI	Cluster	ROI	Cluster	ROI	Cluster	ROI	Cluster
S1BF_R	1	MeA_L	2	CA1_L	3	HB_L	3	ZI_L	3
S2_R	1	BMA_L	2	DG_L	3	MDn_L	3	VPM_R	3
S1BF_L	1	BLA_L	2	DG_R	3	MDn_R	3	Po_R	3
S2_L	1	CeA_L	2	CA1_R	3	HB_R	3	VPM_L	3
S1Tr_L	1	LaA_L	2	CA3_L	3	LPn_L	3	VPL_L	3
S1Tr_R	1	LaA_R	2	CA3_R	3	LPn_R	3	VPL_R	3
RSC_L	1	BLA_R	2	LaHypo_L	3	Po_L	3	PVn_L	3
RSC_R	1	BMA_R	2	LaHypo_R	3	ZI_R	3	PVn_R	3
CPu_L	1	MeA_R	2	mHypo_L	3	VMn_R	3	pvHypo_L	4
CPu_R	1	CeA_R	2	mHypo_R	3	VMn_L	3	pvHypo_R	4

Figure 2.7.2 Functional connectivity-based ROI clustering. (A) Cluster hierarchy. (B) Cluster designation. Cluster 1 contains mainly cortical ROIs and the CPu. Cluster 2 contains the ROIs of the amygdalar nuclei. Cluster 3 contains hippocampal, thalamic subdivisions, and a majority of the hypothalamic nuclei. Cluster 4 contains the bilateral paraventricular hypothalamic nuclei. L and R designators signify left and right hemispheric regions, respectively. ROI abbreviations are defined in Table 2.6.1.

Since PCAs can be used to categorize regions that display similar connectivity patterns and do not require input regarding the connectivity pattern, they can be useful in brain mapping to identify groups with correlated responses (Zhan and Yu, 2015). Therefore, we used this method for genotype prediction. First, we performed a PCA using the effect size values of the entire dataset (p35 – p90), (*pca*, MATLAB function). Next, we used the scores of the first 3 principal components as predictors to train a linear SVM (*fitcsvm*, MATLAB function). To protect against overfitting, we partitioned the data into 5-fold cross validations (*crossval*, MATLAB function). To predict the genotypes at p90 with data from p35 or p42, we calculated independent PCA scores for each age using the same method as above. In this way, the data used for training and predicting were independent of each other.

3. RESULTS

3.1. Study I: Functional ultrasound imaging of recent and remote memory recall in the associative fear neural network in mice

3.1.1. Recent and remote behavioral responses to cued fear expression test

In order to trigger an associative memory trace, animals were trained with Pavlovian auditory cued fear conditioning. A single 80 dB, 9 kHz tone was co-terminated with a 1 mA electric foot shock during the training. After 24 hours and again after 31 days, fear expression to the tone was tested in a different context (context B) of that used during fear conditioning (FC). Several hours after FC, animals were also re-exposed to the conditioning context (context A) without a tone to test for contextually associated fear behavior. Animals displayed significant freezing behavior during both recent and remote cued fear expression tests (52.0 ± 9.4%, $p < 0.001$, and 36.9 ± 6.0%, $p < 0.01$, respectively, ordinary one-way ANOVA with Bonferroni's multiple comparisons post-hoc test) (Figure 3.1.1). When re-exposed to the original training context, animals did not display significant freezing behavior (Figure 3.1.1, Context). Furthermore, after presentation of the tone in the novel context, animals showed minimal freezing behavior, indicating the development of an associative memory that is specific to the cue and not generalized to the context. Three animals were excluded from further analysis in the FC group for exhibiting less than 15% freezing to the tone (FC, n=9). Animals that were only exposed to the tone and were never shocked did not display significant freezing behavior at any time point (UT, n=12) (Grohs-Metz et al., 2022).

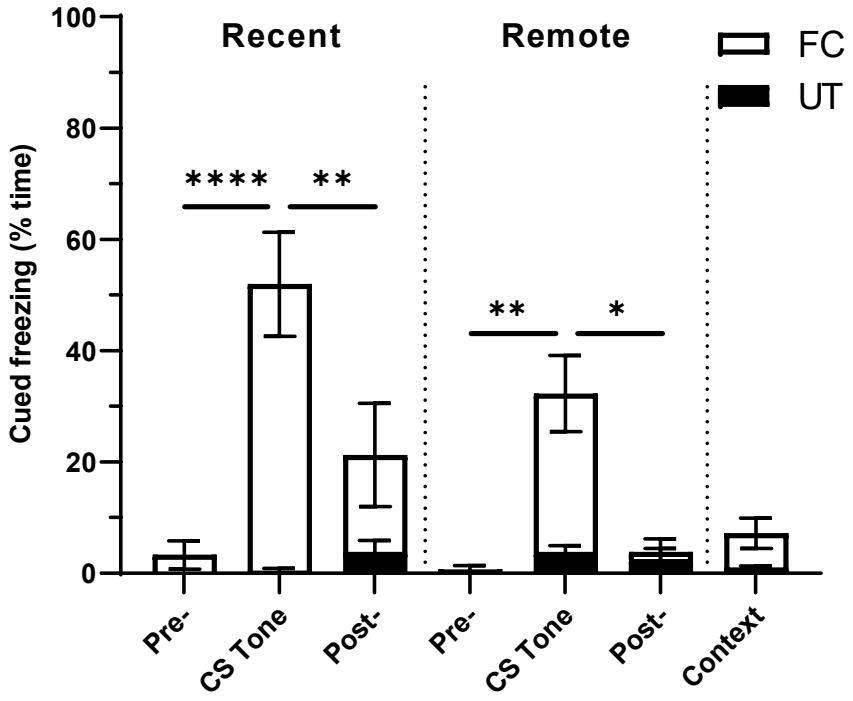

Figure 3.1.1 Average freezing responses to the auditory cue during recent and remote fear expression behavioral tests. FC animals showed significant freezing behavior during the tone in both recall sessions. UT trained animals showed negligible freezing during all time periods. When re-exposed to the conditioning context A after FC, animals exhibited minimal freezing (Context). Thus, validating the single robust US-CS pairing protocol for cued long term fear memory encoding. All data presented as mean ± SEM, significant differences between groups denoted with ** or *** ($p < 0.01$, and $p < 0.001$, respectively); (FC) fear conditioned group, n = 9; (UT) unconditioned tone group, n = 12. (Reprinted with permission from Grohs-Metz et al., 2022 Behav Brain Res.)

3.1.2. Cue-evoked functional connectivity across memory recall imaging sessions

Animals were sedated with dexmedetomidine, and functional connectivity was measured via fUS imaging one day after behavioral expression in recent recall and again after 31 days to investigate memory recall (outlined in Figure 2.2 :1). To calculate cue-evoked changes, pre-tone connectivity was subtracted from connectivity measured during tone presentation, represented as Δz (Figure 3.1.2 A). Significant differences were calculated with a repeated measures two-way ANOVA with multiple comparisons and false discovery rate control by Benjamini, Krieger, and Yekutieli two-stage set up method (Benjamini et al., 2006). During baseline imaging sessions when animals had not been exposed to the tone or a shock, there were only minimal differences in Δz (Figure 3.1.2 A, black data points). However, during recent recall most regions showed increased in cue-evoked connectivity with the exceptions

of the BLA-BMA and PL-HC ROI pairs (Figure 3.1.2 A, red data points, also visualized as cool colored squares in Figure 3.1.2 B). We then used scaled matrices to display the inter-session differences in cue-evoked functional connectivity ($\Delta\Delta z$) between all ROI-ROI pairs (Figure 3.1.2 B-D) for both the FC and UT group. Compared to baseline, global connectivity of the LA was significantly increased with most regions in the FC group during both recall sessions (Figure 3.1.2 B-D, lower triangles, warm colored squares). The CeA also showed increased global connectivity in the recent and remote recall sessions compared to baseline. However, when comparing the recall sessions to each other, FC animals exhibited smaller increases in cue-evoked CeA connectivity during the remote session (Figure 3.1.2 D, bottom row, visualized as cool colored squares). This would suggest that while the amygdala is certainly very active during both recall sessions and the LA is receiving signals, intra-amygdalar processing with the LA decreases during remote memory recall and in parallel output by the CeA is decreased. Interestingly, the TeA showed a somewhat similar pattern of connectivity to the CeA. When compared to recent recall, the TeA showed decreased global connectivity during remote memory retrieval, whereas especially during recent recall, the TeA showed significant cue-evoked connectivity with the A1 and most amygdalar subnuclei in comparison with baseline (Figure 3.1.2 B-D). Another group of anatomical regions, namely the A1, IL, BMA, and HC, showed variable changes in inter-connectivity between the two recall sessions. The IL, for example, showed significant increases in connectivity with the BMA during remote recall while there was only a very minute increase during recent recall. While not reaching statistical significance, the IL did show an increasing connectivity trend during remote recall when compared to recent recall. In comparison, there was a negative association in the PL-HC connection when comparing baseline to recent recall, however, there was a slight increase in cue-evoked connectivity during remote recall, and when comparing the two recall sessions there is a significant increase in HC-PL connectivity during remote recall when compared to recent memory retrieval (Figure 3.1.2 D).

In contrast, the UT group showed small, variable changes without a clear pattern (Figure 3.1.2 B-D, upper triangles). In the regions that were imaged, the cue induced mainly decreases or no change in connectivity in most regions. Compared to baseline, there were significant reductions in specific intra-amygdalar connectivity and only a few non-significant increases in the A1-BMA, and PL-TeA and PL-BLA (Grohs-Metz et al., 2022).

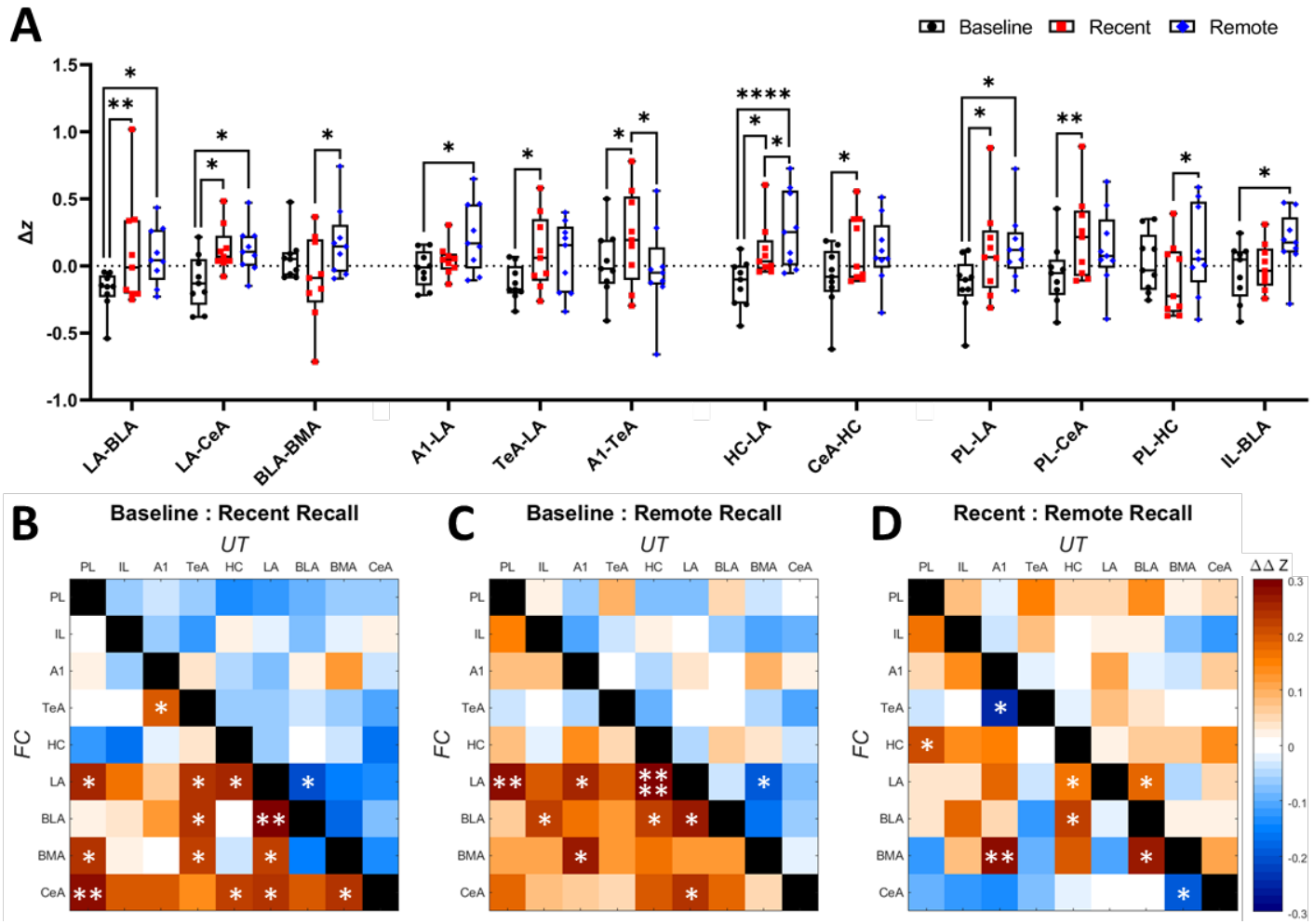

Figure 3.1.2 Functional connectivity changes in response to CS presentation between imaging sessions. (A) Intra-session changes in connectivity for select ROI-ROI pairs in FC group. Inter-session differences in tone-evoked connectivity between baseline and recent recall sessions (B), baseline and remote recall sessions (C), and recent and remote recall sessions (D). FC group data in lower triangles, n = 9, UT group in upper triangles, n = 12. Data presented as median ± 10–90 quartile Δz (A), and mean ΔΔz (B-D). Significant differences between imaging sessions denoted with *, ** or **** ($p < 0.05$, $p < 0.01$, and $p < 0.0001$, respectively**,** two-way ANOVA with multiple comparisons and false discovery rate control). Abbreviations defined in Table 2.6.1. (Reprinted with permission from Grohs-Metz et al., 2022 Behav Brain Res.)

3.1.3. Recent and remote fear associated functional connectivity networks

Using the regions that showed significant differences in cue-evoked connectivity in the FC group, we next built significant functional brain networks using nodes and edges (Figure 3.1.3, nodes = spheres, edges = interconnecting lines). Node diameter size was calculated via the inter-session differences in global connectivity for a given ROI. The edge width and shade are representative of the differences in inter-session connectivity of the ROI-ROI pair. Wide, dark lines represent the greatest $\Delta\Delta z$ increases indicative of increased functional connectivity, white, dashed lines represent decreased connectivity. The largest spheres during recent recall (Figure 3.1.3 A), indicating the regions with the highest global connectivity scores, are the CeA, LA, and TeA; regions typically associated with the recognition and identification of stimuli. Accordingly, these regions also display the largest number of significant edges. During remote recall (Figure 3.1.3 B), most ROIs showed increased global connectivity, except for the TeA and CeA. The majority of interconnecting edges were concentrated with the LA. When comparing the two recall sessions (Figure 3.1.3 C), the HC and BLA are the largest global hubs, which is also reflected in the increased number of edges from the HC. It should be noted that these edges do not reflect directionality (Grohs-Metz et al., 2022).

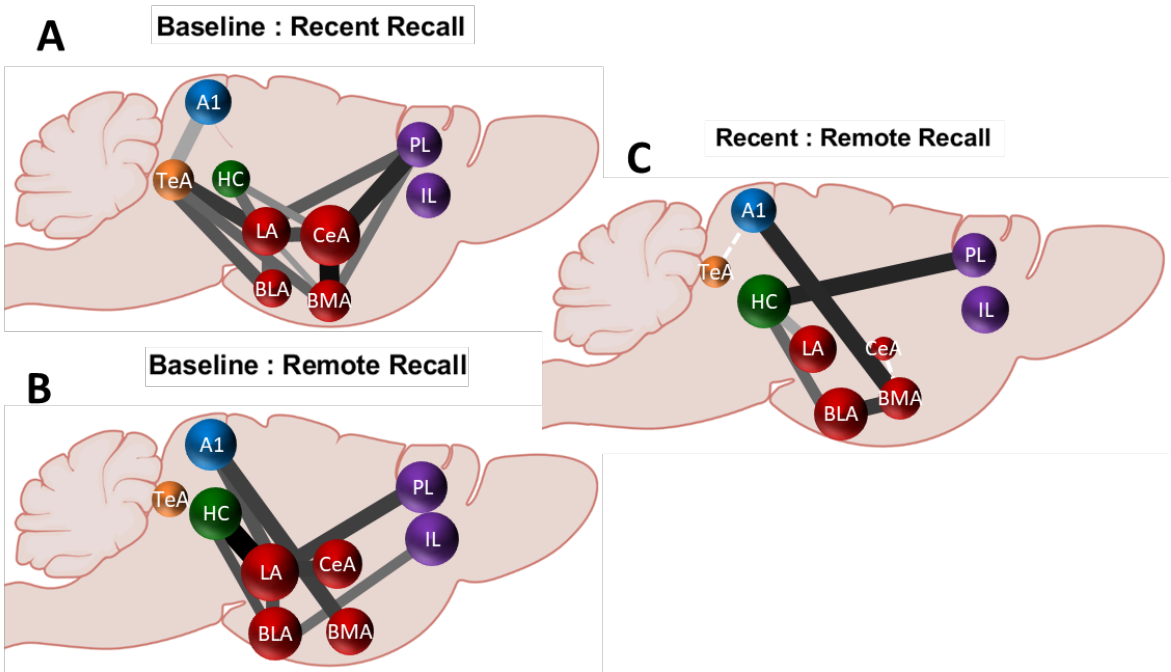

Figure 3.1.3 Brain network functional connectivity diagrams. The node diameter represents inter-session differences in global connectivity. Width and shade of edge color represent ROI-ROI functional connectivity changes (darker & wider = bigger increase), dashed white edges depict negative changes. Figure created with BioRender. (Reprinted with permission from Grohs-Metz et al., 2022 Behav Brain Res.)

3.1.4. Correlation of freezing behavior with functional connectivity

Finally, we sought to associate the changes in functional connectivity with expressed behavior using simple linear regression. We found 2 clusters of ROIs that showed either a negative or positive relationship with freezing behavior. The PL, TeA, HC, and CeA were positively correlated with freezing behavior in both recent and remote recall sessions (Figure 3.1.4 A & C). Contrastingly, regions associated with extinction learning, namely the IL, Al, and BMA, were negatively associated with freezing (Figure 3.1.4 B & D). Therein, these distinct clusters suggest that there might be two networks that are active during both recall sessions. In addition, the slopes of the regression in remote recall are steeper, suggesting a stronger association of activity in these regions to behavioral expression (Grohs-Metz et al., 2022).

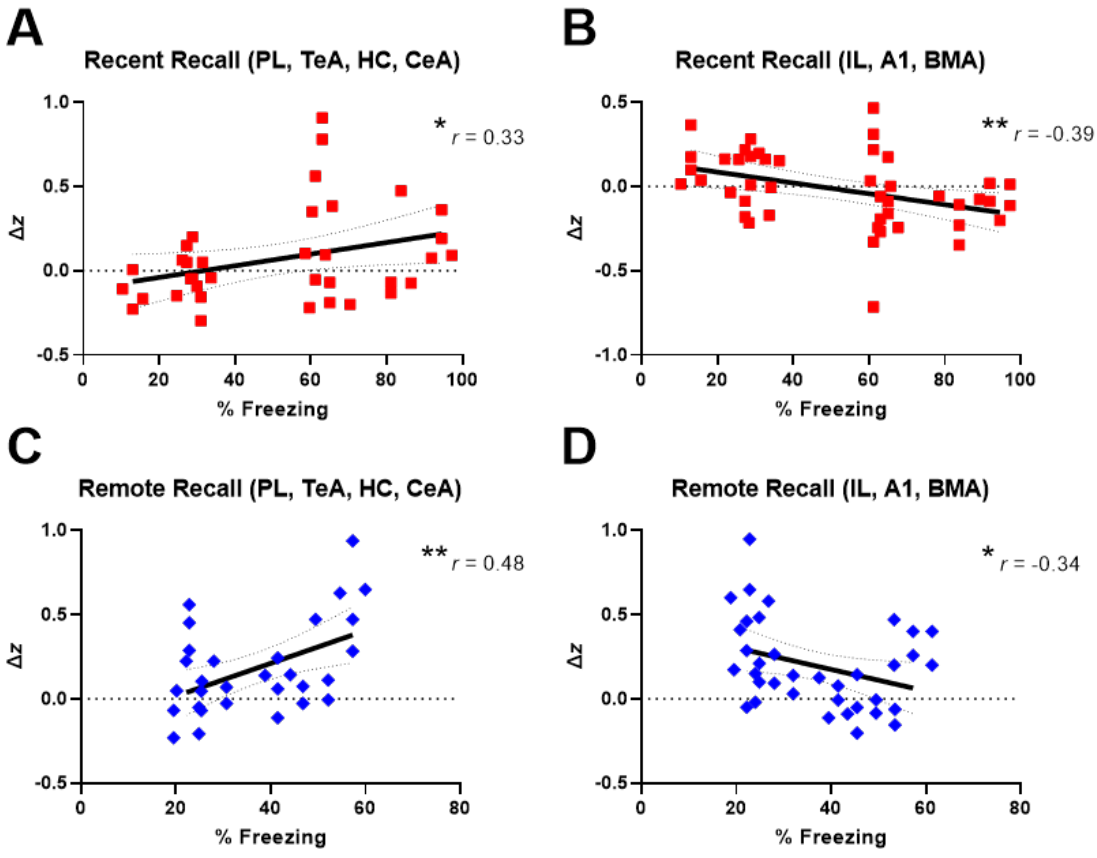

Figure 3.1.4 Correlation of behavioral fear expression and functional connectivity changes between clusters of ROI-ROI pairs in the FC group. (A,C) Connectivity between PL, TeA, HC, and CeA nodes positively correlated with freezing behavior during both recent (A) and remote (C) recall sessions. IL, A1, and BMA inter-nodal connectivity negatively correlated with freezing during recent (B) and remote recall (D). Each point represents a ROI-ROI pair within the denoted cluster for an individual animal in the FC group, n=9. Significant correlations denoted with * or ** ($p < 0.05$ and $p < 0.01$, respectively; simple linear regression; dotted line indicates 95% confidence interval). (Reprinted with permission from Grohs-Metz et al., 2022 Behav Brain Res.)

3.2. Study II: Deviations in network development in the 15q13.3 mouse model: a functional ultrasound study

3.2.1. Developmental trajectory of functional connectivity in 15q13.3 mice

To characterize the trajectory of functional connectivity across development, we longitudinally imaged the same mice during different time points (p35, p42, p60, and p90) thereby monitoring the transitions from pubescence to adolescence and adulthood. Some animals awakened during imaging, therefore only animals that were stable for all 4 imaging sessions were analyzed (WT n=11 and 15q13.3 n=12). To identify the impact of age on functional connectivity at each time point, we computed the effect size (Cohen's d) using the correlation values of WT mice at p35 as the reference dataset (Figure 3.2.1 A), as described in (Zerbi et al., 2019). We then used hierarchical clustering to group brain regions with similar connectivity patterns, where cluster 1 contains cortical ROIs along with the CPu, cluster 2 contains amygdalar ROIs, cluster 3 contains hippocampal, hypothalamic, and thalamic ROIs, and cluster 4 is composed of the paraventricular hypothalamic nucleus (detailed in Figure 2.7.2). To obtain a measure of change in connectivity per developmental time point, we averaged all the effect size values of each brain region and then calculated the mean across all brain regions (Figure 3.2.1 B).

In WT animals we observed an overall decrease in functional connectivity with increasing age (Figure 3.2.1 A, top row of matrices, increasing cool colors). There were some increases in inter-connectivity between regions in clusters 2, 3, and 4 in the WT group at p42 when compared to p35, but these increases were reversed by p60, and this trajectory of decreasing connectivity continued to p90. This effect was accurately reflected when we computed the average effect size for each developmental stage (Figure 3.2.1 B, black bars). In contrast, 15q13.3 mice showed a distinct pattern of functional connectivity at p35 (Figure 3.2.1 A, bottom left matrix) where there was an overall reduced functional connectivity pattern compared to that of the WT at p35 (Figure 3.2.1 B, red bars), though there was increased connectivity between cluster 1 and 3. At p42, the mean effect size between the two genotypes was similar (Figure 3.2.1 B), however, the connectivity patterns were different. WT animals were already showing greater decreases in clusters 1 and 2 and increases in clusters 3 and 4 (Figure 3.2.1 A, top row 2nd matrix from left), whereas the pattern for connectivity in the

15q13.3 was quite similar to that measured at p35, except for some slight increases in intra-connectivity between clusters 3 and 4 (Figure 3.2.1 A, bottom row first 2 matrices from left). Overall, the differences between connectivity from p35 to p42 were slightly greater in WT mice than in 15q13.3 (Figure 3.2.1 A, darker tones for both negative and positive effects). At p60, we found that the differences in the signature of functional connectivity in the 15q13.3 mice were even more substantial compared to WT mice (Figure 3.2.1 A, 3rd column). In 15q13.3 mice, regions in cluster 1, consisting of mainly cortical ROIs, displayed considerably higher inter-functional connectivity with regions in other clusters, while regions in cluster 2 (amygdalar ROIs) and the hippocampal ROIs in cluster 3 showed higher intra-functional connectivity. However, the average change in functional connectivity between genotypes was not different (Figure 3.2.1 B). At p90, the values of functional connectivity of 15q13.3 mice were relatively stable in relation to p60 and did not decrease like the trajectory in the WT group (Figure 3.2.1 A, 4th column and Figure 3.1.1 B). Except for the increased connectivity in the hippocampal ROIs of cluster 3 in the 15q13.3 group, the pattern of intra-connectivity in clusters 3 and 4 were similar between groups at p90. Together, these data indicate that functional connectivity in 15q13.3 mice is already divergent at p35 and follows a different developmental trajectory that results in an overall pattern of hyperconnectivity in adulthood.

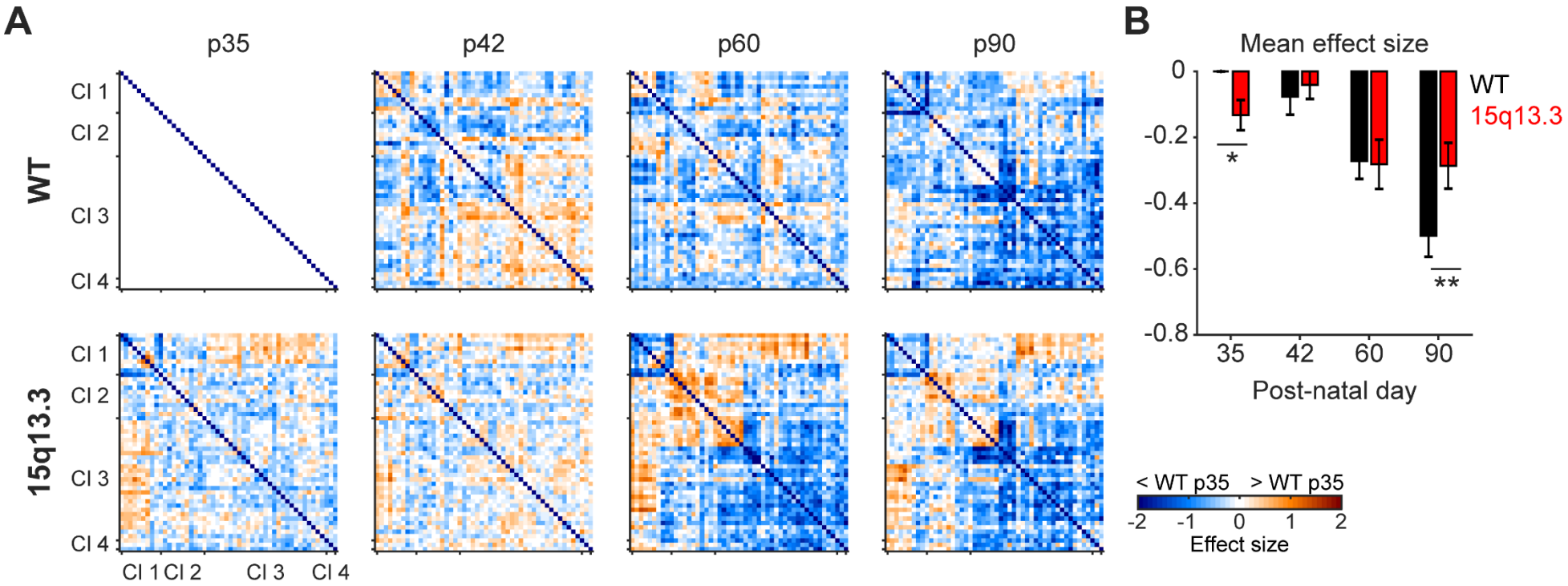

Figure 3.2.1 Differential developmental trajectory of functional connectivity in 15q13.3 mice. (A) Matrices showing the effect size analysis for WT (n=11) and 15q13.3 (n=12) mice across multiple time points through development. (B) Mean effect size across multiple developmental stages for WT and 15q13.3 mice. 2-way repeated measures ANOVA with Bonferroni's multiple comparisons correction, genotype x time interaction $F_{1,49}$= 29.5; p<0.001. * p < 0.05; ** p < 0.001 vs WT. Error bars represent ± SEM.

3.2.2. Identification of a large-scale hyper-connected network in 15q13.3 mice

Having identified a large-scale signature of functional connectivity during development in both WT and 15q13.3 mice, we next sought to identify the specific connections that were different between the genotypes using the entire dataset from all timepoints. Using network-based statistics (NBS) with a stringent threshold (t-value ≥ 3, Figure 3.2.2 A, warm colors), we identified a significant network of brain regions that display higher functional connectivity in 15q13.3 mice than in WT (Figure 3.2.2). Interestingly, this network revealed a pattern of hyperconnectivity within the primary and secondary somatosensory cortices (Figure 3.2.2, blue circles) with different thalamic nuclei (Figure 3.2.2, yellow circles) including the habenula, the medio dorsal thalamus, and the hippocampus (Figure 3.2.2, orange circles). Simultaneously, there was increased connectivity within the amygdalar nuclei (Figure 3.2.2, green circles). Describing overall increased somatosensory, hippocampal, and amygdalar connectivity in 15q13.3 animals.

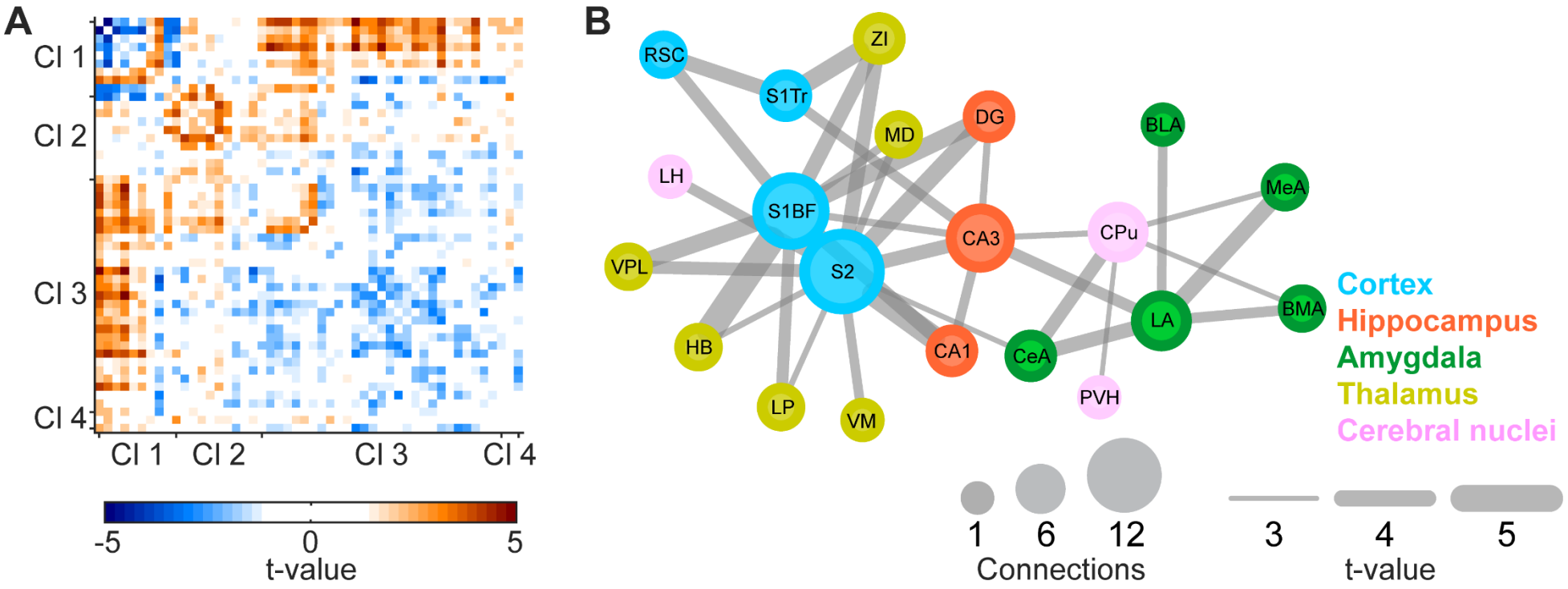

Figure 3.2.2 Identification of a large-scale hyper-connected network in 15q13.3 mice. (A) Scaled matrix of the interregional connections meeting t-value threshold (t-value ≥ 3). (B) Network showing the brain regions (circles) and connections (lines) that were significantly increased in 15q13.3 mice with respect to WT. Bilateral regions were grouped for clarity. Abbreviations are defined in Table 2.6.1.

3.2.3. Genotype prediction based on functional connectivity

Since we found that functional connectivity signature and trajectory was different in 15q13.3 mice, we reasoned that we could use these differences for genotype prediction at later time points. To test this hypothesis, we reduced the dimensionality of the entire dataset with a principal component analysis (PCA) and used the loadings of the first three components to train a linear support vector machine (SVM) learning model. We found that the first three principal components accounted for ~37% of the variance of the entire dataset and that the loading values of individual mice with the same genotype tended to cluster together (Figure 3.2.3 A, left panel). Consequently, the SVM model could predict the correct genotypes with 85% accuracy (Figure 3.2.3 A, right panel), which was not surprising given that the dataset also included values from p90 when the connectivity signatures were most different (Figure 3.2.1). Next, we asked whether it was possible to predict the genotypes at p90 by using the functional connectivity values from a distinct time point in development. When we trained the SVM using data from p35, we found that we could only predict the correct genotype with 52% accuracy (Figure 3.2.3 B, left panel). However, when we used functional connectivity data from p42 to train the SVM, the prediction accuracy of genotypes at p90 increased to 82% (Figure 3.2.3 B, right panel), which was very similar to the accuracy achieved when the entire dataset, including data from p90, was used (Figure 3.2.3 A, right panel). Together, these data suggest that there are already changes in functional connectivity at p42 that allow us to predict with high accuracy the genotype of both groups later in adulthood.

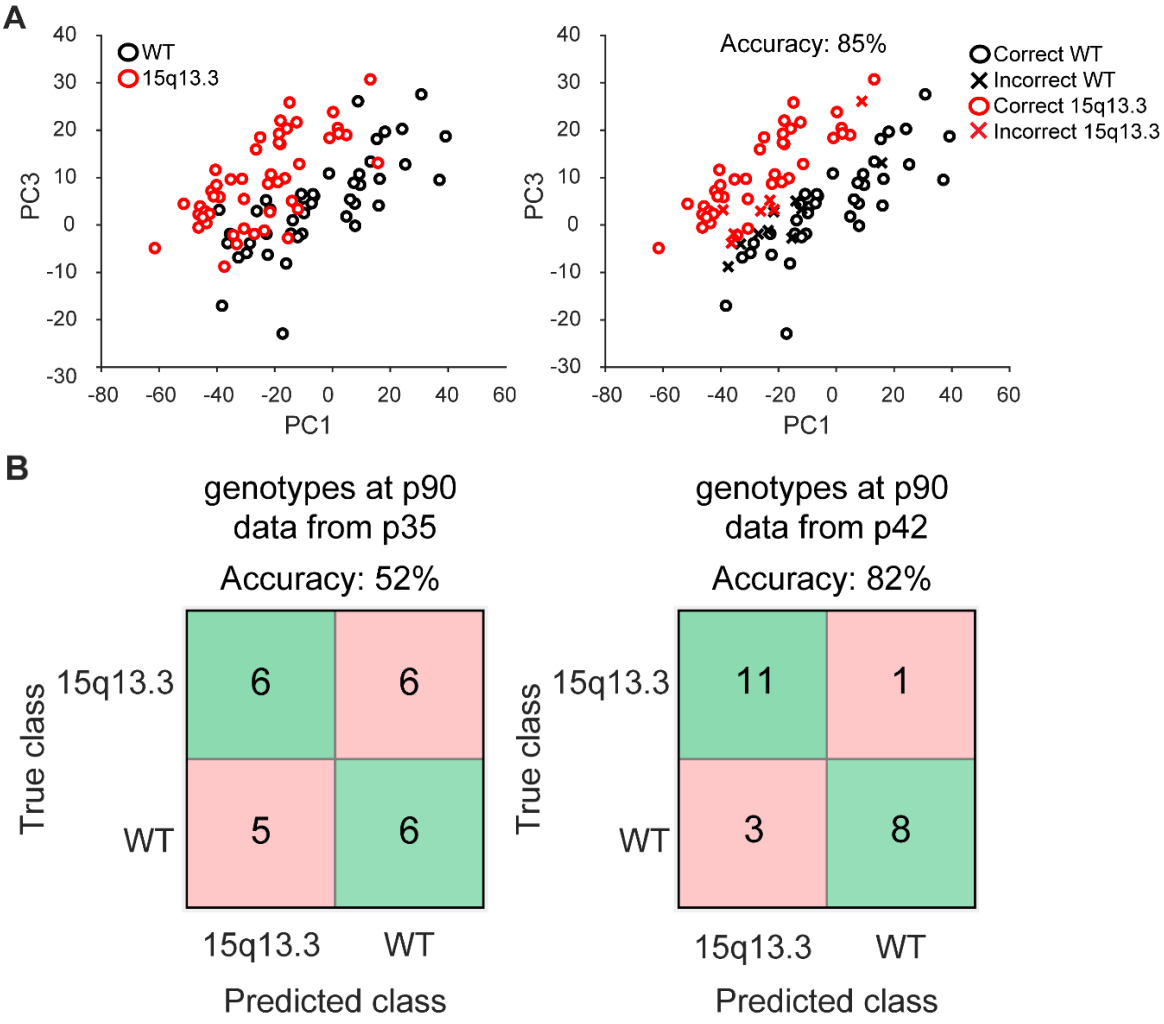

Figure 3.2.3 A machine learning algorithm accurately classifieds genotype based on functional connectivity. (A) Left, plots showing the loadings for PC1 and PC3 of each individual mouse across all imaging time points. Right, decoding accuracy of the SVM model using the entire dataset, where incorrect predictions are denoted with an x. (B) Decoding accuracy of SVM models trained using functional connectivity data from p35 (left) and p42 (right). Pink boxes denote incorrect classifications and green boxes display correct classifications. WT (n=11) and 15q13.3 (n=12).

3.3. Study III: The influence of activation or inhibition of the parvalbumin positive interneuron network in the ventral CA1 on brain-wide networks measured with functional ultrasound

3.3.1. CBV changes resulting from pharmacological modulation of PV+ interneurons in the vCA1

To investigate the role of vCA1 PV+ interneurons in the mesocorticolimbic pathway, we employed a chemogenetic approach to modulate PV+ interneurons with either an inhibitory DREADD (hM4Di), or an activating DREADD (hM3Dq), and compared the changes to a control expressing mCherry only. This approach was important to determine if subtle differences in circuitry would reflect an overall change in regional recruitment and functional network organization.

During imaging, animals were sedated with dexmedetomidine, and an intraperitoneal catheter was placed in the abdomen. After 10 minutes of baseline recording, 6 mg/kg CNO was injected over ~20 seconds and imaging continued for another 45 minutes. Power Doppler signal was extracted from each ROI and normalized to the 10-minute time baseline before CNO administration. Variable changes in CBV were measured after CNO administration (Figure 3.3.1 :1) throughout the ROIs and groups. Depression of PV+ interneuron activity in the vCA1 lead to decreased CBV in the PFC and cingulate cortex (Figure 3.3.1 :1A), with modest increases throughout the cortex. In contrast, vCA1 PV+ activation led to strong increases in CBV in the PL, Cg, and other posterior cortical regions (Figure 3.3.1 :1C). Of note, changes in CBV were also detected in the mCherry control group, although in general, were between the measurements of the 2 study groups.

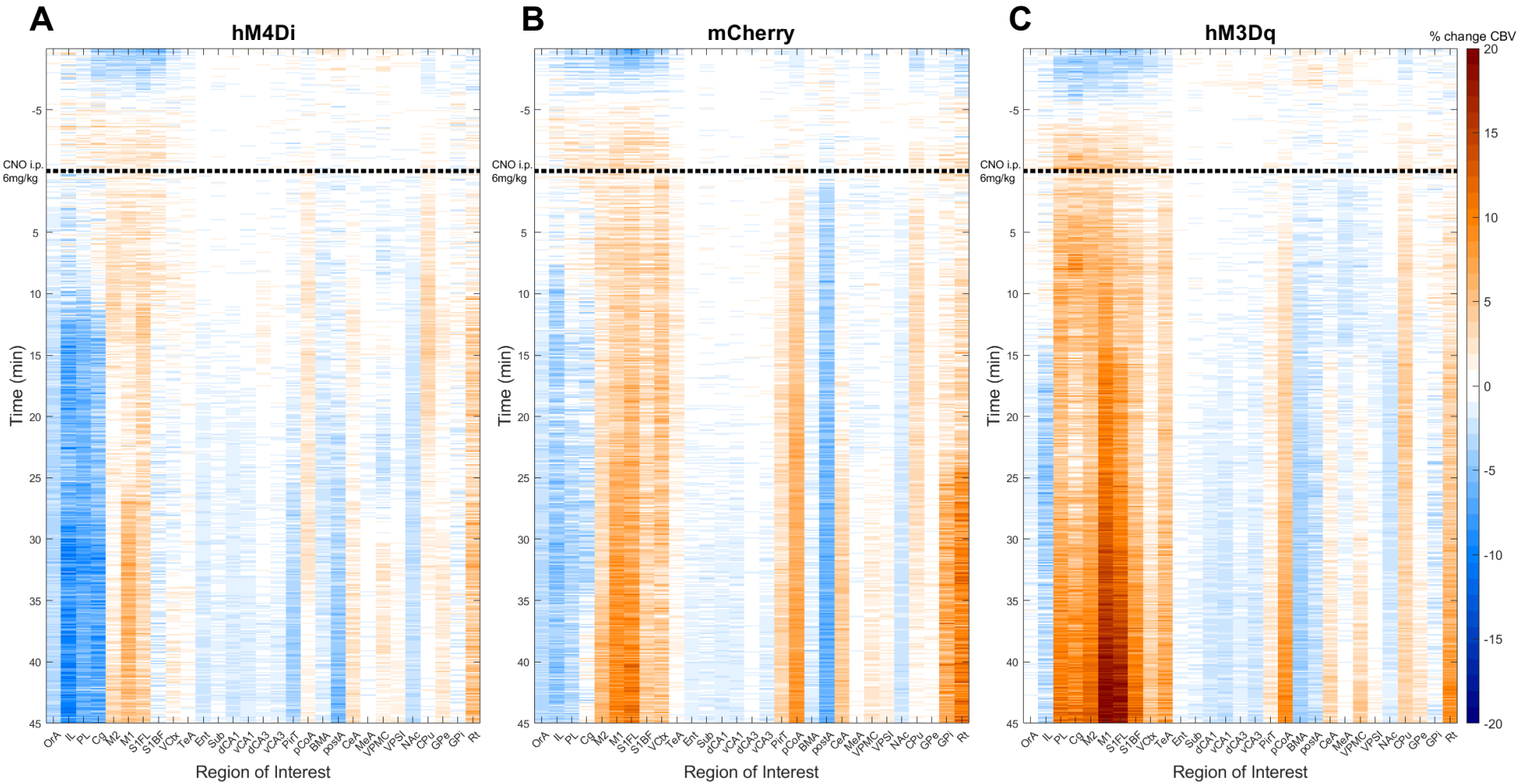

Figure 3.3.1 :1 Compilation of regional changes in CBV over time after DREADD activation in the vCA1. CBV changes both increased (warm colors) and decreased (cool colors) after CNO administration across ROIs and differed between (A) hM4Di, (B) mCherry, and (C) hM3Dq expressing mice. Data is presented as mean percent change from baseline measurements prior to CNO administration. Each small horizontal line represents a 400 ms data point, hM4Di n = 12, mCherry n =11, hM3Dq n = 11. Abbreviations defined in Table 2.6.1.

We were then interested in whether PV+ interneuron modulation would change CBV in the vCA1 itself. Interestingly, increasing PV+ activity in the hM3Dq group resulted in decreased CBV compared to the mCherry group (-2.0 ± 0.9% $p < 0.05$, -2.6 ± 1.1% $p < 0.05$, at 30 minutes and 45 minutes post CNO administration, respectively, Figure 3.3.1 :2A), suggesting that excitatory processes require more energy than tonic inhibition in this particular region. Surprisingly, PV+ inhibition did not have an opposing effect as CBV changes were nearly indistinguishable from the mCherry control (-1.3 ± 1.0% for hM4Di and -1.2 ± 1.1% for mCherry, -1.8 ± 1.5% for hM4Di and -1.7 ± 1.2%, for mCherry at 30 minutes and 45 minutes post CNO administration, respectively, Figure 3.3.1 :2A).

We also further investigated other regions associated with the mesocorticolimbic pathway, namely the NAc, Cg, and PL. We did not see any differences in the NAc in any of the groups (Figure 3.3.1 :2B). A very interesting pattern, however, emerged in the Cg and PL (Figure 3.3.1 :2C & D). After CNO induced PV+ interneuron activation in the vCA1, we detected increases in CBV in these anterior cortical regions. CBV in the hM3Dq group increased in the PL 5.2 ± 4.0% ($p < 0.05$) by 15 minutes, and 10.0 ± 6.8% ($p < 0.05$) at 45 minutes, compared to -5.8 ± 3.0% at 15 minutes, and a -6.9 ± 3.9% at 45 minutes in the hM4Di group, which was reduced compared to the mCherry group, but not significantly. The Cg followed a similar pattern; however, these changes did not pass significance testing. Overall, we did not find that reducing PV+ interneuron activity in the vCA1 resulted in significant differences in CBV throughout the brain when compared to the control group, although there was a trend of decreased CBV in the Cg and PL. However, increasing PV+ interneuron activity resulted in significantly decreased CBV within the vCA1, and in contrast, increased CBV in the Cg and PL anterior cortical regions.

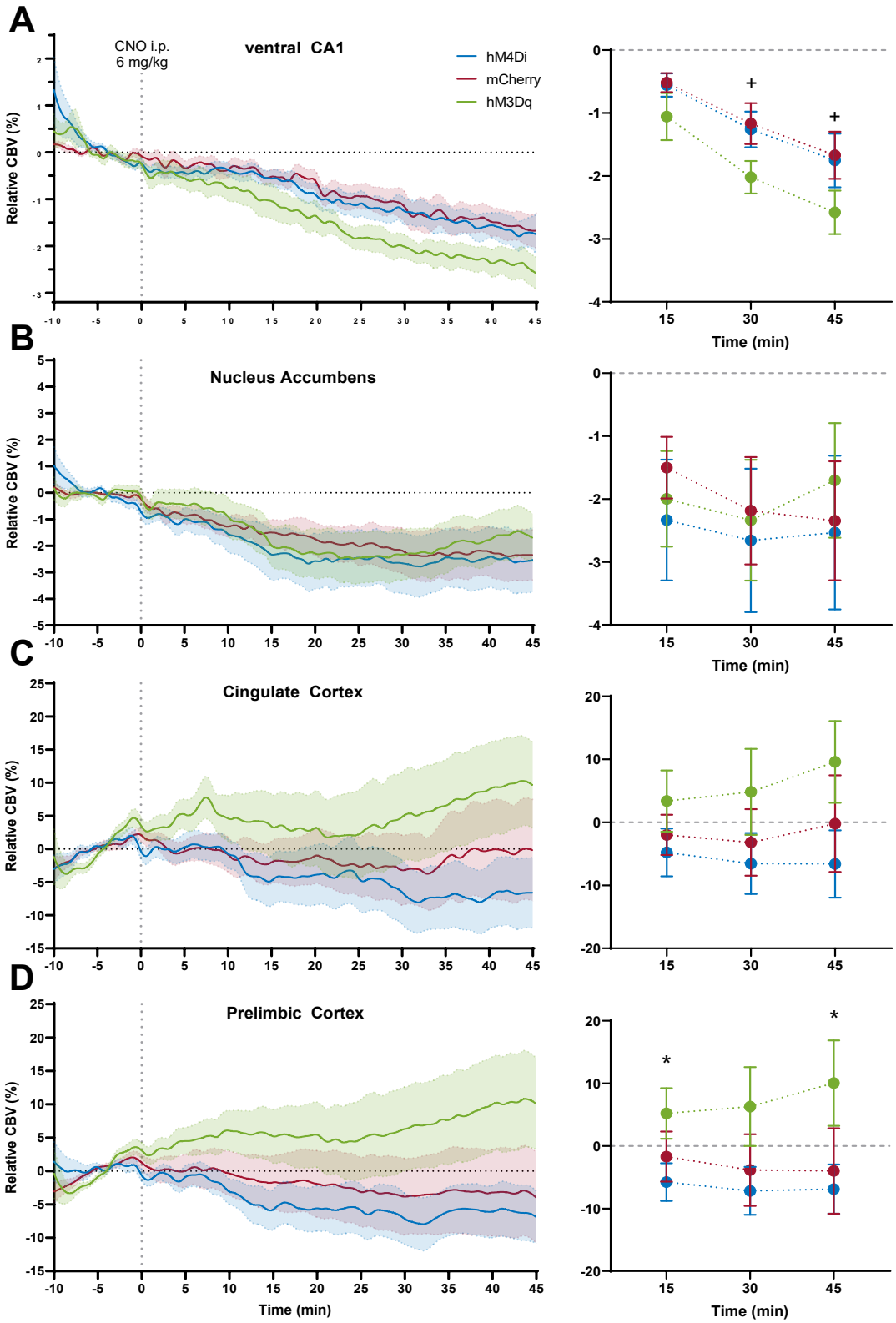

Figure 3.3.1 :2 CBV changes in mesocorticolimbic pathway associated target regions after vCA1 PV+ cell modulation. (A) PV+ cell activation with hM3Dq resulted in decreased CBV in the vCA1. (B) Neither vCA1 PV+ inhibition or activation changed CBV in the NAc. (C & D) Activation of PV+ interneurons in the vCA1 resulted in increased CBV in the Cg and PL while inhibition slightly reduced CBV. Data represented as mean ± SEM, 2-way ANOVA with Tukey's multiple comparisons, significant differences between mCherry and hM3Dq denoted with + ($p < 0.05$), and between hM3Dq and hM4Di with * ($p < 0.05$), hM4Di n = 12, mCherry n =11, hM3Dq n = 11.

3.3.2. Pharmacologically induced changes in connectivity resulting from modulation of PV+ interneurons in the vCA1

We were then interested in how these CBV changes would relate to changes in connectivity. We used Pearson's product moment correlation to generate measurements of connectivity between every ROI-ROI pair, similar to the method used in study I and study II. Since we were interested in the changes over time, we calculated connectivity matrices using 5 minutes of temporal data and slid the window in 1-minute increments across the time course. Windows that encompassed the period of injection were excluded to keep the distinction between pre and post CNO administration. We then normalized the correlation coefficients by creating a z-score using data from the windows prior to CNO administration as reference. To visualize this large amount of data for patterns, we linearized and compacted the matrices and displayed them as Δz over time (Figure 3.3.2 :1).

Prior to this study a technical fault developed in the fUS imaging device. Instability in the grounding of the machine and the power supply of the laboratory building produced large, unpredictable, step artifacts in the raw power Doppler signal during the imaging of some mice. We were able to manually scrub and correct these artifacts from the CBV data, however they left large gaps in the sliding windows of the connectivity data over several animals which therefore had to be excluded from analysis resulting in a final sample size of hM4Di n = 9, mCherry n = 8, hM3Dq n = 9.

After CNO administration, the hM4Di group displayed mostly decreased connectivity throughout a majority of ROIs (cool colors, Figure 3.3.2 :1A) and the hM3Dq group displayed more increases than decreases in connectivity (warm colors, Figure 3.3.2 :1C), while the control group displayed a rather even mix of increased and decreased connectivity values (Figure 3.3.2 :1B) compared to baseline functional connectivity. Furthermore, there appeared to be a swell of increases around 25-30 minutes after CNO administration in the hM4Dq group.

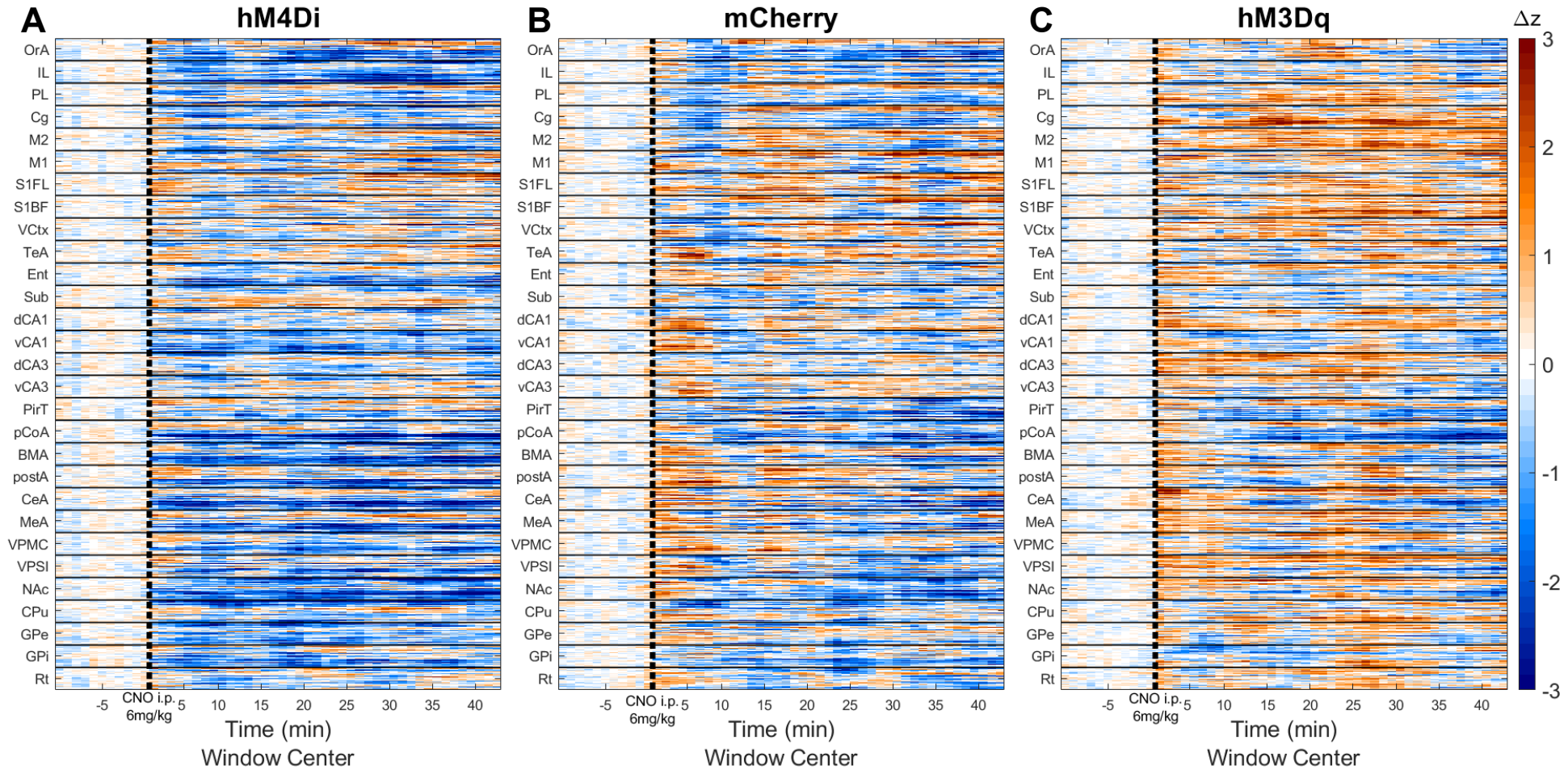

Figure 3.3.2 :1 Regional connectivity changes after PV+ activity modulation in the vCA1. Each ROI block (y-axis) represents the connectivity profile of the hub ROI with every other ROI in the same order as on the y-axis over time (x-axis). (A) vCA1 PV+ interneuron inhibition primarily resulted in reduced connectivity throughout the brain in most ROIs. (B) Control animals displayed a mix of increased and decreased connectivity from baseline while (C) activation of PV+ interneurons in the vCA1 resulted in mostly increases in connectivity. Each data point represents the mean connectivity score normalized to baseline, where a 5-minute sliding window was advanced by 1-minute increments through the time series, hM4Di n = 9, mCherry n =8, hM3Dq n = 9.

We then looked in more detail at the same mesocorticolimbic pathway associated regions as in the CBV analysis by expanding their hub connectivity profiles (Figure 3.3.2 :2). Although activation of PV+ interneurons in the vCA1 resulted in decreased CBV in the hM3Dq group compared to mCherry controls and the hM4Di group, the connectivity profile was very similar to the mCherry group. Substantial decreases in vCA1 connectivity were, however, evident in the hM4Di group, although none of these decreases passed significance testing at the time points measured (Figures 3.3.2 :2A & 3.3.2 :3A-C). In contrast, the NAc displayed a more prominent reduced connectivity profile (Figures 3.3.2 :2B). In the hM4Di group, there were substantial decreases in NAc connectivity with most of the other ROIs measured and connectivity with many regions were increased in the hM3Dq group compared to control. When we looked at the time course of Cg-NAc connectivity in more detail (Figure 3.3.2 :3D), we detected significant differences between the hM3Dq group and the mCherry and hM4Di groups. After 15 minutes, there was significantly more Cg-NAc connectivity in the hM3Dq group than the hM4Di compared to baseline connectivity (2.9 ± 1.9 vs -1.4 ± 0.9 Δz, $p<0.05$). After 30 minutes there was an even greater difference where Cg-NAc connectivity was significantly increased compared to both hM4Di (2.1 ± 1.6 vs -1.9 ± 1.3 Δz, $p<0.05$) and mCherry control (2.1 ± 1.6 vs -3.1 ± 1.8 Δz, $p<0.01$). While Cg-NAc connectivity in the hM4Di group was lower than mCherry for large epochs, there were no significant differences for the specific time points measured. There were many other specific connections that were altered between groups, but we chose to focus on interconnectivity between these select ROIs to highlight activity in the mesocorticolimbic pathway.

Overall, we found that vCA1 PV+ inhibition resulted in lower readouts of connectivity which were especially focused in the NAc, while increasing vCA1 PV+ activity reduced CBV in the vCA1, but increased connectivity throughout the brain.

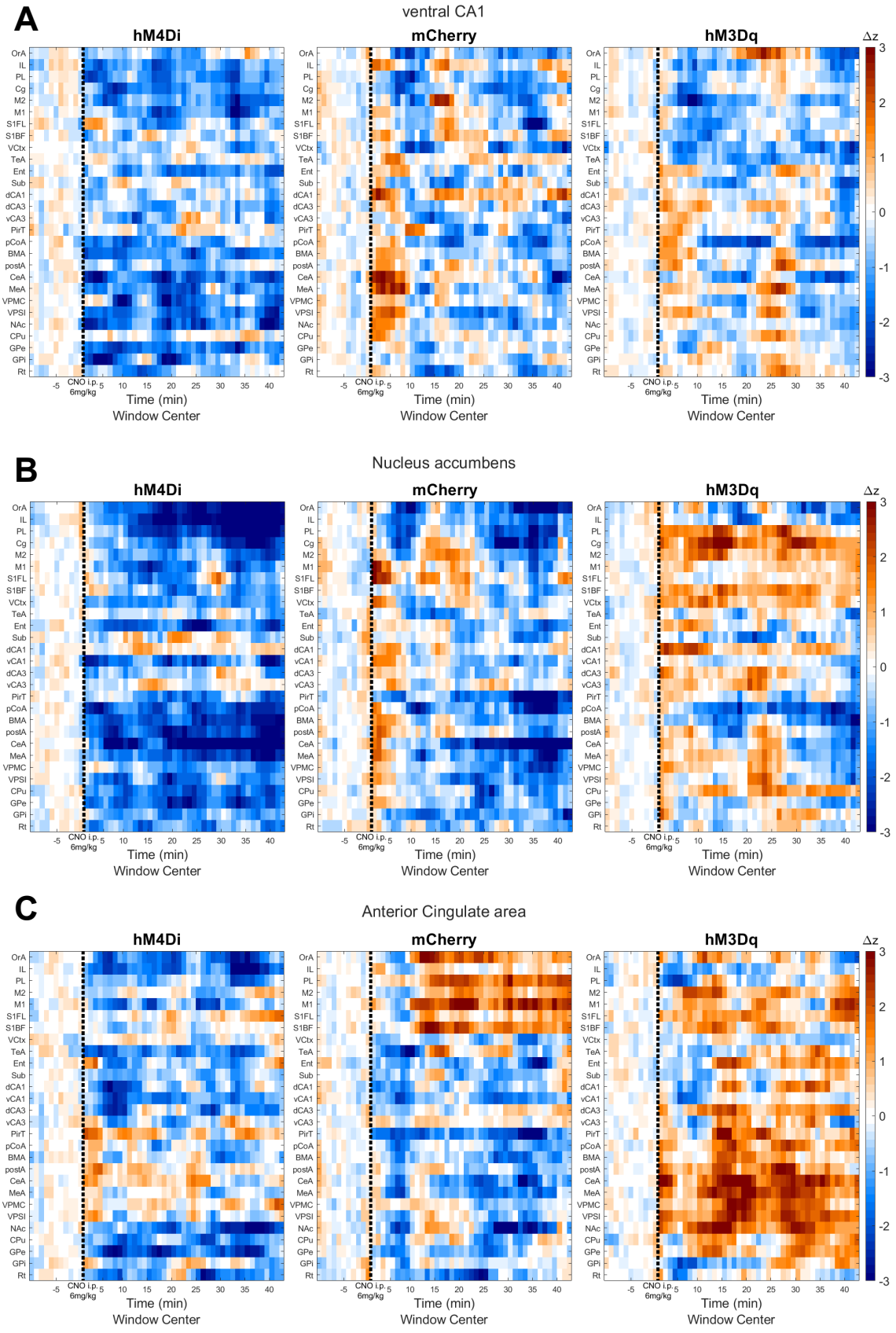

Figure 3.3.2 :2 (continued on next page)

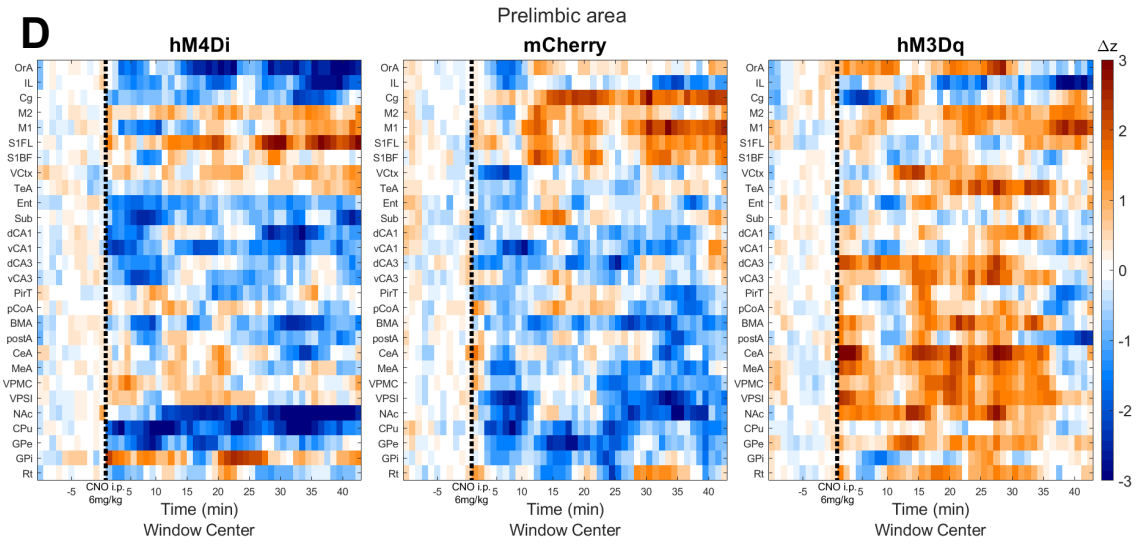

Figure 3.3.2 :2 Expansion of hub connectivity profiles for select mesocorticolimbic associated ROIs. (A) PV+ inhibition (left panel) appeared to slightly reduce global connectivity of the vCA1, whereas the profile of the hM3Dq group (right panel) was similar to control (center panel). (B) Global connectivity of the NAc was greatly reduced after CNO administration in the hM4Di group, whereas many areas displayed increased connectivity in the hM3Dq group compared to the mCherry control. (C & D) PV+ interneuron activation in the hM3Dq group resulted in increased global connectivity throughout the Cg and PL areas. Each data block represents mean connectivity, hM4Di n = 9, mCherry n = 8, hM3Dq n = 9.

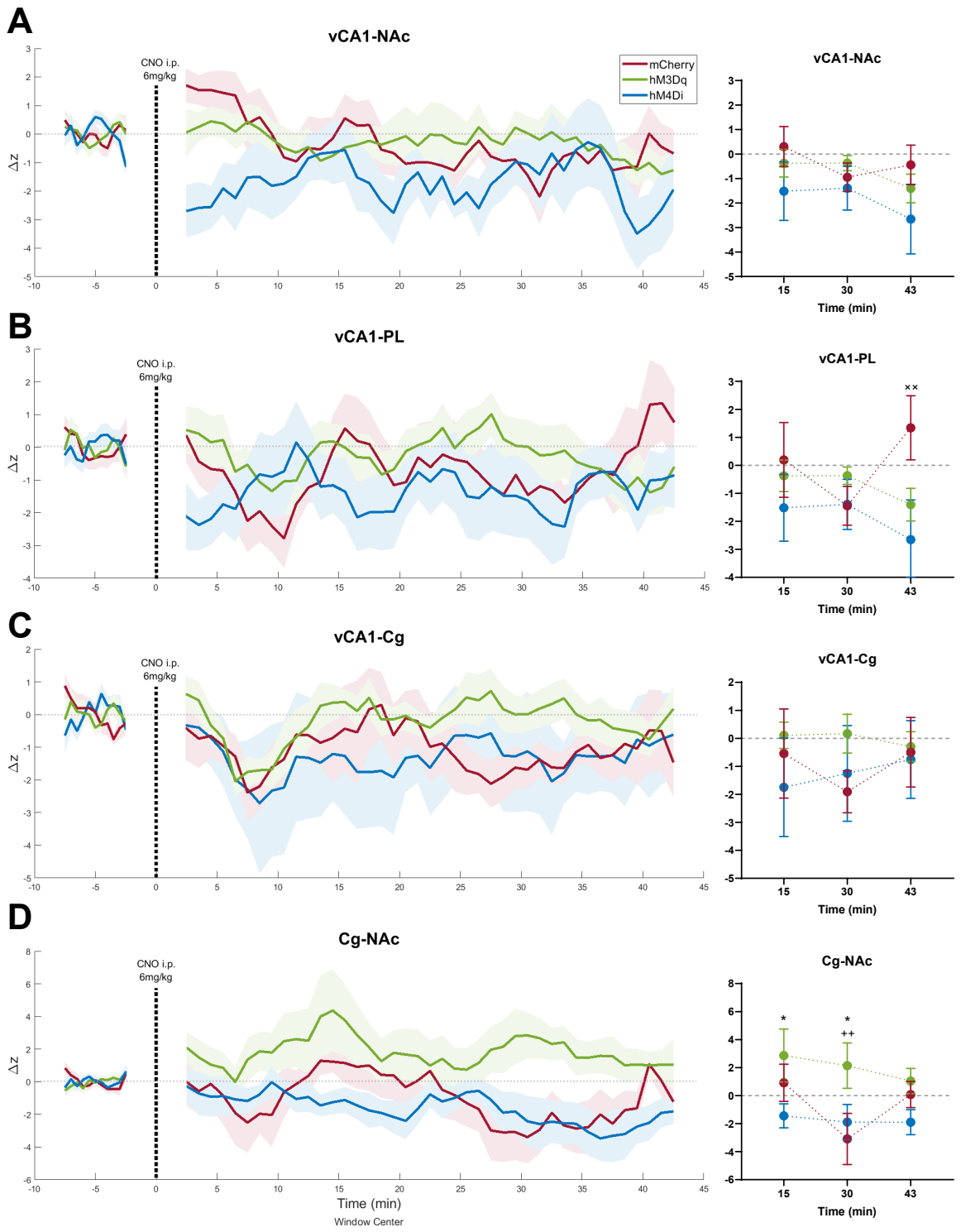

Figure 3.3.2 :3 Effect of PV+ interneuron modulation on specific connections associated with the mesocorticolimbic pathway. There was a trend of reduced connectivity in the hM3Di group, however there are no significant differences in functional connectivity throughout the time course after CNO administration in the connections between (A) the vCA1 and NAc, (B) the vCA1 and PL, and (C) the vCA1 and Cg. However, vCA1 PV+ interneuron activation in the hM4Dq group results in significant increases in connectivity between the NAc and Cg (D) 15 and 30 minutes after CNO administration. Mean ± SEM, 2-way ANOVA with Tukey's multiple comparisons, significant differences between mCherry and hM3Dq denoted with ++ ($p < 0.01$), and between hM3Dq and hM4Di with * ($p < 0.05$), hM4Di n = 9, mCherry n = 8, hM3Dq n = 9.

4. DISCUSSION

Psychiatric diseases remain some of the most studied, but least understood ailments in human health. The inherent heterology of etiology, pathophysiology, and symptom domains in both the broad spectrum of psychiatric disorders and in specific diseases, make them difficult to approach and interpret experimentally. The significant increase in mental illness due to the recent COVID-19 pandemic has further emphasized the importance of mental health and of understanding the biological processes underlying both disease and therapy (Collaborators et al., 2021).

In the clinical setting, the standard method of diagnosing mental disorders is by classifying them based on checklists of observable behavioral symptoms. One of the difficulties with this approach is that virtually all psychiatric disorders have overlapping symptoms and pathology which make it difficult not only to determine specialized care, but in some cases to also measure treatment efficacy (Newson et al., 2021). Crucially, in order to determine the standard of care, symptoms must be present, thwarting the ability to intervene before complications emerge and disrupt the lives of patients.

A neuroimaging approach enables investigation into the physiological elements and neural basis of psychopathology. One of the advantages of using an imaging modality with high spatial and temporal resolution such as functional ultrasound (fUS), is the ability to examine not only sub anatomical regions, but to also investigate neural networks on a larger, more global scale. Multidimensional data, such as that generated through the fUS technique, enable examination of the attributes of psychiatric disease in preclinical animal models. In addition, the non-invasive nature of the technique further allows for longitudinal investigation into biomarker identification and increases the likelihood of predictive validity, features that are essential in drug discovery.

In the present work, we used animal models to recapitulate some of the common features of psychiatric disease, in particular, those observed in schizophrenia. Since schizophrenia patients frequently display disruptions not only in memory (Oertel et al., 2019; Racsmány et al., 2008), but also in the perception of fear (Das et al., 2007; Russell et al., 2007), we first used a behavioral model to conduct an associative fear memory trace (**study I**). We used this proof-of-concept study to verify the capability and robustness of fUS imaging to capture a well-known neural network and any potential subtle changes in that network over time. As

schizophrenic symptoms are well known to present in late adolescence to early adulthood in humans (Angermeyer and Kühnz, 1988; Gogtay et al., 2011), we next investigated the developmental trajectory and predictive validity of a transgenic animal model with a heterogenous phenotype associated with schizophrenia (**study II**). Finally, in a pharmacological model, we investigated whether modulating a specific cell type in a distinct neuroanatomical region could change connectivity in the mesocorticolimbic pathway, a neural network that is highly implicated in schizophrenia (**study III**) (Grace, 2010; Howes and Nour, 2016; Kätzel et al., 2020; Lodge and Grace, 2006; Weinstein et al., 2017).

Each of these studies will be discussed individually in the following sections.

4.1. Study I: Functional ultrasound imaging of recent and remote memory recall in the associative fear neural network in mice

Learning and memory are crucial for an organism to anticipate and adapt to challenges and increase the likelihood of rewards in order to survive and thrive in dynamic environments. While very early researchers theorized that memory was stored in specific neuroanatomical regions (i.e., the hippocampus), that idea has evolved as evidence emerged that memories are encoded, consolidated and stored in distributed networks. The term used to describe this physical ensemble of brain regions involved in a memory is an engram (Josselyn and Tonegawa, 2020; Tonegawa et al., 2018). Many psychiatric disorders display impairments in learning and memory (Pittenger, 2013). In order to effectively develop therapies and guide preclinical and clinical research, it is essential to characterize the underlying circuitry of these processes.

In this study, we aimed to successfully train mice to associate a sound with a foot shock in order to create a cued associative fear memory. We then tested recent and remote memory retrieval using both behavioral expression and neuroimaging. We found that a single CS-US pairing was accompanied by robust freezing behavior and a specific pattern of neural activation (the neural signature of a memory trace), and that this memory trace was also detectable after 31 days. The memory trace involved regions that have been previously linked with the associative fear neural network, including the LA, BLA, CeA, PL, and HC (Bergstrom, 2016; Clark and Squire, 1998; Janak and Tye, 2015; LeDoux, 2000), thus validating our experimental approach. Interestingly, during the remote recall imaging session conducted 31 days after FC, we also detected increased connectivity with regions involved in extinction learning, namely the IL and BMA (Adhikari et al., 2015; Bloodgood et al., 2018; Song et al., 2010), suggesting that fUS can detect not only acute changes in functional connectivity, but also changes pertaining to prolonged processes. Of even more interest, there was a reduction in cue-evoked connectivity of the CeA and TeA in the remote memory retrieval session, suggesting that the neural processing of the auditory cue was also altered during the remote recall session. In compliment, we also found that the degree of behavioral fear expression correlated with connectivity readouts where the PL, TeA, HC, and CeA, regions associated with memory consolidation and fear expression, were positively

correlated with freezing behavior. Moreover, regions associated with fear extinction leaning, namely the IL, A1, and BMA, were negatively associated with freezing behavior (Figure 3.1.4). Further validating the sensitivity of our experimental approach, the UT control group did not show any consistent signatures of fear network connectivity, nor did they express any substantial fear related behavior. Taken together, our data showed for the first time that a memory trace can be detected in a sedated mouse during recent and remote episodic memory retrieval using fUS imaging.

4.1.1. A single CS-US pairing generated robust and specific freezing behavior

A preliminary aim of this study was to ensure that the fear memory was specific to the cue and not associated with the context of the fear conditioning box. In order to achieve this, we performed extensive handling of the mice and familiarization with the FC chamber prior to training. Furthermore, we performed only a single CS-US pairing in contrast to protocols using 3 to 5 pairings that are normally used in contextual and generalized fear experiments (Kim and Cho, 2020; Pan et al., 2020). We then tested this effort by re-exposing the mice to the same FC context without any cue the day after training and we found that the mice, indeed, did not show significant freezing behavior. Furthermore, there was little freezing before and after tone presentation in the novel context (Figure 3.1.1), further supporting that a specific cued associative fear memory had been trained. It was important to establish that the mice had not developed a contextual fear association as this phenomenon can be associated with disparate regions of the brain to cued fear (Kim and Fanselow, 1992; Phillips and LeDoux, 1992).

An important aspect in the study of fear associated memory in the context of therapeutic development, is the ability to diminish the fear response. To accomplish this, the animal or subject is repeatedly exposed to the fear associated stimuli in order to signal that it is no longer coupled to an aversive experience. Rather than this resulting from a reduction in the strength of the fear associated engram, extinction learning is an active process involving the executive function of the PFC (Bloodgood et al., 2018; Maren, 2011). In this study, we did not execute a protocol designed specifically to initiate fear extinction, however, by the second behavioral test the mice had been exposed to the tone on at least 3 occasions, including the 3 presentation blocks during each imaging session. Although the reduction in

freezing behavior between the recent and remote memory retrieval sessions was not statistically significant, there was a clear trend (Figure 3.1.1). In fact, signs of extinction of a cued fear memory can be detected after exposure to as few as 2 cue blocks, though the differences in behavior might not yet be statistically significant (Adhikari et al., 2015; Bloodgood et al., 2018; Wen et al., 2021). In addition to describing the fear associated memory trace, we discuss evidence of the neural signature of extinction learning in the sections below.

4.1.2. Intra-amygdalar connectivity was prominent during both recent and remote memory retrieval

While many regions showed increases in functional connectivity in response to the tone, the changes within the amygdala were the most pronounced. Since the LA is considered the major input nucleus of the amygdala, especially during the processing of fear-related information (Erlich et al., 2012), and is critically involved in fear memory acquisition (Phillips and LeDoux, 1992), it was not surprising that it emerged as a major hub during both fear memory retrieval sessions. This was evidenced by increased connectivity between the LA and BLA, CeA, A1, HC, and PL (Figures 3.1.2 & 3.1.3). Previous studies have substantiated the role of the LA in the integration of auditory and somatosensory inputs from throughout the brain and the LA has also been shown to display significant signatures of gene expression indicative of long-term potentiation, such as CREB (Ploski et al., 2010; Schafe, 2005). Although many theorized that the lateral amygdala was the seat of memory storage and therefore the only region required for memory encoding, a more distributed network is required for a highly robust memory response (Dejean et al., 2015; Maren, 2011; Paré et al., 2004). The entire basolateral complex, including the LA, BLA, and BMA sub anatomical regions, is highly implicated in emotion-related processes, where the major output nuclei of the amygdala is the CeA (Tovote et al., 2015; Whittle et al., 2021). Indeed, we found significant increases in cue-evoked intra-connectivity in the amygdala between these regions in both recent and remote fear memory retrieval in FC mice. While the UT group did show some statistically significant cue-evoked decreases in connectivity between the LA-BLA in the recent retrieval session, and the LA-BMA during the remote retrieval session, these changes were not consistent with a fear associated memory trace (Figures 3.1.2 & 3.1.3).

One of the most pivotal findings of study I, was that CeA showed a global decrease in connectivity to the CS presentation in remote retrieval when compared to recent retrieval. While there was still activation of the CeA during remote recall, connectivity was reduced with all measured ROIs and significantly reduced with the BMA (Figure 3.1.2), reflected by the node weight in the statistically generated functional memory network (Figure 3.1.3). This finding is even more telling since CeA connectivity within the PL, TeA, and HC cluster was positively correlated with freezing behavior, suggesting that the reduced CeA connectivity during the remote memory retrieval session might have been a major factor in the overall trend of reduced freezing behavior in the remote behavioral expression test (Figures 3.1.1 & 3.1.4). Indeed, reduced CeA activity has been associated with extinction behavior (Duvarci et al., 2011; Whittle et al., 2021). However, whether this reduced CeA activity is indicative of a reduction in strength of the memory, or rather of the emergence of extinction learning, cannot be deduced from this finding alone.

4.1.3. The hippocampus is active in cued memory retrieval

The contribution of the hippocampus in cued fear memory is somewhat controversial. There is significant evidence of hippocampal involvement in the formation and retrieval of contextual fear, however, many studies have found that ablation of the hippocampus both before and after FC does not abolish cued fear responses as it does in contextual fear (Kim and Fanselow, 1992; Phillips and LeDoux, 1992). In the current study, however, increased connectivity in response to the cue was evident during both recent and remote fear memory retrieval in the hippocampus (Figures 3.1.2 & 3.1.3). A cue-evoked increase in the HC-LA connection was especially evident during the remote memory retrieval session, where the increase in connectivity was significantly higher than it was during recent retrieval. It is not to say that the hippocampus does not play a role in cued fear memory, indeed increased theta wave synchronicity and auditory evoked potentials can be detected between the HC and LA after successful FC (J. Courtin et al., 2014; Seidenbecher et al., 2003; Stujenske et al., 2014; Tang et al., 2003). It is difficult to distinguish, however, if the HC is playing a role in the retrieval or the reactivation of the cued memory, or alternatively if it is involved in a more active process such as consolidation and reconsolidation. In all likelihood, it is involved in both to some degree. Since global connectivity of the HC positively correlated with freezing behavior, it is more likely that it promotes expression of the associative fear memory rather than supporting extinction learning, however, the influence of the HC in reconsolidation in

the current study cannot be discounted. When examining previous studies, especially some of the seminal studies of FC of the past 2 decades, it is important to note that many utilized chronic methods of inhibiting of the HC. More recent studies have shown that acute silencing of the HC using optogenetics significantly reduces freezing behavior, while again chronic inhibition does not (Goshen et al., 2011; Opalka and Wang, 2020). Together, these published reports and our own findings support the suggestion that while the HC may not be absolutely required for cued fear memory retrieval, when intact it could be involved in reconsolidation and/or recontextualization. In fact, the multiple trace theory hypothesizes that interaction between the PFC and the HC might be playing a role in recontextualization in parallel to classic memory retrieval.

4.1.4. Activity in auditory processing regions during cue-evoked memory

Activity in classical auditory processing A1 and TeA neuroanatomical regions was also significant in memory retrieval. An increase in A1-TeA connectivity during recent memory retrieval was accompanied by significant cue-evoked increases in connectivity of the TeA with the amygdala, in particular. In contrast, during remote memory retrieval, this A1-TeA functional connection was significantly reduced. TeA-amygdalar functional connectivity was still elevated during remote recall but was noticeably reduced, whereas the A1 showed significant increases in cue-evoked connectivity with the LA and BMA during remote memory retrieval compared to what was detected during recent retrieval (Figures 3.1.2 & 3.1.3). This TeA-A1 circuit is critical in auditory processes that are crucial for memory such as signal recognition, discrimination and encoding (Dalmay et al., 2019; Tasaka et al., 2020). It is interesting that during remote memory retrieval, the A1 no longer showed a strong connection with the TeA, but rather showed increased connectivity with the amygdala. This could be interpreted that during remote memory retrieval, the TeA is no longer required to extensively process the incoming auditory signal with the A1 that is rather relayed directly to the amygdala. It is important to note that connectivity between the TeA and amygdala was still elevated during remote recall, a process which is strongly supported in literature (Dalmay et al., 2019; Romanski and LeDoux, 1993), only inter-regional A1-TeA connectivity was reduced. Furthermore, while the TeA was positively correlated with behavioral fear expression, the A1 was negatively associated (Figure 3.1.4), suggesting that the A1 could potentially be involved in extinction learning during remote recall.

4.1.5. Refinement of PFC connectivity during remote fear memory recall

Both the PL and IL showed variable, significant changes in cue-evoked functional connectivity, especially during remote recall. This is in agreement with multiple previous studies which show that the PL and IL regions of the PFC play contrasting roles in associative fear memory (Giustino and Maren, 2015; Sotres-Bayon and Quirk, 2010). Initially, during recent retrieval, significant widespread increases in connectivity between the PL-LA, PL-BMA and PL-CeA were detected. During remote memory retrieval, however, PL connectivity with the more ventricular BMA and CeA nuclei was reduced, while PL-LA connectivity remained significantly elevated. Interestingly, the connection between the PL-HC was considerably changed between imaging sessions where connectivity was drastically increased during remote memory retrieval. It has been proposed that the PL undergoes refinement during the maturation of a memory, where it is shifting from harmonizing the engram, to a more directive role (Feng et al., 2014).

In contrast, the IL is almost exclusively associated with extinction learning (Santini et al., 2008; Senn et al., 2014; Vidal-Gonzalez et al., 2006). We detected increased IL connectivity, especially to the BLA, but also between the PL-IL and PL-A1 during the remote recall session but not during recent memory retrieval. In many previously published studies, increased activity between the IL-BLA has not only been detected during extinction learning, but ablation of this connection inhibits extinction learning and retrieval (Bloodgood et al., 2018; Julien Courtin et al., 2014; Likhtik et al., 2014; Senn et al., 2014). Moreover, in the current study, global IL connectivity negatively correlated with expressed fear behavior (Figure 3.1.4), suggesting that the IL promotes extinction learning to the degree of which our protocol supports extinction, e.g., the multiple exposures to the auditory cue during the recent memory retrieval tests. These results provide key evidence for the argument that some of the changes detected during remote memory retrieval were signs of extinction learning, rather than a reduction in the strength of the fear associated memory.

4.1.6. Shock intensity, frequency, and robustness of memory

We used a relatively mild FC protocol to induce the fear associated memory in this study. While a 1 mA shock is actually considered to be high intensity, the single CS-US pairing is considered to be of low intensity but has been shown to be effective in maintaining freezing

behavior for several weeks (Lux et al., 2016). We too, were still able to detect freezing behavior after 31 days that was specific to the cue. It remains to be determined, however, if stronger behavioral expression is indicative of a stronger memory, or rather reflects increased sensitivity to sensory input administered in close succession to the aversive stimulus in the current study, in light of the high emotional component of the shock, a phenomenon known as fear generalization. We suggest, however, that the strong, positive correlations of cue-evoked functional connectivity with behavior are indicative of a strong memory, especially since the slope of this correlation was greater during remote memory retrieval (Figure 3.1.4). We must also consider the single presentation of the CS-US pairing for memory formation. We used a single, intense shock, rather than multiple mild shocks (i.e., three presentations of 0.2-0.6 mA shocks) which are also frequently used in FC (Lesuis et al., 2018; Scarlata et al., 2019). It is possible that a memory trace involving other neuroanatomical regions or signatures of generalized fear could be induced by increasing the number of CS-US pairings, aspects that are of value in translational research.

4.1.7. Major conclusions of study I

We used a preclinical, behavioral model of cued associative fear to examine an episodic memory trace over time. We showed that we could utilize the fUS imaging technique along with behavioral readouts to detect neural networks involved in emotional processing and memory retrieval. Our approach was validated by the detectable increases in amygdalar functional connectivity, a well-established feature of associative fear memory. A more controversial aspect of cued memory, we also detected more increases in hippocampal cue-evoked functional connectivity during remote memory retrieval than in recent recall. We do not suspect that this was attributable to the contextual fear network, since the mice did not display this behavior during fear expression experiments and there is substantial evidence in literature that the HC plays an active role in reconsolidation and recontextualization during memory retrieval. Connectivity increases in regions highly involved in auditory processing were also evident but were interestingly segregated during remote memory recall. Finally, we found contrasting correlations of the proximal but distinct regions of the PFC especially during remote memory, where the refinement of connections may indicate a more directive role in memory recall as well as the introduction of extinction learning. Thus, fUS can be utilized to measure evoked network connectivity and monitor changes in the contributions of distinct anatomical regions over time.

4.2. Study II: Deviations in network development in the 15q13.3 mouse model: a functional ultrasound study

The ability to detect and measure functional biomarkers in developmental models offers great promise to guide early intervention in psychiatric diseases such as schizophrenia. Pinpointing specific changes in the transition from risk to the presentation of psychosis will enable strategic therapeutic targeting that could drastically improve patient quality of life and prevent the substantial health, social, and economic burdens associated with mental illness.

To the best of our knowledge, this was the first study to monitor functional connectivity through development with fUS imaging and to subsequently use this data for graph theory analysis and prediction modeling. Our network analysis revealed divergent trajectories for 15q13.3 mice and WT littermate controls where global connectivity was reduced for both genotypes with age, but to a lesser extent for 15q mice. We were then able to isolate the distinct differences between genotypes to identify a large-scale network where 15q13.3 mice displayed global cortical hyperconnectivity and elevated intra-connectivity within the hippocampus and amygdala, in particular. In order to determine the stage of development where the connectivity trajectories bifurcated, we used machine learning to predict genotype classification. We found that the connectivity profile from p42, but not p35, predicted the genotype of individual mice at p90 with the most accuracy. All together, these results suggest a crucial period of network maturation from early to late pubescence that is pivotal in the transition of network connectivity into adulthood.

4.2.1. Delays and deviations in connectivity patterns in 15q13.3 mice through development

When we analyzed the patterns of functional connectivity, we found that in WT mice there was an incremental pattern of decreasing functional connectivity through development (Figure 3.2.1). While there is less data from animal models regarding this phenomenon, these results are in line with longitudinal and cross-sectional studies in humans that show decreases in network functional connectivity from adolescence to adulthood, especially in within network connectivity (Fair et al., 2009; Jiang et al., 2018; Jolles et al., 2011; Marek et al., 2015). These studies found that this was mostly due to decreased segregation and

increased integration between networks thought to come about due to synaptic pruning, increased myelination, and an increase in inhibitory signaling as depicted in figure 1.1 (Fair et al., 2007; Supekar et al., 2009). As the brain matures and increases in cognitive functioning, it is necessary to refine network connectivity for faster and more efficient processing. It has been proposed that during development, resting state networks are continually interrogating connections to find the most efficient configuration for a particular function or task. As these connections are reinforced, either through experience or spontaneous waves of synchrony, redundant connections are pruned leading to an overall refined network that presents with decreased functional connectivity (Deco et al., 2011; Fair et al., 2007), comparable to the trajectory detected in WT mice in this study. It is important to note, however, that the changes in functional connectivity have been presented as differences from WT connectivity on p35. That is, there are still strong functional connections between many of these regions, they are simply reduced in comparison to this time point.

Connectivity in 15q13.3 mice, however, displayed a significantly different trajectory of functional connectivity through development. The overall differences in connectivity showed very few changes from p35 to p42. However, the connectivity patterns were noticeably different at p42 in 15q13.3 mice compared to WT. At p60 the differences between genotypes were even more perceptible. There was an overall reduction of functional connectivity in the WT mice and here the 15q13.3 mice showed higher magnitudes of change. Hyperconnectivity was evident in global cortical, intra-amygdalar, and intra hippocampal ROIs. At the later adult stage of p90, WT mice showed significant reductions in connectivity, whereas the 15q13.3 mice showed few differences from the young adult p60 time point. A significantly increased functional connectivity profile was also reported in adult 15q13.3 mice in an extensive article from N. Gass et al, (2016). Furthermore, a reversal of this hyperconnectivity was accomplished through administration of a positive allosteric modulator of the acetylcholine alpha7 receptor, one of the genes in the 15q13.3 locus. The same group later reported increased brain volume (Reinwald et al., 2020), which could be related to reduced pruning compared to WT and reflect the hyperconnectivity signature that we have detected in this study. The *OTUD7A* gene has also been identified as a key player in the pathogenesis of the 15q13.3 genotype, where reduced expression of this deubiquitinating enzyme correlated with dendritic spine morphology and outgrowth deficits (Uddin et al., 2018). Interestingly, *OTUD7A* expression peaks around p14 in mice (Uddin et

al., 2018). The reduced levels of acetylcholine transmission and abnormal dendritic spine stability generated from deficiencies in these two genes could be key drivers of the hyperconnectivity profile detected in the 15q13.3 group. It could be suggested that a combination of abnormal gene expression at specific time points in development and the subsequent inappropriate neuronal responses to external stimuli coalesce to create the developmental abnormalities we detected in the 15q13.3 mice.

4.2.2. The hyperconnectivity network of 15q13.3 mice

A hyperconnected network was revealed using network-based statistics on the entire data set (Figure 3.2.2). We found hyperconnectivity throughout the primary and secondary somatosensory cortices along with thalamic nuclei and subdivisions of the hippocampus. Thalamocortical hyperconnectivity is frequently reported in patients with first-episode psychosis as well as those with high risk and first-degree relatives (Cao et al., 2018; Klingner et al., 2014; Walther et al., 2017). This aberrant connectivity can have several implications in patients. Firstly, both hypo and hyperkinesia are frequently reported in schizophrenia affected individuals (Lund et al., 1991; Peralta et al., 2010). These features have been associated with differences in myelination and cortical thickness (Bai et al., 2009; Walther et al., 2011), phenomena that are congruent with hyperconnectivity. Secondly, abnormalities in the thalamic relay of sensory information can have implications for the interpretation of external information. Indeed, thalamocortical connectivity has been found to be inversely related to processing speed and attention (Chen et al., 2019) which could be related to abnormal filtering and transmission of sensory information.

We also detected a hyperconnected network within the sub anatomical regions of the amygdala. This feature, in particular, has been linked to some of the positive symptoms of schizophrenia, such as paranoia. Increased connectivity of the amygdala with the visual cortices, for example, is prevalent in schizophrenia patients that experience visual hallucinations (Ford et al., 2015). Patients with paranoid ideation have also shown increased connectivity between the amygdala and prefrontal cortex (Fan et al., 2021), a distinguishing trait of schizophrenia and potential diagnostic marker.

Hippocampal hyperactivity is a prominent feature of many psychiatric diseases and especially of schizophrenia. Interestingly, hippocampal connectivity has been correlated to both positive and negative symptoms (Duan et al., 2015; Schobel et al., 2009; Uscătescu et

al., 2021). Hallucinations themselves are thought to be in part attributed to the inappropriate recall of memories. Increased resting state connectivity between the hippocampus and somatosensory cortices, even in the absence of a task, can correlate with the severity of hallucination in patients with chronic hallucinations (Sommer et al., 2012). Furthermore, patients with paranoia show increased resting state connectivity between the hippocampus and amygdala, another prominent feature in our study (Walther et al., 2021). These characteristics all hold the potential for biomarkers for schizophrenia diagnosis as well as therapeutic efficacy evaluation.

4.2.3. Genotype prediction from developmental network signatures

Finally, we used a PCA and machine learning to see if we could accurately predict genotypes using functional connectivity measures from different points in development. We found that the connectivity profile from p35 could only predict the genotype at p90 with 52% accuracy but that data from p42 increased accuracy to 82% (Figure 3.2.3). The ability to predict the conversion from risk to psychosis is of great interest in the treatment and development of therapeutics for schizophrenia. Many of the features detected in this study have been used for that purpose. For example, thalamocortical and amygdalar hyperconnectivity is more prevalent in converters than non-converters (Gee et al., 2012; Ramsay, 2019). Furthermore, the degree of connectivity can be used to predict the time to conversion (Cao et al., 2018). A similar result has been found in the hippocampus, where CA1 hyperactivity could be used to time hippocampal atrophy (Schobel et al., 2013), a feature commonly associated with the conversion to psychosis.

Connectivity profiles can also predict the severity of symptoms (Gheiratmand et al., 2017; Kottaram et al., 2020; Uscătescu et al., 2021), suggesting a direct link between functional connectivity and phenotype. Indeed, measures of connectivity have been shown to most accurately predict symptom severity during follow up after treatment (Collin et al., 2020). Identification of individuals that are at a high clinical risk for conversion to psychosis in addition to predicting which of these patients will convert, and when that change might occur, could help to thwart illness and improve outcomes. In fact, only a third of subjects deemed clinical high risk eventually receive a formal diagnosis of psychosis (Ellis et al.,

2020). Our results show that these same analyses can be applied to a preclinical model, providing a translational tool that can further enhance drug development.

4.2.4. Major Conclusions of study II

We showed that the 15q13.3 mouse model can be effectively used to investigate alterations in the trajectory of functional connectivity through development. We found a network of hyperconnectivity that reflects clinical measurements in schizophrenic patients. Finally, we showed that the connectivity profile at early adolescence best predicts the network signature during adulthood. Together, these results show promise in improving translation in drug development for psychiatric diseases.

4.3. Study III: The influence of activation or inhibition of the parvalbumin positive interneuron network in the ventral CA1 on brain-wide networks measured with functional ultrasound

Hyperactive dopaminergic transmission is the dominant theory of the etiology of schizophrenia. The ventral hippocampus, in particular, has been identified as a potential driver of aberrant dopamine signaling through increased glutamatergic transmission to regions involved in the regulation of activity in the mesocorticolimbic pathway (Floresco et al., 2001; Legault et al., 2000). Within the hippocampus, parvalbumin containing interneurons (PV+) set the intrinsic tone for rhythmic oscillations, which are central in system responsiveness as well as functional connectivity (Amilhon et al., 2015; Marissal et al., 2018). In the current study we used phenotypically normal, heterozygous PV-Cre mice to either decrease (hM4Di) or increase (hM3Dq) PV+ interneuron activity in the vCA1, effectively shifting the excitatory/inhibitory (E/I) balance. We then measured changes in both CBV and functional connectivity in various anatomical regions associated with the mesocorticolimbic pathway using functional ultrasound.

4.3.1. CBV alterations after chemogenetic vCA1 PV+ interneuron modulation

We found that pharmacologically inhibiting the PV+ interneuron population through virally expressed hM4Di in the vCA1 did not significantly change CBV from that of mCherry control over time (Figure 3.3.1 :2A). Activation of these inhibitory interneurons via hM3Dq, however, resulted in a significant decrease in CBV 30- and 45- minutes after i.p. CNO administration. This suggests that when the E/I balance is shifted toward inhibition in the vCA1, there is a reduction in metabolic demand which manifests as a reduction in regional CBV (Mathiesen et al., 1998; Sanganahalli et al., 2016). Contrastingly, it can be hypothesized that the reduction of PV+ activity and the subsequently expected increase in excitatory activity in the hM4Di group was not, however, strong enough to necessitate an increase in CBV. While there are few published findings regarding PV+ evoked changes of CBV in the vCA1 specifically, the inhibition of PV+ interneurons in the cortex has been found to trigger a regional increase in CBV, whereas inhibition of cortical excitatory

signaling reduces CBV (Markicevic et al., 2020), a finding we were not able to recapitulate here. It should be considered that in the context of schizophrenia, the decreased activity of interneurons in the vCA1 is thought to lower the threshold of the region for stimulation but is not necessarily capable of generating increased excitatory output unaided (Lodge and Grace, 2006). We took precautions to reduce stress during all phases of experiments and since it is unlikely the animals experienced novel stressors after the onset of sedation, it could be that without an external stimulus any potential pharmacologically induced increases in CBV are below the range of detection in the vCA1.

In parallel to the changes detected in the vCA1, we measured increased CBV in the PL after activation of PV+ interneurons in the vCA1 which was statistically significant at the 15- and 45-minute post CNO administration time points (Figure 3.3.1 :2D). Here, decreased CBV was evident in the contrasting hM4Di group. Although this difference was consistent after CNO administration, statistical significance was not met. A similar pattern was observed in the Cg, but the differences all failed to pass statistical testing for any of the groups. While literature is sparse regarding CBV responses after vCA1 interneuron modulation as mentioned previously, a thorough fMRI study by the Adan and Dijkhuizen groups (2017) showed that activation of the projection from the ventral tegmental area (VTA) to the NAc resulted in significantly increased BOLD signal in the mPFC in anesthetized rats. It cannot be ruled out that an indirect pathway between the vCA1 and PL/Cg, for example through the NAc, could contribute the CBV response detected in the anterior cortical regions, even if CBV in the NAc was relatively unchanged.

4.3.2. Influence of vCA1 PV+ activity on functional connectivity in the mesocorticolimbic pathway

We then created a time series of functional connectivity for every ROI-ROI pair using 5-minute sliding windows with 1-minute increments normalized to baseline connectivity prior to CNO administration. We calculated over 42,000 connectivity points which were displayed in a large matrix of matrices to visualize trends in the evolution of connectivity after vCA1 PV+ modulation for each group (Figure 3.3.2 :1). We found that inhibition of vCA1 PV+ interneurons largely resulted in decreases in connectivity, while PV+ activation gave rise to more increases in connectivity than decreases, and the mCherry control group showed a fairly even mix of directional changes. Initially, it may seem counterintuitive that decreasing

regional inhibition reduced connectivity and increasing inhibitory signals increased connectivity, but it is important to note that functional connectivity is calculated from low frequency oscillations (< 0.2 Hz, Section 2.7.1). In a study of high relevance to the one presented here, Marissal et al., (2018) conducted a thorough investigation of the influence of PV+ interneurons on CA1 network dynamics using calcium imaging and electrophysiology. They found that inhibition of PV+ almost completely abolished spontaneous calcium assembly synchrony in the CA1. In contrast, hM3Dq activation of PV+ interneurons increased coactivation of neurons to produce even more precise synchrony than that seen in the control group. Since the low frequency oscillations that characterize functional connectivity in methods such as fUS and fMRI are thought to be highly related to rhythmic interneuron activity (Amilhon et al., 2015; Anenberg et al., 2015), our data suggests that the decreased and increased functional connectivity measured here can be primarily attributed to changes in the synchrony of interneuron firing, rather than the simple release or suppression of excitation.

When we looked in depth at ROIs of interest in the mesocorticolimbic pathway, we did see a trend of decreased vCA1 connectivity after PV+ inhibition and increased connectivity after PV+ activation, but this was neither robust nor significant with any of the other target mesocorticolimbic ROIs (Figure 3.3.2 :2). Connectivity between the vCA1 and NAc did appear to be lower during certain epochs in the hM4Di group but this was not consistent. That is not to say that the vCA1 could not still be having an indirect effect on the NAc. Unfortunately, we were not able to collect data from the VTA in this study, however, many groups have shown that the VTA is a key intermediary in this pathway (Legault et al., 2000; Roelofs et al., 2017). We also looked more closely at the Cg-NAc connectivity profile and found that there was significantly increased connectivity between the two regions 15- and 30- minutes after CNO administration in the hM3Dq group. While the hM4Di group once again showed consistent decreases, these were not significant. Instability in the mCherry connectivity profile could be a reason for this statistical variability, alternatively our viral transfection protocol may not have met a physiological threshold for robust inhibition. In either case, this result does not necessarily align with many studies in schizophrenic patients that show increased connectivity between the PFC and NAc correlates with symptom severity (Cao et al., 2022). Yet, if we consider functional connectivity in the context of synchrony, it could be that activation of the PV+ interneurons in the hM3Dq group generates synchrony throughout the system and therein increased connectivity. Furthermore, although

we did not see increased connectivity in the hM4Di group which is more likely to model hippocampal hyperactivity in schizophrenia, it could be that chronic reinforcement of this activity is necessary to produce this effect since we performed these experiments in phenotypically normal, healthy animals. In fact, it has been shown that there is decreased connectivity between the striatum and PFC in first episode, treatment-naïve patients (Lin et al., 2018) and this feature could then progress to the increased connectivity detected in chronic patients (Cao et al., 2022), an outcome that could be investigated with chronic CNO treatment in the current study.

4.3.3. Major Conclusions of study III

Since many forms of mental illness are likely caused by abnormalities in the overall organization and function of brain networks, pinpointing certain regions that can then change connectivity through an entire network is of substantial interest in the development of therapies. Given the pivotal role of the vCA1 in modulating dopamine in the mesocorticolimbic pathway and the prevalence of PV+ interneuron abnormalities in schizophrenia, we sought to examine how PV+ inhibition as well as activation in the vCA1 would affect connectivity and CBV throughout the brain with functional ultrasound imaging. We found that inhibiting PV+ interneurons in the vCA1 did not produce statistically significant differences in CBV and functional connectivity, however there was a trend of reduction in both measures. Interestingly, increasing PV+ interneuron activity resulted in decreased CBV in the vCA1 but increased CBV in the PL and Cg. These findings correlated with increased connectivity between the Cg and NAc, a feature which could be modulated in chronic disease. Separating the cause from the effect of circuit abnormalities enables isolation of upstream and downstream features which can inform further research that rather than solely alleviating symptoms, might impede disease progression and potentially lead to a cure for schizophrenia.

4.4. Limitations

While we believe that our results reveal impactful findings in multiple fields, there are some limitations that should be discussed when interpreting the findings described here.

To send and receive power Doppler signal, we used an ultrasonic probe with a linear array. This means we had to isolate single, cross-sectional imaging planes to maximize coverage of given ROIs. We therefore were unable to acquire data from certain regions that would have been of interest in these studies (the VTA in study III, for example). An ultrasonic matrix array is currently in development that would help to overcome this limitation and allow for empirical evaluation of distributed networks. Additionally, while the current probe delivers excellent spatial and temporal resolution, the rate of image compilation would need to be increased to determine directionality of functional connectivity, a characteristic that would have increased the level of information in all of the studies presented here.

It must also be mentioned that we have made conclusions regarding neuronal activity through indirect measurements of blood flow. While there are many studies that combine electrophysiology with measurements from the blood, we cannot say for certain that those features are present in every measurement. We also cannot be certain how much the variability in neurovascular coupling between animals and in various regions affects the interpretation of functional connectivity. Even EEG measurements that record neuronal activity directly can only give regional information and cannot acquire data at a cellular level. It could be that in the future a technique is developed that allows for direct and specific monitoring of neuronal activity in a non-invasive manner suitable for both humans and animals, however, at the moment indirect measurement of blood flow provides some of the best translational value.

We used sedated mice for the current studies. Although the animals were only lightly sedated there were certainly effects on functional connectivity due to this point. A recent fUS study in awake mice did, however, show that dexmedetomidine at the level used here did not affect the pattern and only slightly affected the strength of functional connectivity in comparison to conscious mice (Ferrier et al., 2020). While it would be ideal to study conscious animals, it is virtually impossible to disentangle resting state networks in behaving mice. Although humans can be directed to lay still in an MRI scanner, it is not feasible to do this in rodents without some form of restraint and is still very difficult to measure without significant

movement artifacts and immense stress on the animal. We did attempt to set up a technique for head fixed imaging in conscious mice, however, significant and frequent movement artifacts made this data impossible to analyze with any reliability. In addition, the analytical complexities, time constraints and labor intensities of surgical implantation of the head plates substantially reduced the feasibility of exploratory studies. Furthermore, we feel that the stable measurements and reduced variability in attention and cognitive state that sedation entails, provided the best method for achieving the aims of this project.

Limitations in the realm of data analysis are also relevant in this project. Within and between subject variability is a frequent issue in neuroimaging, requiring large sample sizes that do not necessarily adhere to the 3R principals (Wachsmuth et al., 2021). Increasing the number of animals in each group may have reduced variability but a compromise was necessary. No formal power analyses were made here and instead group sizes were estimated from those used in published literature. In addition, we were limited by the analytical techniques available. fUS is a relatively novel technique with a distinct data format. Programs for the analysis of MRI data have been in development for decades and have streamlined analytical pipelines. There is no standard way of converting fUS data to be used in these software packages, though they would provide innumerable methods for analyzing the data presented here. In relation to this topic, the seed-based functional connectivity analyses used in these studies required *a priori* selection of ROIs. Although functional connectivity readouts using this method can be more easily assigned statistical value and are also more transparent to interpret, there are potential biases from this approach. Since the studies here were exploratory and we intended to investigate the pattern of activation across certain ROIs, we do not feel these limitations negate the interpretation of our results.

4.5. General Conclusions

We have shown that functional ultrasound imaging can be effectively used to investigate many aspects of the neural networks involved in psychiatric disease. We found that a memory trace can be measured and monitored through time and that subtle differences in networks at rest can be correlated with behavior. We also tracked network maturation through development and compared the trajectory of a transgenic model of psychiatric disease. We found that the shift in connectivity from early to late pubescence most accurately predicts network connectivity in adulthood, an aspect that is applicable in studies for early intervention in schizophrenia. Finally, we showed that modulating a sub-population of interneurons in a distinct anatomical region can affect global circuitry using a chemogenetic pharmacological model of network dysfunction in schizophrenia. All together supporting the role for fUS imaging in drug development for psychiatric disease.

5. SUMMARY

Psychiatric diseases remain some of the most studied, but least understood ailments in human health. The inherent heterology of etiology, pathophysiology, and symptom domains in both the broad spectrum of psychiatric disorders, make them difficult to approach and interpret experimentally. Various properties of cerebral hemodynamics have proven invaluable in research as a method of indirectly measuring neural activity. The novel imaging modality, functional ultrasound (fUS), which measures blood flow directly via reflected power Doppler signal, has shown a high correlation of cerebral blood volume (CBV) with neural activity. Functional connectivity, a measure of network integration through the temporal correlation of regional neural activity, has emerged as a highly informative approach to understanding the basis of cognition, behavior, and mood.

In the present work, we used animal models in combination with fUS imaging to investigate some of the common features of psychiatric disease, in particular, those observed in schizophrenia. Since schizophrenia patients frequently display disruptions not only in memory, but also in the processing of fear-related stimuli, we first used a behavioral model to conduct an associative fear memory trace (**study I**). We used this proof-of-concept study to verify the capability and robustness of fUS imaging to capture a well-known neural network and any potential subtle changes in that network over time. As schizophrenic symptoms are well known to present in late adolescence to early adulthood in humans, we next investigated the developmental trajectory and predictive validity of a transgenic animal model with a heterogenous phenotype associated with schizophrenia (**study II**). Finally, in a pharmacological model, we investigated whether modulating a specific cell type in a distinct neuroanatomical region could change connectivity in the mesocorticolimbic pathway, a neural network that is highly implicated in schizophrenia (**study III**).

During **study I**, "*Functional ultrasound imaging of recent and remote memory recall in the associative fear neural network in mice*", we used fear conditioning to encode an auditory cued associative fear memory to investigate if we could detect and monitor the evolution of a memory trace over time. We also sought to correlate cue-evoked functional connectivity with expressed behavior. We showed that we could utilize the fUS imaging technique along with behavioral readouts to detect neural networks involved in emotional processing and

memory retrieval. Thus, fUS could be utilized to measure evoked network connectivity and monitor changes in the contributions of distinct anatomical regions over time.

In **study II**, "*Deviations in network development in the 15q13.3 mouse model: a functional ultrasound study*", we used the 15q13.3 transgenic copy number variant animal model to recapitulate the post pubescent onset of schizophrenic symptoms. We measured functional connectivity at 4 separate developmental milestones from pubescence to adulthood, thereby detecting a hyperconnected network in 15q13.3 mice and identified a critical transition in network connectivity between early and late pubescence that could predict the conversion to an adult neural signature.

Study III, "*The influence of activation or inhibition of the parvalbumin positive interneuron network in the ventral CA1 on brain-wide networks measured with functional ultrasound*", aimed to further elucidate the role of the ventral CA1 parvalbumin expressing (PV+) interneurons in the mesocorticolimbic network using a pharmacological fUS approach in combination with designer receptors exclusively activated by designer drugs (DREADD)-based chemogenetics. We detected a bidirectional effect after either inhibiting or activating PV+ interneurons throughout the network. This showed that subtle differences in circuitry can trigger an overall change in regional recruitment and functional network organization.

We have shown that functional ultrasound imaging can be effectively used to investigate multidimensional aspects of the neural networks involved in psychiatric disease. Since many forms of mental illness are likely caused by abnormalities in the overall organization and function of brain networks, pinpointing certain regions that can then change connectivity through an entire network is of substantial interest in the development of therapies. Ultimately, the methods and results presented here can contribute to the translatability of preclinical research for the development of therapies that effectively improve patient lives.

6. LIST OF REFERENCES

Adhikari, A., Lerner, T.N., Finkelstein, J., Pak, S., Jennings, J.H., Davidson, T.J., Ferenczi, E., Gunaydin, L.A., Mirzabekov, J.J., Ye, L., Kim, S.-Y., Lei, A., Deisseroth, K., 2015. Basomedial amygdala mediates top–down control of anxiety and fear. Nature 527, 179–185. https://doi.org/10.1038/nature15698

Amaral, D.G., Dolorfo, C., Alvarez-Royo, P., 1991. Organization of CA1 projections to the subiculum: A PHA-L analysis in the rat. Hippocampus 1, 415–435. https://doi.org/10.1002/hipo.450010410

Amilhon, B., Huh, C.Y.L., Manseau, F., Ducharme, G., Nichol, H., Adamantidis, A., Williams, S., 2015. Parvalbumin Interneurons of Hippocampus Tune Population Activity at Theta Frequency. Neuron 86, 1277–1289. https://doi.org/10.1016/j.neuron.2015.05.027

Anagnostaras, S.G., Wood, S.C., Shuman, T., Cai, D.J., LeDuc, A.D., Zurn, K.R., Zurn, J.B., Sage, J.R., Herrera, G.M., 2010. Automated Assessment of Pavlovian Conditioned Freezing and Shock Reactivity in Mice Using the Video Freeze System. Front Behav Neurosci 4, 158. https://doi.org/10.3389/fnbeh.2010.00158

Anenberg, E., Chan, A.W., Xie, Y., LeDue, J.M., Murphy, T.H., 2015. Optogenetic Stimulation of GABA Neurons can Decrease Local Neuronal Activity While Increasing Cortical Blood Flow. J Cereb Blood Flow Metabolism 35, 1579–1586. https://doi.org/10.1038/jcbfm.2015.140

Angermeyer, M.C., Kühnz, L., 1988. Gender differences in age at onset of Schizophrenia. European Archives Psychiatry Neurological Sci 237, 351–364. https://doi.org/10.1007/bf00380979

Assaf, Y., Bouznach, A., Zomet, O., Marom, A., Yovel, Y., 2020. Conservation of brain connectivity and wiring across the mammalian class. Nat Neurosci 23, 805–808. https://doi.org/10.1038/s41593-020-0641-7

Bai, Y.M., Chou, K.-H., Lin, C.-P., Chen, I.-Y., Li, C.-T., Yang, K.C., Chou, Y.-H., Su, T.-P., 2009. White matter abnormalities in schizophrenia patients with tardive dyskinesia: A diffusion tensor image study. Schizophr Res 109, 167–181. https://doi.org/10.1016/j.schres.2009.02.003

Baker, N.J., Schofield, J.C., Caswell, 2 Mark D, McLellan, A.D., 2011. Effects of Early Atipamezole Reversal of Medetomidine–Ketamine Anesthesia in Mice. J Am Assoc Lab Anim Sci 6, 916–920. https://doi.org/10.1111/j.1467-2995.2009.00463.x

Baloch, S., Verma, R., Huang, H., Khurd, P., Clark, S., Yarowsky, P., Abel, T., Mori, S., Davatzikos, C., 2009. Quantification of Brain Maturation and Growth Patterns in C57BL/6J Mice via Computational Neuroanatomy of Diffusion Tensor Images. Cereb Cortex 19, 675–687. https://doi.org/10.1093/cercor/bhn112

Bansal, R., Gerber, A.J., Peterson, B.S., 2008. Brain Morphometry Using Anatomical Magnetic Resonance Imaging. J Am Acad Child Adolesc Psychiatry 47, 619–621. https://doi.org/10.1097/chi.0b013e31816c54ed

Barrett, D., Shumake, J., Jones, D., Gonzalez-Lima, F., 2003. Metabolic Mapping of Mouse Brain Activity after Extinction of a Conditioned Emotional Response. J Neurosci 23, 5740–5749. https://doi.org/10.1523/jneurosci.23-13-05740.2003

Bast, T., Zhang, W., Feldon, J., 2003. Dorsal hippocampus and classical fear conditioning to tone and context in rats: Effects of local NMDA-receptor blockade and stimulation. Hippocampus 13, 657–675. https://doi.org/10.1002/hipo.10115

Benjamini, Y., Krieger, A.M., Yekutieli, D., 2006. Adaptive linear step-up procedures that control the false discovery rate. Biometrika 93, 491–507. https://doi.org/10.1093/biomet/93.3.491

Bergstrom, H.C., 2016. The neurocircuitry of remote cued fear memory. Neurosci Biobehav Rev 71, 409–417. https://doi.org/10.1016/j.neubiorev.2016.09.028

Bergstrom, H.C., McDonald, C.G., Johnson, L.R., 2011. Pavlovian Fear Conditioning Activates a Common Pattern of Neurons in the Lateral Amygdala of Individual Brains. Plos One 6, e15698. https://doi.org/10.1371/journal.pone.0015698

Bloodgood, D.W., Sugam, J.A., Holmes, A., Kash, T.L., 2018. Fear extinction requires infralimbic cortex projections to the basolateral amygdala. Transl Psychiat 8, 60. https://doi.org/10.1038/s41398-018-0106-x

Boido, D., Rungta, R.L., Osmanski, B.-F., Roche, M., Tsurugizawa, T., Bihan, D.L., Ciobanu, L., Charpak, S., 2019. Mesoscopic and microscopic imaging of sensory responses in the same animal. Nat Commun 10, 1110. https://doi.org/10.1038/s41467-019-09082-4

Breier, A., Su, T.-P., Saunders, R., Carson, R.E., Kolachana, B.S., Bartolomeis, A. de, Weinberger, D.R., Weisenfeld, N., Malhotra, A.K., Eckelman, W.C., Pickar, D., 1997. Schizophrenia is associated with elevated amphetamine-induced synaptic dopamine concentrations: Evidence from a novel positron emission tomography method. Proc National Acad Sci 94, 2569–2574. https://doi.org/10.1073/pnas.94.6.2569

Burgos-Robles, A., Vidal-Gonzalez, I., Santini, E., Quirk, G.J., 2007. Consolidation of Fear Extinction Requires NMDA Receptor-Dependent Bursting in the Ventromedial Prefrontal Cortex. Neuron 53, 871–880. https://doi.org/10.1016/j.neuron.2007.02.021

Călin, A., Stancu, M., Zagrean, A.-M., Jefferys, J.G.R., Ilie, A.S., Akerman, C.J., 2018. Chemogenetic Recruitment of Specific Interneurons Suppresses Seizure Activity. Front Cell Neurosci 12, 293. https://doi.org/10.3389/fncel.2018.00293

Cao, H., Chén, O.Y., Chung, Y., Forsyth, J.K., McEwen, S.C., Gee, D.G., Bearden, C.E., Addington, J., Goodyear, B., Cadenhead, K.S., Mirzakhanian, H., Cornblatt, B.A., Carrión, R.E., Mathalon, D.H., McGlashan, T.H., Perkins, D.O., Belger, A., Seidman, L.J., Thermenos, H., Tsuang, M.T., Erp, T.G.M. van, Walker, E.F., Hamann, S., Anticevic, A., Woods, S.W., Cannon, T.D., 2018. Cerebello-thalamo-cortical hyperconnectivity as a state-independent functional neural signature for psychosis prediction and characterization. Nat Commun 9, 3836. https://doi.org/10.1038/s41467-018-06350-7

Cao, X., Li, Q., Liu, S., Li, Z., Wang, Y., Cheng, L., Yang, C., Xu, Y., 2022. Enhanced Resting-State Functional Connectivity of the Nucleus Accumbens in First-Episode, Medication-Naïve Patients With Early Onset Schizophrenia. Front Neurosci-switz 16, 844519. https://doi.org/10.3389/fnins.2022.844519

Cardno, A.G., Marshall, E.J., Coid, B., Macdonald, A.M., Ribchester, T.R., Davies, N.J., Venturi, P., Jones, L.A., Lewis, S.W., Sham, P.C., Gottesman, I.I., Farmer, A.E., McGuffin, P., Reveley, A.M., Murray, R.M., 1999. Heritability Estimates for Psychotic Disorders: The Maudsley Twin Psychosis Series. Arch Gen Psychiat 56, 162–168. https://doi.org/10.1001/archpsyc.56.2.162

Catana, C., 2019. Development of Dedicated Brain PET Imaging Devices: Recent Advances and Future Perspectives. J Nucl Med 60, 1044–1052. https://doi.org/10.2967/jnumed.118.217901

Cenquizca, L.A., Swanson, L.W., 2007. Spatial organization of direct hippocampal field CA1 axonal projections to the rest of the cerebral cortex. Brain Res Rev 56, 1–26. https://doi.org/10.1016/j.brainresrev.2007.05.002

Chahboune, H., Ment, L.R., Stewart, W.B., Ma, X., Rothman, D.L., Hyder, F., 2007. Neurodevelopment of C57B/L6 mouse brain assessed by in vivo diffusion tensor imaging. Nmr Biomed 20, 375–382. https://doi.org/10.1002/nbm.1130

Chang, C., Maren, S., 2010. Strain Difference in the Effect of Infralimbic Cortex Lesions on Fear Extinction in Rats. Behav Neurosci 124, 391–397. https://doi.org/10.1037/a0019479

Charlson, F.J., Ferrari, A.J., Santomauro, D.F., Diminic, S., Stockings, E., Scott, J.G., McGrath, J.J., Whiteford, H.A., 2018. Global Epidemiology and Burden of Schizophrenia: Findings From the Global Burden of Disease Study 2016. Schizophrenia Bull 44, 1195–1203. https://doi.org/10.1093/schbul/sby058

Chen, G., Zhang, Y., Li, X., Zhao, X., Ye, Q., Lin, Y., Tao, H.W., Rasch, M.J., Zhang, X., 2017. Distinct Inhibitory Circuits Orchestrate Cortical beta and gamma Band Oscillations. Neuron 96, 1403-1418.e6. https://doi.org/10.1016/j.neuron.2017.11.033

Chen, P., Ye, E., Jin, X., Zhu, Y., Wang, L., 2019. Association between Thalamocortical Functional Connectivity Abnormalities and Cognitive Deficits in Schizophrenia. Sci Rep-uk 9, 2952. https://doi.org/10.1038/s41598-019-39367-z

Cho, J.-H., Huang, B.S., Gray, J.M., 2016. RNA sequencing from neural ensembles activated during fear conditioning in the mouse temporal association cortex. Sci Rep-uk 6, 31753. https://doi.org/10.1038/srep31753

Clark, R.E., Squire, L.R., 1998. Classical Conditioning and Brain Systems: The Role of Awareness. Science 280, 77–81. https://doi.org/10.1126/science.280.5360.77

Cole, M.W., Bassett, D.S., Power, J.D., Braver, T.S., Petersen, S.E., 2014. Intrinsic and Task-Evoked Network Architectures of the Human Brain. Neuron 83, 238–251. https://doi.org/10.1016/j.neuron.2014.05.014

Collaborators, C.-19 M.D., Santomauro, D.F., Herrera, A.M.M., Shadid, J., Zheng, P., Ashbaugh, C., Pigott, D.M., Abbafati, C., Adolph, C., Amlag, J.O., Aravkin, A.Y., Bang-Jensen, B.L., Bertolacci, G.J., Bloom, S.S., Castellano, R., Castro, E., Chakrabarti, S., Chattopadhyay, J., Cogen, R.M., Collins, J.K., Dai, X., Dangel, W.J., Dapper, C., Deen, A., Erickson, M., Ewald, S.B., Flaxman, A.D., Frostad, J.J., Fullman, N., Giles, J.R., Giref, A.Z., Guo, G., He, J., Helak, M., Hulland, E.N., Idrisov, B., Lindstrom, A., Linebarger, E., Lotufo, P.A., Lozano, R., Magistro, B., Malta, D.C., Månsson, J.C., Marinho, F., Mokdad, A.H., Monasta, L., Naik, P., Nomura, S., O'Halloran, J.K., Ostroff, S.M., Pasovic, M., Penberthy, L., Jr, R.C.R., Reinke, G., Ribeiro, A.L.P., Sholokhov, A., Sorensen, R.J.D., Varavikova, E., Vo, A.T., Walcott, R., Watson, S., Wiysonge, C.S., Zigler, B., Hay, S.I., Vos, T., Murray, C.J.L., Whiteford, H.A., Ferrari, A.J., 2021. Global prevalence and burden of depressive and anxiety disorders in 204 countries and territories in 2020 due to the COVID-19 pandemic. Lancet 398, 1700–1712. https://doi.org/10.1016/s0140-6736(21)02143-7

Collin, G., Nieto-Castanon, A., Shenton, M.E., Pasternak, O., Kelly, S., Keshavan, M.S., Seidman, L.J., McCarley, R.W., Niznikiewicz, M.A., Li, H., Zhang, T., Tang, Y., Stone, W.S., Wang, J., Whitfield-Gabrieli, S., 2020. Brain functional connectivity data enhance prediction of clinical outcome in youth at risk for psychosis. Neuroimage Clin 26, 102108. https://doi.org/10.1016/j.nicl.2019.102108

Collo, G., Mucci, A., Giordano, G.M., Pich, E.M., Galderisi, S., 2020. Negative Symptoms of Schizophrenia and Dopaminergic Transmission: Translational Models and Perspectives Opened by iPSC Techniques. Front Neurosci-switz 14, 632. https://doi.org/10.3389/fnins.2020.00632

Courtin, Julien, Chaudun, F., Rozeske, R.R., Karalis, N., Gonzalez-Campo, C., Wurtz, H., Abdi, A., Baufreton, J., Bienvenu, T.C.M., Herry, C., 2014. Prefrontal parvalbumin interneurons shape neuronal activity to drive fear expression. Nature 505, 92–96. https://doi.org/10.1038/nature12755

Courtin, J., Karalis, N., Gonzalez-Campo, C., Wurtz, H., Herry, C., 2014. Persistence of amygdala gamma oscillations during extinction learning predicts spontaneous fear recovery. Neurobiol Learn Mem 113, 82–89. https://doi.org/10.1016/j.nlm.2013.09.015

Dalmay, T., Abs, E., Poorthuis, R.B., Hartung, J., Pu, D.-L., Onasch, S., Lozano, Y.R., Signoret-Genest, J., Tovote, P., Gjorgjieva, J., Letzkus, J.J., 2019. A Critical Role for Neocortical Processing of Threat Memory. Neuron 104, 1180-1194.e7. https://doi.org/10.1016/j.neuron.2019.09.025

Das, P., Kemp, A.H., Flynn, G., Harris, A.W.F., Liddell, B.J., Whitford, T.J., Peduto, A., Gordon, E., Williams, L.M., 2007. Functional disconnections in the direct and indirect amygdala pathways for fear processing in schizophrenia. Schizophr Res 90, 284–294. https://doi.org/10.1016/j.schres.2006.11.023

Deco, G., Jirsa, V.K., McIntosh, A.R., 2011. Emerging concepts for the dynamical organization of resting-state activity in the brain. Nat Rev Neurosci 12, 43–56. https://doi.org/10.1038/nrn2961

Deffieux, T., Demené, C., Tanter, M., 2021. Functional ultrasound imaging: a new imaging modality for neuroscience. Neuroscience 474, 110–121. https://doi.org/10.1016/j.neuroscience.2021.03.005

Dejean, C., Courtin, J., Rozeske, R.R., Bonnet, M.C., Dousset, V., Michelet, T., Herry, C., 2015. Neuronal Circuits for Fear Expression and Recovery: Recent Advances and Potential Therapeutic Strategies. Biol Psychiat 78, 298–306. https://doi.org/10.1016/j.biopsych.2015.03.017

Demené, C., Deffieux, T., Pernot, M., Osmanski, B.-F., Biran, V., Gennisson, J.-L., Sieu, L.-A., Bergel, A., Franqui, S., Correas, J.-M., Cohen, I., Baud, O., Tanter, M., 2015. Spatiotemporal Clutter Filtering of Ultrafast Ultrasound Data Highly Increases Doppler and fUltrasound Sensitivity. Ieee T Med Imaging 34, 2271–2285. https://doi.org/10.1109/tmi.2015.2428634

Duan, H.-F., Gan, J.-L., Yang, J.-M., Cheng, Z.-X., Gao, C.-Y., Shi, Z.-J., Zhu, X.-Q., Liang, X.-J., Zhao, L.-M., 2015. A longitudinal study on intrinsic connectivity of hippocampus associated with positive symptom in first-episode schizophrenia. Behav Brain Res 283, 78–86. https://doi.org/10.1016/j.bbr.2015.01.022

Dugré, J.R., Dumais, A., Tikasz, A., Mendrek, A., Potvin, S., 2021. Functional connectivity abnormalities of the long-axis hippocampal subregions in schizophrenia during episodic memory. Npj Schizophrenia 7, 19. https://doi.org/10.1038/s41537-021-00147-2

Durston, S., Pol, H.E.H., Casey, B.J., Giedd, J.N., Buitelaar, J.K., Engeland, H.V., 2001. Anatomical MRI of the Developing Human Brain: What Have We Learned? J Am Acad Child Adolesc Psychiatry 40, 1012–1020. https://doi.org/10.1097/00004583-200109000-00009

Duvarci, S., Popa, D., Pare, D., 2011. Central Amygdala Activity during Fear Conditioning. J Neurosci 31, 289–294. https://doi.org/10.1523/jneurosci.4985-10.2011

Edmiston, E.K., Song, Y., Chang, M., Yin, Z., Zhou, Q., Zhou, Y., Jiang, X., Wei, S., Xu, K., Tang, Y., Wang, F., 2020. Hippocampal Resting State Functional Connectivity in Patients With Schizophrenia and Unaffected Family Members. Frontiers Psychiatry 11, 278. https://doi.org/10.3389/fpsyt.2020.00278

Ellis, J.K., Walker, E.F., Goldsmith, D.R., 2020. Selective Review of Neuroimaging Findings in Youth at Clinical High Risk for Psychosis: On the Path to Biomarkers for Conversion. Frontiers Psychiatry 11, 567534. https://doi.org/10.3389/fpsyt.2020.567534

Erlich, J.C., Bush, D.E.A., LeDoux, J.E., 2012. The role of the lateral amygdala in the retrieval and maintenance of fear-memories formed by repeated probabilistic reinforcement. Front Behav Neurosci 6, 16. https://doi.org/10.3389/fnbeh.2012.00016

Erp, T.G.M. van, Hibar, D.P., Rasmussen, J.M., Glahn, D.C., Pearlson, G.D., Andreassen, O.A., Agartz, I., Westlye, L.T., Haukvik, U.K., Dale, A.M., Melle, I., Hartberg, C.B., Gruber, O., Kraemer, B., Zilles, D., Donohoe, G., Kelly, S., McDonald, C., Morris, D.W., Cannon, D.M., Corvin, A., Machielsen, M.W.J., Koenders, L., Haan, L. de, Veltman, D.J., Satterthwaite, T.D., Wolf, D.H., Gur, R.C., Gur, R.E., Potkin, S.G., Mathalon, D.H., Mueller, B.A., Preda, A., Macciardi, F., Ehrlich, S., Walton, E., Hass, J., Calhoun, V.D., Bockholt, H.J., Sponheim, S.R., Shoemaker, J.M., Haren, N.E.M. van, Pol, H E Hulshoff, Pol, H E H, Ophoff, R.A., Kahn, R.S., Roiz-Santiañez, R., Crespo-Facorro, B., Wang, L., Alpert, K.I., Jönsson, E.G., Dimitrova, R., Bois, C., Whalley, H.C., McIntosh, A.M., Lawrie, S.M., Hashimoto, R., Thompson, P.M., Turner, J.A., 2016. Subcortical brain volume abnormalities in 2028 individuals with schizophrenia and 2540 healthy controls via the ENIGMA consortium. Mol Psychiatr 21, 547–553. https://doi.org/10.1038/mp.2015.63

Fair, D.A., Cohen, A.L., Power, J.D., Dosenbach, N.U.F., Church, J.A., Miezin, F.M., Schlaggar, B.L., Petersen, S.E., 2009. Functional Brain Networks Develop from a "Local to Distributed" Organization. Plos Comput Biol 5, e1000381. https://doi.org/10.1371/journal.pcbi.1000381

Fair, D.A., Dosenbach, N.U.F., Church, J.A., Cohen, A.L., Brahmbhatt, S., Miezin, F.M., Barch, D.M., Raichle, M.E., Petersen, S.E., Schlaggar, B.L., 2007. Development of distinct control networks through segregation and integration. Proc National Acad Sci 104, 13507–13512. https://doi.org/10.1073/pnas.0705843104

Fan, L., Klein, H., Bass, E., Springfield, C., Pinkham, A., 2021. Amygdala hyperconnectivity in the paranoid state: A transdiagnostic study. J Psychiatr Res 138, 117–124. https://doi.org/10.1016/j.jpsychires.2021.03.049

Fejgin, K., Nielsen, J., Birknow, M.R., Bastlund, J.F., Nielsen, V., Lauridsen, J.B., Stefansson, H., Steinberg, S., Sorensen, H.B.D., Mortensen, T.E., Larsen, P.H., Klewe, I.V., Rasmussen, S.V., Stefansson, K., Werge, T.M., Kallunki, P., Christensen, K.V., Didriksen, M., 2014. A Mouse Model that Recapitulates Cardinal Features of the 15q13.3 Microdeletion Syndrome Including Schizophrenia- and Epilepsy-Related Alterations. Biol Psychiat 76, 128–137. https://doi.org/10.1016/j.biopsych.2013.08.014

Feng, P., Feng, T., Chen, Z., Lei, X., 2014. Memory consolidation of fear conditioning: Bi-stable amygdala connectivity with dorsal anterior cingulate and medial prefrontal cortex. Soc Cogn Affect Neur 9, 1730–1737. https://doi.org/10.1093/scan/nst170

Ferrier, J., Tiran, E., Deffieux, T., Tanter, M., Lenkei, Z., 2020. Functional imaging evidence for task-induced deactivation and disconnection of a major default mode network hub in the mouse brain. P Natl Acad Sci Usa 117, 15270–15280. https://doi.org/10.1073/pnas.1920475117

Floresco, S.B., Todd, C.L., Grace, A.A., 2001. Glutamatergic Afferents from the Hippocampus to the Nucleus Accumbens Regulate Activity of Ventral Tegmental Area Dopamine Neurons. J Neurosci 21, 4915–4922. https://doi.org/10.1523/jneurosci.21-13-04915.2001

Ford, J.M., Palzes, V.A., Roach, B.J., Potkin, S.G., Erp, T.G.M. van, Turner, J.A., Mueller, B.A., Calhoun, V.D., Voyvodic, J., Belger, A., Bustillo, J., Vaidya, J.G., Preda, A., McEwen, S.C., Network, F.I.B.I.R., Mathalon, D.H., 2015. Visual Hallucinations Are Associated With Hyperconnectivity Between the Amygdala and Visual Cortex in People With a Diagnosis of Schizophrenia. Schizophrenia Bull 41, 223–232. https://doi.org/10.1093/schbul/sbu031

Foxe, J.J., Wylie, G.R., Martinez, A., Schroeder, C.E., Javitt, D.C., Guilfoyle, D., Ritter, W., Murray, M.M., 2002. Auditory-Somatosensory Multisensory Processing in Auditory Association Cortex: An fMRI Study. J Neurophysiol 88, 540–543. https://doi.org/10.1152/jn.2002.88.1.540

Gardner, D.M., Baldessarini, R.J., Waraich, P., 2005. Modern antipsychotic drugs: a critical overview. Can Med Assoc J 172, 1703–1711. https://doi.org/10.1503/cmaj.1041064

Gass, N., Weber-Fahr, W., Sartorius, A., Becker, R., Didriksen, M., Stensbøl, T.B., Bastlund, J.F., Meyer-Lindenberg, A., Schwarz, A.J., 2016. An acetylcholine alpha7 positive allosteric modulator rescues a schizophrenia-associated brain endophenotype in the 15q13.3 microdeletion, encompassing CHRNA7. Eur Neuropsychopharm 26, 1150–1160. https://doi.org/10.1016/j.euroneuro.2016.03.013

Gee, D.G., Karlsgodt, K.H., Erp, T.G.M. van, Bearden, C.E., Lieberman, M.D., Belger, A., Perkins, D.O., Olvet, D.M., Cornblatt, B.A., Constable, T., Woods, S.W., Addington, J., Cadenhead, K.S., McGlashan, T.H., Seidman, L.J., Tsuang, M.T., Walker, E.F., Cannon, T.D., Consortium, on behalf of the N., 2012. Altered age-related trajectories of amygdala-prefrontal circuitry in adolescents at clinical high risk for psychosis: A preliminary study. Schizophr Res 134, 1–9. https://doi.org/10.1016/j.schres.2011.10.005

Gesnik, M., Blaize, K., Deffieux, T., Gennisson, J.-L., Sahel, J.-A., Fink, M., Picaud, S., Tanter, M., 2017. 3D functional ultrasound imaging of the cerebral visual system in rodents. Neuroimage 149, 267–274. https://doi.org/10.1016/j.neuroimage.2017.01.071

Gheiratmand, M., Rish, I., Cecchi, G.A., Brown, M.R.G., Greiner, R., Polosecki, P.I., Bashivan, P., Greenshaw, A.J., Ramasubbu, R., Dursun, S.M., 2017. Learning stable and predictive network-based patterns of schizophrenia and its clinical symptoms. Npj Schizophrenia 3, 22. https://doi.org/10.1038/s41537-017-0022-8

Giedd, J.N., Blumenthal, J., Jeffries, N.O., Castellanos, F.X., Liu, H., Zijdenbos, A., Paus, T., Evans, A.C., Rapoport, J.L., 1999. Brain development during childhood and adolescence: a longitudinal MRI study. Nat Neurosci 2, 861–863. https://doi.org/10.1038/13158

Giustino, T.F., Maren, S., 2015. The Role of the Medial Prefrontal Cortex in the Conditioning and Extinction of Fear. Front Behav Neurosci 9, 298. https://doi.org/10.3389/fnbeh.2015.00298

Goense, J., Bohraus, Y., Logothetis, N.K., 2016. fMRI at High Spatial Resolution: Implications for BOLD-Models. Front Comput Neurosc 10, 66. https://doi.org/10.3389/fncom.2016.00066

Gogtay, N., Vyas, N.S., Testa, R., Wood, S.J., Pantelis, C., 2011. Age of Onset of Schizophrenia: Perspectives From Structural Neuroimaging Studies. Schizophrenia Bull 37, 504–513. https://doi.org/10.1093/schbul/sbr030

Goshen, I., Brodsky, M., Prakash, R., Wallace, J., Gradinaru, V., Ramakrishnan, C., Deisseroth, K., 2011. Dynamics of Retrieval Strategies for Remote Memories. Cell 147, 678–689. https://doi.org/10.1016/j.cell.2011.09.033

Grace, A.A., 2010. Ventral Hippocampus, Interneurons, and Schizophrenia. Curr Dir Psychol Sci 19, 232–237. https://doi.org/10.1177/0963721410378032

Grewe, B.F., Gründemann, J., Kitch, L.J., Lecoq, J.A., Parker, J.G., Marshall, J.D., Larkin, M.C., Jercog, P.E., Grenier, F., Li, J.Z., Lüthi, A., Schnitzer, M.J., 2017. Neural ensemble dynamics underlying a long-term associative memory. Nature 543, 670–675. https://doi.org/10.1038/nature21682

Grohs-Metz, G., Smausz, R., Gigg, J., Boeckers, T., Hengerer, B., 2022. Functional ultrasound imaging of recent and remote memory recall in the associative fear neural network in mice. Behav Brain Res 428, 113862. https://doi.org/10.1016/j.bbr.2022.113862

Holt, D.J., Lebron-Milad, K., Milad, M.R., Rauch, S.L., Pitman, R.K., Orr, S.P., Cassidy, B.S., Walsh, J.P., Goff, D.C., 2009. Extinction Memory Is Impaired in Schizophrenia. Biol Psychiat 65, 455–463. https://doi.org/10.1016/j.biopsych.2008.09.017

Honey, C.J., Thivierge, J.-P., Sporns, O., 2010. Can structure predict function in the human brain? Neuroimage 52, 766–776. https://doi.org/10.1016/j.neuroimage.2010.01.071

Howes, O.D., Nour, M.M., 2016. Dopamine and the aberrant salience hypothesis of schizophrenia. World Psychiatry 15, 3–4. https://doi.org/10.1002/wps.20276

Huttenlocher, P.R., 1979. Synaptic density in human frontal cortex — Developmental changes and effects of aging. Brain Res 163, 195–205. https://doi.org/10.1016/0006-8993(79)90349-4

Insel, T.R., 2010. Rethinking schizophrenia. Nature 468, 187–193. https://doi.org/10.1038/nature09552

James, S.L., Abate, D., Abate, K.H., Abay, S.M., Abbafati, C., Abbasi, N., Abbastabar, H., Abd-Allah, F., Abdela, J., Abdelalim, A., Abdollahpour, I., Abdulkader, R.S., Abebe, Z., Abera, S.F., Abil, O.Z., Abraha, H.N., Abu-Raddad, L.J., Abu-Rmeileh, N.M.E., Accrombessi, M.M.K., Acharya, D., Acharya, P., Ackerman, I.N., Adamu, A.A., Adebayo, O.M., Adekanmbi, V., Adetokunboh, O.O., Adib, M.G., Adsuar, J.C., Afanvi, K.A., Afarideh, M., Afshin, A., Agarwal, G., Agesa, K.M., Aggarwal, R., Aghayan, S.A., Agrawal, S., Ahmadi, A., Ahmadi, M., Ahmadieh, H., Ahmed, M.B., Aichour, A.N., Aichour, I., Aichour, M.T.E., Akinyemiju, T., Akseer, N., Al-Aly, Z., Al-Eyadhy, A., Al-Mekhlafi, H.M., Al-Raddadi, R.M., Alahdab, F., Alam, K., Alam, T., Alashi, A., Alavian, S.M., Alene, K.A., Alijanzadeh, M., Alizadeh-Navaei, R., Aljunid, S.M., Alkerwi, A., Alla, F., Allebeck, P., Alouani, M.M.L., Altirkawi, K., Alvis-Guzman, N., Amare, A.T., Aminde, L.N., Ammar, W., Amoako, Y.A., Anber, N.H., Andrei, C.L., Androudi, S., Animut, M.D., Anjomshoa, M., Ansha, M.G., Antonio, C.A.T., Anwari, P., Arabloo, J., Arauz, A., Aremu, O., Ariani, F., Armoon, B., Ärnlöv, J., Arora, A., Artaman, A., Aryal, K.K., Asayesh, H., Asghar, R.J., Ataro, Z., Atre, S.R., Ausloos, M., Avila-Burgos, L., Avokpaho, E.F.G.A., Awasthi, A., Quintanilla, B.P.A., Ayer, R., Azzopardi, P.S., Babazadeh, A., Badali, H., Badawi, A., Bali, A.G., Ballesteros, K.E., Ballew, S.H., Banach, M., Banoub, J.A.M., Banstola, A., Barac, A., Barboza, M.A., Barker-Collo, S.L., Bärnighausen, T.W., Barrero, L.H., Baune, B.T., Bazargan-Hejazi, S., Bedi, N., Beghi, E., Behzadifar, Masoud, Behzadifar, Meysam, Béjot, Y., Belachew, A.B., Belay, Y.A., Bell, M.L., Bello, A.K., Bensenor, I.M., Bernabe, E., Bernstein, R.S., Beuran, M., Beyranvand, T., Bhala, N., Bhattarai, S., Bhaumik, S., Bhutta, Z.A., Biadgo, B., Bijani, A., Bikbov, B., Bilano, V., Bililign, N., Sayeed, M.S.B., Bisanzio, D., Blacker, B.F., Blyth, F.M., Bou-Orm, I.R., Boufous, S., Bourne, R., Brady, O.J., Brainin, M., Brant, L.C., Brazinova, A., Breitborde, N.J.K., Brenner, H., Briant, P.S., Briggs, A.M., Briko, A.N., Britton, G., Brugha, T., Buchbinder, R., Busse, R., Butt, Z.A., Cahuana-Hurtado, L., Cano, J., Cárdenas, R., Carrero, J.J., Carter, A., Carvalho, F., Castañeda-Orjuela, C.A., Rivas, J.C., Castro, F., Catalá-López, F., Cercy, K.M., Cerin, E., Chaiah, Y., Chang, A.R., Chang, H.-Y., Chang, J.-C., Charlson, F.J., Chattopadhyay, A., Chattu, V.K., Chaturvedi, P., Chiang, P.P.-C., Chin, K.L., Chitheer, A., Choi, J.-Y.J., Chowdhury, R., Christensen, H., Christopher, D.J., Cicuttini, F.M., Ciobanu, L.G., Cirillo, M., Claro, R.M., Collado-Mateo, D., Cooper, C., Coresh, J., Cortesi, P.A., Cortinovis, M., Costa, M., Cousin, E., Criqui, M.H., Cromwell, E.A., Cross, M., Crump, J.A., Dadi, A.F., Dandona, L., Dandona, R., Dargan, P.I., Daryani, A., Gupta, R.D., Neves, J.D., Dasa, T.T., Davey, G., Davis, A.C., Davitoiu, D.V., Courten, B.D., Hoz, F.P.D.L., Leo, D.D., Neve, J.-W.D., Degefa, M.G., Degenhardt, L., Deiparine, S., Dellavalle, R.P., Demoz, G.T., Deribe, K., Dervenis, N., Jarlais, D.C.D., Dessie, G.A., Dey, S., Dharmaratne, S.D., Dinberu, M.T., Dirac, M.A., Djalalinia, S., Doan, L., Dokova, K., Doku, D.T., Dorsey, E.R., Doyle, K.E., Driscoll, T.R., Dubey, M., Dubljanin, E., Duken, E.E., Duncan, B.B., Duraes, A.R., Ebrahimi, H., Ebrahimpour, S., Echko, M.M., Edvardsson, D., Effiong, A., Ehrlich, J.R., Bcheraoui, C.E., Zaki, M.E.S., El-Khatib, Z., Elkout, H., Elyazar, I.R.F., Enayati, A., Endries, A.Y., Er, B., Erskine, H.E., Eshrati, B., Eskandarieh, S., Esteghamati, A., Esteghamati, S., Fakhim, H., Omrani, V.F., Faramarzi, M., Fareed, M., Farhadi, F., Farid, T.A., Farinha, C.S.E. sá, Farioli, A., Faro, A., Farvid, M.S., Farzadfar, F., Feigin, V.L., Fentahun, N., Fereshtehnejad, S.-M., Fernandes, E., Fernandes, J.C., Ferrari, A.J., Feyissa, G.T., Filip, I., Fischer, F., Fitzmaurice, C., Foigt, N.A., Foreman, K.J., Fox, J., Frank, T.D., Fukumoto, T., Fullman, N., Fürst, T., Furtado, J.M., Futran, N.D., Gall, S., Ganji, M., Gankpe, F.G., Garcia-Basteiro, A.L., Gardner, W.M., Gebre, A.K., Gebremedhin, A.T., Gebremichael, T.G., Gelano, T.F., Geleijnse, J.M., Genova-

Maleras, R., Geramo, Y.C.D., Gething, P.W., Gezae, K.E., Ghadiri, K., Falavarjani, K.G., Ghasemi-Kasman, M., Ghimire, M., Ghosh, R., Ghoshal, A.G., Giampaoli, S., Gill, P.S., Gill, T.K., Ginawi, I.A., Giussani, G., Gnedovskaya, E.V., Goldberg, E.M., Goli, S., Gómez-Dantés, H., Gona, P.N., Gopalani, S.V., Gorman, T.M., Goulart, A.C., Goulart, B.N.G., Grada, A., Grams, M.E., Grosso, G., Gugnani, H.C., Guo, Y., Gupta, P.C., Gupta, Rahul, Gupta, Rajeev, Gupta, T., Gyawali, B., Haagsma, J.A., Hachinski, V., Hafezi-Nejad, N., Bidgoli, H.H., Hagos, T.B., Hailu, G.B., Haj-Mirzaian, Arvin, Haj-Mirzaian, Arya, Hamadeh, R.R., Hamidi, S., Handal, A.J., Hankey, G.J., Hao, Y., Harb, H.L., Harikrishnan, S., Haro, J.M., Hasan, M., Hassankhani, H., Hassen, H.Y., Havmoeller, R., Hawley, C.N., Hay, R.J., Hay, S.I., Hedayatizadeh-Omran, A., Heibati, B., Hendrie, D., Henok, A., Herteliu, C., Heydarpour, S., Hibstu, D.T., Hoang, H.T., Hoek, H.W., Hoffman, H.J., Hole, M.K., Rad, E.H., Hoogar, P., Hosgood, H.D., Hosseini, S.M., Hosseinzadeh, M., Hostiuc, M., Hostiuc, S., Hotez, P.J., Hoy, D.G., Hsairi, M., Htet, A.S., Hu, G., Huang, J.J., Huynh, C.K., Iburg, K.M., Ikeda, C.T., Ileanu, B., Ilesanmi, O.S., Iqbal, U., Irvani, S.S.N., Irvine, C.M.S., Islam, S.M.S., Islami, F., Jacobsen, K.H., Jahangiry, L., Jahanmehr, N., Jain, S.K., Jakovljevic, M., Javanbakht, M., Jayatilleke, A.U., Jeemon, P., Jha, R.P., Jha, V., Ji, J.S., Johnson, C.O., Jonas, J.B., Jozwiak, J.J., Jungari, S.B., Jürisson, M., Kabir, Z., Kadel, R., Kahsay, A., Kalani, R., Kanchan, T., Karami, M., Matin, B.K., Karch, A., Karema, C., Karimi, N., Karimi, S.M., Kasaeian, A., Kassa, D.H., Kassa, G.M., Kassa, T.D., Kassebaum, N.J., Katikireddi, S.V., Kawakami, N., Karyani, A.K., Keighobadi, M.M., Keiyoro, P.N., Kemmer, L., Kemp, G.R., Kengne, A.P., Keren, A., Khader, Y.S., Khafaei, B., Khafaie, M.A., Khajavi, A., Khalil, I.A., Khan, E.A., Khan, M.S., Khan, M.A., Khang, Y.-H., Khazaei, M., Khoja, A.T., Khosravi, A., Khosravi, M.H., Kiadaliri, A.A., Kiirithio, D.N., Kim, C.-I., Kim, D., Kim, P., Kim, Y.-E., Kim, Y.J., Kimokoti, R.W., Kinfu, Y., Kisa, A., Kissimova-Skarbek, K., Kivimäki, M., Knudsen, A.K.S., Kocarnik, J.M., Kochhar, S., Kokubo, Y., Kolola, T., Kopec, J.A., Kosen, S., Kotsakis, G.A., Koul, P.A., Koyanagi, A., Kravchenko, M.A., Krishan, K., Krohn, K.J., Defo, B.K., Bicer, B.K., Kumar, G.A., Kumar, M., Kyu, H.H., Lad, D.P., Lad, S.D., Lafranconi, A., Lalloo, R., Lallukka, T., Lami, F.H., Lansingh, V.C., Latifi, A., Lau, K.M.-M., Lazarus, J.V., Leasher, J.L., Ledesma, J.R., Lee, P.H., Leigh, J., Leung, J., Levi, M., Lewycka, S., Li, S., Li, Y., Liao, Y., Liben, M.L., Lim, L.-L., Lim, S.S., Liu, S., Lodha, R., Looker, K.J., Lopez, A.D., Lorkowski, S., Lotufo, P.A., Low, N., Lozano, R., Lucas, T.C.D., Lucchesi, L.R., Lunevicius, R., Lyons, R.A., Ma, S., Macarayan, E.R.K., Mackay, M.T., Madotto, F., Razek, H.M.A.E., Razek, M.M.A.E., Maghavani, D.P., Mahotra, N.B., Mai, H.T., Majdan, M., Majdzadeh, R., Majeed, A., Malekzadeh, R., Malta, D.C., Mamun, A.A., Manda, A.-L., Manguerra, H., Manhertz, T., Mansournia, M.A., Mantovani, L.G., Mapoma, C.C., Maravilla, J.C., Marcenes, W., Marks, A., Martins-Melo, F.R., Martopullo, I., März, W., Marzan, M.B., Mashamba-Thompson, T.P., Massenburg, B.B., Mathur, M.R., Matsushita, K., Maulik, P.K., Mazidi, M., McAlinden, C., McGrath, J.J., McKee, M., Mehndiratta, M.M., Mehrotra, R., Mehta, K.M., Mehta, V., Mejia-Rodriguez, F., Mekonen, T., Melese, A., Melku, M., Meltzer, M., Memiah, P.T.N., Memish, Z.A., Mendoza, W., Mengistu, D.T., Mengistu, G., Mensah, G.A., Mereta, S.T., Meretoja, A., Meretoja, T.J., Mestrovic, T., Mezerji, N.M.G., Miazgowski, B., Miazgowski, T., Millear, A.I., Miller, T.R., Miltz, B., Mini, G.K., Mirarefin, M., Mirrakhimov, E.M., Misganaw, A.T., Mitchell, P.B., Mitiku, H., Moazen, B., Mohajer, B., Mohammad, K.A., Mohammadifard, N., Mohammadnia-Afrouzi, M., Mohammed, M.A., Mohammed, S., Mohebi, F., Moitra, M., Mokdad, A.H., Molokhia, M., Monasta, L., Moodley, Y., Moosazadeh, M., Moradi, G., Moradi-Lakeh, M., Moradinazar, M., Moraga, P., Morawska, L., Velásquez, I.M., Morgado-Da-

Costa, J., Morrison, S.D., Moschos, M.M., Mountjoy-Venning, W.C., Mousavi, S.M., Mruts, K.B., Muche, A.A., Muchie, K.F., Mueller, U.O., Muhammed, O.S., Mukhopadhyay, S., Muller, K., Mumford, J.E., Murhekar, M., Musa, J., Musa, K.I., Mustafa, G., Nabhan, A.F., Nagata, C., Naghavi, M., Naheed, A., Nahvijou, A., Naik, G., Naik, N., Najafi, F., Naldi, L., Nam, H.S., Nangia, V., Nansseu, J.R., Nascimento, B.R., Natarajan, G., Neamati, N., Negoi, I., Negoi, R.I., Neupane, S., Newton, C.R.J., Ngunjiri, J.W., Nguyen, A.Q., Nguyen, Ha Thu, Nguyen, H.L.T., Nguyen, Huong Thanh, Nguyen, L.H., Nguyen, M., Nguyen, N.B., Nguyen, S.H., Nichols, E., Ningrum, D.N.A., Nixon, M.R., Nolutshungu, N., Nomura, S., Norheim, O.F., Noroozi, M., Norrving, B., Noubiap, J.J., Nouri, H.R., Shiadeh, M.N., Nowroozi, M.R., Nsoesie, E.O., Nyasulu, P.S., Odell, C.M., Ofori-Asenso, R., Ogbo, F.A., Oh, I.-H., Oladimeji, O., Olagunju, A.T., Olagunju, T.O., Olivares, P.R., Olsen, H.E., Olusanya, B.O., Ong, K.L., Ong, S.K., Oren, E., Ortiz, A., Ota, E., Otstavnov, S.S., Øverland, S., Owolabi, M.O., A, M.P., Pacella, R., Pakpour, A.H., Pana, A., Panda-Jonas, S., Parisi, A., Park, E.-K., Parry, C.D.H., Patel, S., Pati, S., Patil, S.T., Patle, A., Patton, G.C., Paturi, V.R., Paulson, K.R., Pearce, N., Pereira, D.M., Perico, N., Pesudovs, K., Pham, H.Q., Phillips, M.R., Pigott, D.M., Pillay, J.D., Piradov, M.A., Pirsaheb, M., Pishgar, F., Plana-Ripoll, O., Plass, D., Polinder, S., Popova, S., Postma, M.J., Pourshams, A., Poustchi, H., Prabhakaran, D., Prakash, S., Prakash, V., Purcell, C.A., Purwar, M.B., Qorbani, M., Quistberg, D.A., Radfar, A., Rafay, A., Rafiei, A., Rahim, F., Rahimi, K., Rahimi-Movaghar, A., Rahimi-Movaghar, V., Rahman, M., Rahman, M.H. ur, Rahman, M.A., Rahman, S.U., Rai, R.K., Rajati, F., Ram, U., Ranjan, P., Ranta, A., Rao, P.C., Rawaf, D.L., Rawaf, S., Reddy, K.S., Reiner, R.C., Reinig, N., Reitsma, M.B., Remuzzi, G., Renzaho, A.M.N., Resnikoff, S., Rezaei, S., Rezai, M.S., Ribeiro, A.L.P., Roberts, N.L.S., Robinson, S.R., Roever, L., Ronfani, L., Roshandel, G., Rostami, A., Roth, G.A., Roy, A., Rubagotti, E., Sachdev, P.S., Sadat, N., Saddik, B., Sadeghi, E., Moghaddam, S.S., Safari, H., Safari, Y., Safari-Faramani, R., Safdarian, M., Safi, S., Safiri, S., Sagar, R., Sahebkar, A., Sahraian, M.A., Sajadi, H.S., Salam, N., Salama, J.S., Salamati, P., Saleem, K., Saleem, Z., Salimi, Y., Salomon, J.A., Salvi, S.S., Salz, I., Samy, A.M., Sanabria, J., Sang, Y., Santomauro, D.F., Santos, I.S., Santos, J.V., Milicevic, M.M.S., Jose, B.P.S., Sardana, M., Sarker, A.R., Sarrafzadegan, N., Sartorius, B., Sarvi, S., Sathian, B., Satpathy, M., Sawant, A.R., Sawhney, M., Saxena, S., Saylan, M., Schaeffner, E., Schmidt, M.I., Schneider, I.J.C., Schöttker, B., Schwebel, D.C., Schwendicke, F., Scott, J.G., Sekerija, M., Sepanlou, S.G., Serván-Mori, E., Seyedmousavi, S., Shabaninejad, H., Shafieesabet, A., Shahbazi, M., Shaheen, A.A., Shaikh, M.A., Shams-Beyranvand, M., Shamsi, M., Shamsizadeh, M., Sharafi, H., Sharafi, K., Sharif, M., Sharif-Alhoseini, M., Sharma, M., Sharma, R., She, J., Sheikh, A., Shi, P., Shibuya, K., Shigematsu, M., Shiri, R., Shirkoohi, R., Shishani, K., Shiue, I., Shokraneh, F., Shoman, H., Shrime, M.G., Si, S., Siabani, S., Siddiqi, T.J., Sigfusdottir, I.D., Sigurvinsdottir, R., Silva, J.P., Silveira, D.G.A., Singam, N.S.V., Singh, J.A., Singh, N.P., Singh, V., Sinha, D.N., Skiadaresi, E., Slepak, E.L.N., Sliwa, K., Smith, D.L., Smith, M., Filho, A.M.S., Sobaih, B.H., Sobhani, S., Sobngwi, E., Soneji, S.S., Soofi, M., Soosaraei, M., Sorensen, R.J.D., Soriano, J.B., Soyiri, I.N., Sposato, L.A., Sreeramareddy, C.T., Srinivasan, V., Stanaway, J.D., Stein, D.J., Steiner, C., Steiner, T.J., Stokes, M.A., Stovner, L.J., Subart, M.L., Sudaryanto, A., Sufiyan, M.B., Sunguya, B.F., Sur, P.J., Sutradhar, I., Sykes, B.L., Sylte, D.O., Tabarés-Seisdedos, R., Tadakamadla, S.K., Tadesse, B.T., Tandon, N., Tassew, S.G., Tavakkoli, M., Taveira, N., Taylor, H.R., Tehrani-Banihashemi, A., Tekalign, T.G., Tekelemedhin, S.W., Tekle, M.G., Temesgen, H., Temsah, M.-H., Temsah, O., Terkawi, A.S., Teweldemedhin, M., Thankappan, K.R., Thomas, N., Tilahun, B., To, Q.G., Tonelli,

M., Topor-Madry, R., Topouzis, F., Torre, A.E., Tortajada-Girbés, M., Touvier, M., Tovani-Palone, M.R., Towbin, J.A., Tran, B.X., Tran, K.B., Troeger, C.E., Truelsen, T.C., Tsilimbaris, M.K., Tsoi, D., Car, L.T., Tuzcu, E.M., Ukwaja, K.N., Ullah, I., Undurraga, E.A., Unutzer, J., Updike, R.L., Usman, M.S., Uthman, O.A., Vaduganathan, M., Vaezi, A., Valdez, P.R., Varughese, S., Vasankari, T.J., Venketasubramanian, N., Villafaina, S., Violante, F.S., Vladimirov, S.K., Vlassov, V., Vollset, S.E., Vosoughi, K., Vujcic, I.S., Wagnew, F.S., Waheed, Y., Waller, S.G., Wang, Y., Wang, Y.-P., Weiderpass, E., Weintraub, R.G., Weiss, D.J., Weldegebreal, F., Weldegwergs, K.G., Werdecker, A., West, T.E., Whiteford, H.A., Widecka, J., Wijeratne, T., Wilner, L.B., Wilson, S., Winkler, A.S., Wiyeh, A.B., Wiysonge, C.S., Wolfe, C.D.A., Woolf, A.D., Wu, S., Wu, Y.-C., Wyper, G.M.A., Xavier, D., Xu, G., Yadgir, S., Yadollahpour, A., Jabbari, S.H.Y., Yamada, T., Yan, L.L., Yano, Y., Yaseri, M., Yasin, Y.J., Yeshaneh, A., Yimer, E.M., Yip, P., Yisma, E., Yonemoto, N., Yoon, S.-J., Yotebieng, M., Younis, M.Z., Yousefifard, M., Yu, C., Zadnik, V., Zaidi, Z., Zaman, S.B., Zamani, M., Zare, Z., Zeleke, A.J., Zenebe, Z.M., Zhang, K., Zhao, Z., Zhou, M., Zodpey, S., Zucker, I., Vos, T., Murray, C.J.L., 2018. Global, regional, and national incidence, prevalence, and years lived with disability for 354 diseases and injuries for 195 countries and territories, 1990–2017: a systematic analysis for the Global Burden of Disease Study 2017. Lancet 392, 1789–1858. https://doi.org/10.1016/s0140-6736(18)32279-7

Janak, P.H., Tye, K.M., 2015. From circuits to behaviour in the amygdala. Nature 517, 284–292. https://doi.org/10.1038/nature14188

Jarome, T.J., Helmstetter, F.J., 2014. Protein degradation and protein synthesis in long-term memory formation. Front Mol Neurosci 7, 61. https://doi.org/10.3389/fnmol.2014.00061

Jendryka, M., Palchaudhuri, M., Ursu, D., Veen, B. van der, Liss, B., Kätzel, D., Nissen, W., Pekcec, A., 2019. Pharmacokinetic and pharmacodynamic actions of clozapine-N-oxide, clozapine, and compound 21 in DREADD-based chemogenetics in mice. Sci Rep-uk 9, 4522. https://doi.org/10.1038/s41598-019-41088-2

Jiang, P., Vuontela, V., Tokariev, M., Lin, H., Aronen, E.T., Ma, Y., Carlson, S., 2018. Functional connectivity of intrinsic cognitive networks during resting state and task performance in preadolescent children. Plos One 13, e0205690. https://doi.org/10.1371/journal.pone.0205690

Jolles, D.D., Buchem, M.A. van, Crone, E.A., Rombouts, S.A.R.B., 2011. A Comprehensive Study of Whole-Brain Functional Connectivity in Children and Young Adults. Cereb Cortex 21, 385–391. https://doi.org/10.1093/cercor/bhq104

Josselyn, S.A., Tonegawa, S., 2020. Memory engrams: Recalling the past and imagining the future. Science 367. https://doi.org/10.1126/science.aaw4325

Jung, H., Dasen, J.S., 2015. Evolution of Patterning Systems and Circuit Elements for Locomotion. Dev Cell 32, 408–422. https://doi.org/10.1016/j.devcel.2015.01.008

Kamprath, K., Wotjak, C.T., 2004. Nonassociative learning processes determine expression and extinction of conditioned fear in mice. Learn Memory 11, 770–786. https://doi.org/10.1101/lm.86104

Kätzel, D., Wolff, A.R., Bygrave, A.M., Bannerman, D.M., 2020. Hippocampal Hyperactivity as a Druggable Circuit-Level Origin of Aberrant Salience in Schizophrenia. Front Pharmacol 11, 486811. https://doi.org/10.3389/fphar.2020.486811

Kim, J.J., Fanselow, M.S., 1992. Modality-Specific Retrograde Amnesia of Fear. Science 256, 675–677. https://doi.org/10.1126/science.1585183

Kim, J.J., Jung, M.W., 2006. Neural circuits and mechanisms involved in Pavlovian fear conditioning: A critical review. Neurosci Biobehav Rev 30, 188–202. https://doi.org/10.1016/j.neubiorev.2005.06.005

Kim, W.B., Cho, J.-H., 2020. Encoding of contextual fear memory in hippocampal–amygdala circuit. Nat Commun 11, 1382. https://doi.org/10.1038/s41467-020-15121-2

Klingner, C.M., Langbein, K., Dietzek, M., Smesny, S., Witte, O.W., Sauer, H., Nenadic, I., 2014. Thalamocortical connectivity during resting state in schizophrenia. Eur Arch Psy Clin N 264, 111–119. https://doi.org/10.1007/s00406-013-0417-0

Kottaram, A., Johnston, L.A., Tian, Y., Ganella, E.P., Laskaris, L., Cocchi, L., McGorry, P., Pantelis, C., Kotagiri, R., Cropley, V., Zalesky, A., 2020. Predicting individual improvement in schizophrenia symptom severity at 1-year follow-up: Comparison of connectomic, structural, and clinical predictors. Hum Brain Mapp 41, 3342–3357. https://doi.org/10.1002/hbm.25020

Krieckhaus, E.E., Donahoe, J.W., Morgan, M.A., 1992. Paranoid schizophrenia may be caused by dopamine hyperactivity of CA1 hippocampus. Biol Psychiat 31, 560–570. https://doi.org/10.1016/0006-3223(92)90242-r

Krishnadas, R., Ryali, S., Chen, T., Uddin, L., Supekar, K., Palaniyappan, L., Menon, V., 2014. Resting state functional hyperconnectivity within a triple network model in paranoid schizophrenia. Lancet 383, S65. https://doi.org/10.1016/s0140-6736(14)60328-7

Kwon, J.-T., Jhang, J., Kim, H.-S., Lee, S., Han, J.-H., 2012. Brain region-specific activity patterns after recent or remote memory retrieval of auditory conditioned fear. Learn Memory 19, 487–494. https://doi.org/10.1101/lm.025502.112

Lebel, C., Beaulieu, C., 2011. Longitudinal Development of Human Brain Wiring Continues from Childhood into Adulthood. J Neurosci 31, 10937–10947. https://doi.org/10.1523/jneurosci.5302-10.2011

LeDoux, J.E., 2000. Emotion Circuits in the Brain. Annu Rev Neurosci 23, 155–184. https://doi.org/10.1146/annurev.neuro.23.1.155

Lee, S., Kim, S.-J., Kwon, O.-B., Lee, J.H., Kim, J.-H., 2013. Inhibitory networks of the amygdala for emotional memory. Front Neural Circuit 7, 129. https://doi.org/10.3389/fncir.2013.00129

Legault, M., Rompré, P.-P., Wise, R.A., 2000. Chemical Stimulation of the Ventral Hippocampus Elevates Nucleus Accumbens Dopamine by Activating Dopaminergic Neurons of the Ventral Tegmental Area. J Neurosci 20, 1635–1642. https://doi.org/10.1523/jneurosci.20-04-01635.2000

Lesuis, S.L., Catsburg, L.A.E., Lucassen, P.J., Krugers, H.J., 2018. Effects of corticosterone on mild auditory fear conditioning and extinction; role of sex and training paradigm. Learn Memory 25, 544–549. https://doi.org/10.1101/lm.047811.118

Likhtik, E., Stujenske, J.M., Topiwala, M.A., Harris, A.Z., Gordon, J.A., 2014. Prefrontal entrainment of amygdala activity signals safety in learned fear and innate anxiety. Nat Neurosci 17, 106–113. https://doi.org/10.1038/nn.3582

Lima, B., Cardoso, M.M.B., Sirotin, Y.B., Das, A., 2014. Stimulus-Related Neuroimaging in Task-Engaged Subjects Is Best Predicted by Concurrent Spiking. J Neurosci 34, 13878–13891. https://doi.org/10.1523/jneurosci.1595-14.2014

Lin, P., Wang, Xiaosheng, Zhang, B., Kirkpatrick, B., Öngür, D., Levitt, J.J., Jovicich, J., Yao, S., Wang, Xiang, 2018. Functional dysconnectivity of the limbic loop of frontostriatal circuits in first-episode, treatment-naive schizophrenia. Hum Brain Mapp 39, 747–757. https://doi.org/10.1002/hbm.23879

Linke, R., Braune, G., Schwegler, H., 2000. Differential projection of the posterior paralaminar thalamic nuclei to the amygdaloid complex in the rat. Exp Brain Res 134, 520–532. https://doi.org/10.1007/s002210000475

Liu, X., Pu, Y., Wu, D., Zhang, Z., Hu, X., Liu, L., 2019. Cross-Frequency Coupling Between Cerebral Blood Flow Velocity and EEG in Ischemic Stroke Patients With Large Vessel Occlusion. Front Neurol 10, 194. https://doi.org/10.3389/fneur.2019.00194

Lodge, D.J., Behrens, M.M., Grace, A.A., 2009. A Loss of Parvalbumin-Containing Interneurons Is Associated with Diminished Oscillatory Activity in an Animal Model of Schizophrenia. J Neurosci 29, 2344–2354. https://doi.org/10.1523/jneurosci.5419-08.2009

Lodge, D.J., Grace, A.A., 2006. The Hippocampus Modulates Dopamine Neuron Responsivity by Regulating the Intensity of Phasic Neuron Activation. Neuropsychopharmacol 31, 1356–1361. https://doi.org/10.1038/sj.npp.1300963

Logothetis, N.K., Pauls, J., Augath, M., Trinath, T., Oeltermann, A., 2001. Neurophysiological investigation of the basis of the fMRI signal. Nature 412, 150–157. https://doi.org/10.1038/35084005

Lui, S., Yao, L., Xiao, Y., Keedy, S.K., Reilly, J.L., Keefe, R.S., Tamminga, C.A., Keshavan, M.S., Pearlson, G.D., Gong, Q., Sweeney, J.A., 2015. Resting-state brain function in schizophrenia and psychotic bipolar probands and their first-degree relatives. Psychol Med 45, 97–108. https://doi.org/10.1017/s003329171400110x

Lund, C.E., Mortimer, A.M., Rogers, D., McKenna, P.J., 1991. Motor, Volitional and Behavioural Disorders in Schizophrenia. Brit J Psychiat 158, 323–327. https://doi.org/10.1192/bjp.158.3.323

Lux, V., Atucha, E., Kitsukawa, T., Sauvage, M.M., 2016. Imaging a memory trace over half a life-time in the medial temporal lobe reveals a time-limited role of CA3 neurons in retrieval. Elife 5, e11862. https://doi.org/10.7554/elife.11862

Ma, Y., Shaik, M.A., Kozberg, M.G., Kim, S.H., Portes, J.P., Timerman, D., Hillman, E.M.C., 2016. Resting-state hemodynamics are spatiotemporally coupled to synchronized and symmetric neural activity in excitatory neurons. Proc National Acad Sci 113, E8463–E8471. https://doi.org/10.1073/pnas.1525369113

Macé, E., Montaldo, G., Cohen, I., Baulac, M., Fink, M., Tanter, M., 2011. Functional ultrasound imaging of the brain. Nat Methods 8, 662–664. https://doi.org/10.1038/nmeth.1641

Malaspina, D., Storer, S., Furman, V., Esser, P., Printz, D., Berman, A., Lignelli, A., Gorman, J., Heertum, R.V., 1999. SPECT study of visual fixation in schizophrenia and comparison subjects. Biol Psychiat 46, 89–93. https://doi.org/10.1016/s0006-3223(98)00306-0

Mandino, F., Cerri, D.H., Garin, C.M., Straathof, M., Tilborg, G.A.F. van, Chakravarty, M.M., Dhenain, M., Dijkhuizen, R.M., Gozzi, A., Hess, A., Keilholz, S.D., Lerch, J.P., Shih, Y.-Y.I., Grandjean, J., 2020. Animal Functional Magnetic Resonance Imaging: Trends and Path Toward Standardization. Front Neuroinform 13, 78. https://doi.org/10.3389/fninf.2019.00078

Marek, R., Jin, J., Goode, T.D., Giustino, T.F., Wang, Q., Acca, G.M., Holehonnur, R., Ploski, J.E., Fitzgerald, P.J., Lynagh, T., Lynch, J.W., Maren, S., Sah, P., 2018. Hippocampus-driven feed-forward inhibition of the prefrontal cortex mediates relapse of extinguished fear. Nat Neurosci 21, 384–392. https://doi.org/10.1038/s41593-018-0073-9

Marek, S., Hwang, K., Foran, W., Hallquist, M.N., Luna, B., 2015. The Contribution of Network Organization and Integration to the Development of Cognitive Control. Plos Biol 13, e1002328. https://doi.org/10.1371/journal.pbio.1002328

Maren, S., 2011. Seeking a Spotless Mind: Extinction, Deconsolidation, and Erasure of Fear Memory. Neuron 70, 830–845. https://doi.org/10.1016/j.neuron.2011.04.023

Maren, S., Aharonov, G., Fanselow, M.S., 1997. Neurotoxic lesions of the dorsal hippocampus and Pavlovian fear conditioning in rats. Behav Brain Res 88, 261–274. https://doi.org/10.1016/s0166-4328(97)00088-0

Marissal, T., Salazar, R.F., Bertollini, C., Mutel, S., Roo, M.D., Rodriguez, I., Müller, D., Carleton, A., 2018. Restoring wild-type-like CA1 network dynamics and behavior during adulthood in a mouse model of schizophrenia. Nat Neurosci 21, 1412–1420. https://doi.org/10.1038/s41593-018-0225-y

Markicevic, M., Fulcher, B.D., Lewis, C., Helmchen, F., Rudin, M., Zerbi, V., Wenderoth, N., 2020. Cortical Excitation:Inhibition Imbalance Causes Abnormal Brain Network Dynamics as Observed in Neurodevelopmental Disorders. Cereb Cortex 30, 4922–4937. https://doi.org/10.1093/cercor/bhaa084

Mathiesen, C., Caesar, K., Akgören, N., Lauritzen, M., 1998. Modification of activity-dependent increases of cerebral blood flow by excitatory synaptic activity and spikes in rat cerebellar cortex. J Physiology 512, 555–566. https://doi.org/10.1111/j.1469-7793.1998.555be.x

McHugo, M., Talati, P., Armstrong, K., Vandekar, S.N., Blackford, J.U., Woodward, N.D., Heckers, S., 2019. Hyperactivity and Reduced Activation of Anterior Hippocampus in Early Psychosis. Am J Psychiat 176, 1030–1038. https://doi.org/10.1176/appi.ajp.2019.19020151

McTeague, L.M., Huemer, J., Carreon, D.M., Jiang, Y., Eickhoff, S.B., Etkin, A., 2017. Identification of Common Neural Circuit Disruptions in Cognitive Control Across Psychiatric Disorders. Am J Psychiat 174, 676–685. https://doi.org/10.1176/appi.ajp.2017.16040400

McTeague, L.M., Rosenberg, B.M., Lopez, J.W., Carreon, D.M., Huemer, J., Jiang, Y., Chick, C.F., Eickhoff, S.B., Etkin, A., 2020. Identification of Common Neural Circuit Disruptions in Emotional Processing Across Psychiatric Disorders. Am J Psychiat 177, 411–421. https://doi.org/10.1176/appi.ajp.2019.18111271

Menon, V., Ford, J.M., Lim, K.O., Glover, G.H., Pfefferbaum, A., 1997. Combined event-related fMRI and EEG evidence for temporal—parietal cortex activation during target detection. Neuroreport 8, 3029–3037. https://doi.org/10.1097/00001756-199709290-00007

Metzner, C., Zurowski, B., Steuber, V., 2019. The Role of Parvalbumin-positive Interneurons in Auditory Steady-State Response Deficits in Schizophrenia. Sci Rep-uk 9, 18525. https://doi.org/10.1038/s41598-019-53682-5

Moghaddam, B., Javitt, D., 2012. From Revolution to Evolution: The Glutamate Hypothesis of Schizophrenia and its Implication for Treatment. Neuropsychopharmacol 37, 4–15. https://doi.org/10.1038/npp.2011.181

Nabel, E.M., Garkun, Y., Koike, H., Sadahiro, M., Liang, A., Norman, K.J., Taccheri, G., Demars, M.P., Im, S., Caro, K., Lopez, S., Bateh, J., Hof, P.R., Clem, R.L., Morishita, H., 2020. Adolescent frontal top-down neurons receive heightened local drive to establish adult attentional behavior in mice. Nat Commun 11, 3983. https://doi.org/10.1038/s41467-020-17787-0

Nader, K., Schafe, G.E., Doux, J.E.L., 2000. Fear memories require protein synthesis in the amygdala for reconsolidation after retrieval. Nature 406, 722–726. https://doi.org/10.1038/35021052

Nasrallah, F.A., Tay, H.-C., Chuang, K.-H., 2014. Detection of functional connectivity in the resting mouse brain. Neuroimage 86, 417–424. https://doi.org/10.1016/j.neuroimage.2013.10.025

Newson, J.J., Pastukh, V., Thiagarajan, T.C., 2021. Poor Separation of Clinical Symptom Profiles by DSM-5 Disorder Criteria. Frontiers Psychiatry 12, 775762. https://doi.org/10.3389/fpsyt.2021.775762

Nouhoum, M., Ferrier, J., Osmanski, B.-F., Ialy-Radio, N., Pezet, S., Tanter, M., Deffieux, T., 2021. A functional ultrasound brain GPS for automatic vascular-based neuronavigation. Sci Rep-uk 11, 15197. https://doi.org/10.1038/s41598-021-94764-7

Nunez-Elizalde, A.O., Krumin, M., Reddy, C.B., Montaldo, G., Urban, A., Harris, K.D., Carandini, M., 2022. Neural correlates of blood flow measured by ultrasound. Neuron. https://doi.org/10.1016/j.neuron.2022.02.012

Oertel, V., Kraft, D., Alves, G., Knöchel, C., Ghinea, D., Storchak, H., Matura, S., Prvulovic, D., Bittner, R.A., Linden, D.E.J., Reif, A., Stäblein, M., 2019. Associative Memory Impairments Are Associated With Functional Alterations Within the Memory Network in Schizophrenia Patients and Their Unaffected First-Degree Relatives: An fMRI Study. Frontiers Psychiatry 10, 33. https://doi.org/10.3389/fpsyt.2019.00033

Oh, J.-P., Han, J.-H., 2020. A critical role of hippocampus for formation of remote cued fear memory. Mol Brain 13, 112. https://doi.org/10.1186/s13041-020-00652-y

Opalka, A.N., Wang, D.V., 2020. Hippocampal efferents to retrosplenial cortex and lateral septum are required for memory acquisition. Learn Memory 27, 310–318. https://doi.org/10.1101/lm.051797.120

Osmanski, B.-F., Pezet, S., Ricobaraza, A., Lenkei, Z., Tanter, M., 2014. Functional ultrasound imaging of intrinsic connectivity in the living rat brain with high spatiotemporal resolution. Nat Commun 5, 5023. https://doi.org/10.1038/ncomms6023

Pan, S., Mayoral, S.R., Choi, H.S., Chan, J.R., Kheirbek, M.A., 2020. Preservation of a remote fear memory requires new myelin formation. Nat Neurosci 23, 487–499. https://doi.org/10.1038/s41593-019-0582-1

Paré, D., Quirk, G.J., Ledoux, J.E., 2004. New Vistas on Amygdala Networks in Conditioned Fear. J Neurophysiol 92, 1–9. https://doi.org/10.1152/jn.00153.2004

Pati, S., Salvi, S.S., Kallianpur, M., Vaidya, B., Banerjee, A., Maiti, S., Clement, J.P., Vaidya, V.A., 2019. Chemogenetic Activation of Excitatory Neurons Alters Hippocampal Neurotransmission in a Dose-Dependent Manner. Eneuro 6, ENEURO.0124-19.2019. https://doi.org/10.1523/eneuro.0124-19.2019

Peralta, V., Campos, M.S., Jalón, E.G.D., Cuesta, M.J., 2010. Motor behavior abnormalities in drug-naïve patients with schizophrenia spectrum disorders. Movement Disord 25, 1068–1076. https://doi.org/10.1002/mds.23050

Phillips, R.G., LeDoux, J.E., 1992. Differential contribution of amygdala and hippocampus to cued and contextual fear conditioning. Behav Neurosci 106, 274–285. https://doi.org/10.1037//0735-7044.106.2.274

Pittenger, C., 2013. Disorders of memory and plasticity in psychiatric disease. Dialogues Clin Neurosci 15, 455–463. https://doi.org/10.31887/dcns.2013.15.4/cpittenger

Ploski, J.E., Park, K.W., Ping, J., Monsey, M.S., Schafe, G.E., 2010. Identification of plasticity-associated genes regulated by Pavlovian fear conditioning in the lateral amygdala. J Neurochem 112, 636–650. https://doi.org/10.1111/j.1471-4159.2009.06491.x

Pol, H.E.H., Brans, R.G.H., Haren, N.E.M. van, Schnack, H.G., Langen, M., Baaré, W.F.C., Oel, C.J. van, Kahn, R.S., 2004. Gray and white matter volume abnormalities in monozygotic and same-gender dizygotic twins discordant for schizophrenia. Biol Psychiat 55, 126–130. https://doi.org/10.1016/s0006-3223(03)00728-5

Quinn, J.J., Wied, H.M., Ma, Q.D., Tinsley, M.R., Fanselow, M.S., 2008. Dorsal hippocampus involvement in delay fear conditioning depends upon the strength of the tone-footshock association. Hippocampus 18, 640–654. https://doi.org/10.1002/hipo.20424

Rabut, C., Ferrier, J., Bertolo, A., Osmanski, B., Mousset, X., Pezet, S., Deffieux, T., Lenkei, Z., Tanter, M., 2020. Pharmaco-fUS: Quantification of pharmacologically-induced dynamic changes in brain perfusion and connectivity by functional ultrasound imaging in awake mice. Neuroimage 222, 117231. https://doi.org/10.1016/j.neuroimage.2020.117231

Racsmány, M., Conway, M.A., Garab, E.A., Cimmer, C., Janka, Z., Kurimay, T., Pléh, C., Szendi, I., 2008. Disrupted memory inhibition in schizophrenia. Schizophr Res 101, 218–224. https://doi.org/10.1016/j.schres.2008.01.002

Ramsay, I.S., 2019. An Activation Likelihood Estimate Meta-analysis of Thalamocortical Dysconnectivity in Psychosis. Biological Psychiatry Cognitive Neurosci Neuroimaging 4, 859–869. https://doi.org/10.1016/j.bpsc.2019.04.007

Rees, E., Walters, J.T.R., Georgieva, L., Isles, A.R., Chambert, K.D., Richards, A.L., Mahoney-Davies, G., Legge, S.E., Moran, J.L., McCarroll, S.A., O'Donovan, M.C., Owen, M.J., Kirov, G., 2014. Analysis of copy number variations at 15 schizophrenia-associated loci. Brit J Psychiat 204, 108–114. https://doi.org/10.1192/bjp.bp.113.131052

Reichert, H., 2009. Evolutionary conservation of mechanisms for neural regionalization, proliferation and interconnection in brain development. Biol Letters 5, 112–116. https://doi.org/10.1098/rsbl.2008.0337

Reinwald, J.R., Sartorius, A., Weber-Fahr, W., Sack, M., Becker, R., Didriksen, M., Stensbøl, T.B., Schwarz, A.J., Meyer-Lindenberg, A., Gass, N., 2020. Separable neural mechanisms for the pleiotropic association of copy number variants with neuropsychiatric traits. Transl Psychiat 10, 93. https://doi.org/10.1038/s41398-020-0771-4

Roelofs, T.J.M., Verharen, J.P.H., Tilborg, G.A.F. van, Boekhoudt, L., Toorn, A. van der, Jong, J.W. de, Luijendijk, M.C.M., Otte, W.M., Adan, R.A.H., Dijkhuizen, R.M., 2017. A novel approach to map induced activation of neuronal networks using chemogenetics and functional neuroimaging in rats: A proof-of-concept study on the mesocorticolimbic system. Neuroimage 156, 109–118. https://doi.org/10.1016/j.neuroimage.2017.05.021

Romanski, L.M., LeDoux, J.E., 1993. Information Cascade from Primary Auditory Cortex to the Amygdala: Corticocortical and Corticoamygdaloid Projections of Temporal Cortex in the Rat. Cereb Cortex 3, 515–532. https://doi.org/10.1093/cercor/3.6.515

Roth, B.L., 2016. DREADDs for Neuroscientists. Neuron 89, 683–694. https://doi.org/10.1016/j.neuron.2016.01.040

Russell, T.A., Reynaud, E., Kucharska-Pietura, K., Ecker, C., Benson, P.J., Zelaya, F., Giampietro, V., Brammer, M., David, A., Phillips, M.L., 2007. Neural responses to dynamic expressions of fear in schizophrenia. Neuropsychologia 45, 107–123. https://doi.org/10.1016/j.neuropsychologia.2006.04.026

Sacco, T., Sacchetti, B., 2010. Role of Secondary Sensory Cortices in Emotional Memory Storage and Retrieval in Rats. Science 329, 649–656. https://doi.org/10.1126/science.1183165

Sanders, M.J., Wiltgen, B.J., Fanselow, M.S., 2003. The place of the hippocampus in fear conditioning. Eur J Pharmacol 463, 217–223. https://doi.org/10.1016/s0014-2999(03)01283-4

Sanganahalli, B.G., Herman, P., Rothman, D.L., Blumenfeld, H., Hyder, F., 2016. Metabolic demands of neural-hemodynamic associated and disassociated areas in brain. J Cereb Blood Flow Metabolism 36, 1695–1707. https://doi.org/10.1177/0271678x16664531

Santini, E., Quirk, G.J., Porter, J.T., 2008. Fear Conditioning and Extinction Differentially Modify the Intrinsic Excitability of Infralimbic Neurons. J Neurosci 28, 4028–4036. https://doi.org/10.1523/jneurosci.2623-07.2008

Scarlata, M.J., Lee, S.H., Lee, D., Kandigian, S.E., Hiller, A.J., Dishart, J.G., Mintz, G.E., Wang, Z., Coste, G.I., Mousley, A.L., Soler, I., Lawson, K., Ng, A.J., Bezek, J.L., Bergstrom, H.C., 2019. Chemogenetic stimulation of the infralimbic cortex reverses alcohol-induced fear memory overgeneralization. Sci Rep-uk 9, 6730. https://doi.org/10.1038/s41598-019-43159-w

Schafe, G.E., 2005. Tracking the Fear Engram: The Lateral Amygdala Is an Essential Locus of Fear Memory Storage. J Neurosci 25, 10010–10014. https://doi.org/10.1523/jneurosci.3307-05.2005

Schobel, S.A., Chaudhury, N.H., Khan, U.A., Paniagua, B., Styner, M.A., Asllani, I., Inbar, B.P., Corcoran, C.M., Lieberman, J.A., Moore, H., Small, S.A., 2013. Imaging Patients with Psychosis and a Mouse Model Establishes a Spreading Pattern of Hippocampal Dysfunction and Implicates Glutamate as a Driver. Neuron 78, 81–93. https://doi.org/10.1016/j.neuron.2013.02.011

Schobel, S.A., Lewandowski, N.M., Corcoran, C.M., Moore, H., Brown, T., Malaspina, D., Small, S.A., 2009. Differential Targeting of the CA1 Subfield of the Hippocampal Formation by Schizophrenia and Related Psychotic Disorders. Arch Gen Psychiat 66, 938–946. https://doi.org/10.1001/archgenpsychiatry.2009.115

Seidenbecher, T., Laxmi, T.R., Stork, O., Pape, H.-C., 2003. Amygdalar and Hippocampal Theta Rhythm Synchronization During Fear Memory Retrieval. Science 301, 846–850. https://doi.org/10.1126/science.1085818

Senn, V., Wolff, S.B.E., Herry, C., Grenier, F., Ehrlich, I., Gründemann, J., Fadok, J.P., Müller, C., Letzkus, J.J., Lüthi, A., 2014. Long-Range Connectivity Defines Behavioral Specificity of Amygdala Neurons. Neuron 81, 428–437. https://doi.org/10.1016/j.neuron.2013.11.006

Shen, M., Guo, Y., Dong, Q., Gao, Y., Stockton, M.E., Li, M., Kannan, S., Korabelnikov, T., Schoeller, K.A., Sirois, C.L., Zhou, C., Le, J., Wang, D., Chang, Q., Sun, Q.-Q., Zhao, X., 2021. FXR1 regulation of parvalbumin interneurons in the prefrontal cortex is critical for schizophrenia-like behaviors. Mol Psychiatr 26, 6845–6867. https://doi.org/10.1038/s41380-021-01096-z

Sieu, L.-A., Bergel, A., Tiran, E., Deffieux, T., Pernot, M., Gennisson, J.-L., Tanter, M., Cohen, I., 2015. EEG and functional ultrasound imaging in mobile rats. Nat Methods 12, 831–834. https://doi.org/10.1038/nmeth.3506

Slifstein, M., Giessen, E. van de, Snellenberg, J.V., Thompson, J.L., Narendran, R., Gil, R., Hackett, E., Girgis, R., Ojeil, N., Moore, H., D'Souza, D., Malison, R.T., Huang, Y., Lim, K., Nabulsi, N., Carson, R.E., Lieberman, J.A., Abi-Dargham, A., 2015. Deficits in Prefrontal Cortical and Extrastriatal Dopamine Release in Schizophrenia: A Positron Emission Tomographic Functional Magnetic Resonance Imaging Study. Jama Psychiat 72, 316–324. https://doi.org/10.1001/jamapsychiatry.2014.2414

Smith, S.M., Fox, P.T., Miller, K.L., Glahn, D.C., Fox, P.M., Mackay, C.E., Filippini, N., Watkins, K.E., Toro, R., Laird, A.R., Beckmann, C.F., 2009. Correspondence of the brain's functional architecture during activation and rest. Proc National Acad Sci 106, 13040–13045. https://doi.org/10.1073/pnas.0905267106

Sommer, I.E., Clos, M., Meijering, A.L., Diederen, K.M.J., Eickhoff, S.B., 2012. Resting State Functional Connectivity in Patients with Chronic Hallucinations. Plos One 7, e43516. https://doi.org/10.1371/journal.pone.0043516

Song, E.Y., Boatman, J.A., Jung, M.W., Kim, J.J., 2010. Auditory Cortex is Important in the Extinction of Two Different Tone-Based Conditioned Fear Memories in Rats. Front Behav Neurosci 4, 24. https://doi.org/10.3389/fnbeh.2010.00024

Sotres-Bayon, F., Quirk, G.J., 2010. Prefrontal control of fear: more than just extinction. Curr Opin Neurobiol 20, 231–235. https://doi.org/10.1016/j.conb.2010.02.005

Stujenske, J.M., Likhtik, E., Topiwala, M.A., Gordon, J.A., 2014. Fear and Safety Engage Competing Patterns of Theta-Gamma Coupling in the Basolateral Amygdala. Neuron 83, 919–933. https://doi.org/10.1016/j.neuron.2014.07.026

Sullivan, P.F., Kendler, K.S., Neale, M.C., 2003. Schizophrenia as a Complex Trait: Evidence From a Meta-analysis of Twin Studies. Arch Gen Psychiat 60, 1187–1192. https://doi.org/10.1001/archpsyc.60.12.1187

Supekar, K., Musen, M., Menon, V., 2009. Development of Large-Scale Functional Brain Networks in Children. Plos Biol 7, e1000157. https://doi.org/10.1371/journal.pbio.1000157

Tang, J., Wagner, S., Schachner, M., Dityatev, A., Wotjak, C.T., 2003. Potentiation of amygdaloid and hippocampal auditory-evoked potentials in a discriminatory fear-conditioning task in mice as a function of tone pattern and context. Eur J Neurosci 18, 639–650. https://doi.org/10.1046/j.1460-9568.2003.02758.x

Tasaka, G., Feigin, L., Maor, I., Groysman, M., DeNardo, L.A., Schiavo, J.K., Froemke, R.C., Luo, L., Mizrahi, A., 2020. The Temporal Association Cortex Plays a Key Role in Auditory-Driven Maternal Plasticity. Neuron 107, 566-579.e7. https://doi.org/10.1016/j.neuron.2020.05.004

Tonegawa, S., Morrissey, M.D., Kitamura, T., 2018. The role of engram cells in the systems consolidation of memory. Nat Rev Neurosci 19, 485–498. https://doi.org/10.1038/s41583-018-0031-2

Tosches, M.A., 2017. Developmental and genetic mechanisms of neural circuit evolution. Dev Biol 431, 16–25. https://doi.org/10.1016/j.ydbio.2017.06.016

Tovote, P., Fadok, J.P., Lüthi, A., 2015. Neuronal circuits for fear and anxiety. Nat Rev Neurosci 16, 317–331. https://doi.org/10.1038/nrn3945

Tuominen, L., Romaniuk, L., Milad, M.R., Goff, D.C., Hall, J., Holt, D.J., 2022. Impairment in acquisition of conditioned fear in schizophrenia. Neuropsychopharmacol 47, 681–686. https://doi.org/10.1038/s41386-021-01193-1

Uddin, M., Unda, B.K., Kwan, V., Holzapfel, N.T., White, S.H., Chalil, L., Woodbury-Smith, M., Ho, K.S., Harward, E., Murtaza, N., Dave, B., Pellecchia, G., D'Abate, L., Nalpathamkalam, T., Lamoureux, S., Wei, J., Speevak, M., Stavropoulos, J., Hope, K.J., Doble, B.W., Nielsen, J., Wassman, E.R., Scherer, S.W., Singh, K.K., 2018. OTUD7A Regulates Neurodevelopmental Phenotypes in the 15q13.3 Microdeletion Syndrome. Am J Hum Genet 102, 278–295. https://doi.org/10.1016/j.ajhg.2018.01.006

Uscătescu, L.C., Kronbichler, L., Stelzig-Schöler, R., Pearce, B.-G., Said-Yürekli, S., Reich, L.A., Weber, S., Aichhorn, W., Kronbichler, M., 2021. Effective Connectivity of the Hippocampus Can Differentiate Patients with Schizophrenia from Healthy Controls: A Spectral DCM Approach. Brain Topogr 34, 762–778. https://doi.org/10.1007/s10548-021-00868-8

Vidal-Gonzalez, I., Vidal-Gonzalez, B., Rauch, S.L., Quirk, G.J., 2006. Microstimulation reveals opposing influences of prelimbic and infralimbic cortex on the expression of conditioned fear. Learn Memory 13, 728–733. https://doi.org/10.1101/lm.306106

Vita, A., Peri, L.D., Deste, G., Sacchetti, E., 2012. Progressive loss of cortical gray matter in schizophrenia: a meta-analysis and meta-regression of longitudinal MRI studies. Transl Psychiat 2, e190–e190. https://doi.org/10.1038/tp.2012.116

Wachsmuth, L., Mensen, A., Barca, C., Wiart, M., Tristão-Pereira, C., Busato, A., Waiczies, S., Himmelreich, U., Millward, J.M., Reimann, H.M., Jelescu, I., Marzola, P., Pradier, B., Viola, A., Faber, C., 2021. Contribution of preclinical MRI to responsible animal research: living up to the 3R principle. Magnetic Reson Mater Phys Biology Medicine 34, 469–474. https://doi.org/10.1007/s10334-021-00929-w

Walther, S., Federspiel, A., Horn, H., Razavi, N., Wiest, R., Dierks, T., Strik, W., Müller, T.J., 2011. Alterations of white matter integrity related to motor activity in schizophrenia. Neurobiol Dis 42, 276–283. https://doi.org/10.1016/j.nbd.2011.01.017

Walther, S., Lefebvre, S., Conring, F., Gangl, N., Nadesalingam, N., Alexaki, D., Wüthrich, F., Rüter, M., Viher, P.V., Federspiel, A., Wiest, R., Stegmayer, K., 2021. Limbic links to paranoia: increased resting-state functional connectivity between amygdala, hippocampus and orbitofrontal cortex in schizophrenia patients with paranoia. Eur Arch Psy Clin N 1–12. https://doi.org/10.1007/s00406-021-01337-w

Walther, S., Stegmayer, K., Federspiel, A., Bohlhalter, S., Wiest, R., Viher, P.V., 2017. Aberrant Hyperconnectivity in the Motor System at Rest Is Linked to Motor Abnormalities in Schizophrenia Spectrum Disorders. Schizophrenia Bull 43, 982–992. https://doi.org/10.1093/schbul/sbx091

Wang, M., Pei, L., Fletcher, P.J., Kapur, S., Seeman, P., Liu, F., 2010. Schizophrenia, amphetamine-induced sensitized state and acute amphetamine exposure all show a common alteration: increased dopamine D2 receptor dimerization. Mol Brain 3, 25–25. https://doi.org/10.1186/1756-6606-3-25

Wang, P.S., Aguilar-Gaxiola, S., Alonso, J., Angermeyer, M.C., Borges, G., Bromet, E.J., Bruffaerts, R., Girolamo, G. de, Graaf, R. de, Gureje, O., Haro, J.M., Karam, E.G., Kessler, R.C., Kovess, V., Lane, M.C., Lee, S., Levinson, D., Ono, Y., Petukhova, M., Posada-Villa, J., Seedat, S., Wells, J.E., 2007. Use of mental health services for anxiety, mood, and substance disorders in 17 countries in the WHO world mental health surveys. Lancet 370, 841–850. https://doi.org/10.1016/s0140-6736(07)61414-7

Wang, Q., Ding, S.-L., Li, Y., Royall, J., Feng, D., Lesnar, P., Graddis, N., Naeemi, M., Facer, B., Ho, A., Dolbeare, T., Blanchard, B., Dee, N., Wakeman, W., Hirokawa, K.E., Szafer, A., Sunkin, S.M., Oh, S.W., Bernard, A., Phillips, J.W., Hawrylycz, M., Koch, C., Zeng, H., Harris, J.A., Ng, L., 2020. The Allen Mouse Brain Common Coordinate Framework: A 3D Reference Atlas. Cell 181, 936-953.e20. https://doi.org/10.1016/j.cell.2020.04.007

Weerink, M.A.S., Struys, M.M.R.F., Hannivoort, L.N., Barends, C.R.M., Absalom, A.R., Colin, P., 2017. Clinical Pharmacokinetics and Pharmacodynamics of Dexmedetomidine. Clin Pharmacokinet 56, 893–913. https://doi.org/10.1007/s40262-017-0507-7

Weinstein, J.J., Chohan, M.O., Slifstein, M., Kegeles, L.S., Moore, H., Abi-Dargham, A., 2017. Pathway-Specific Dopamine Abnormalities in Schizophrenia. Biol Psychiat 81, 31–42. https://doi.org/10.1016/j.biopsych.2016.03.2104

Wen, Z., Chen, Z.S., Milad, M.R., 2021. Fear extinction learning modulates large-scale brain connectivity. Neuroimage 238, 118261–118261. https://doi.org/10.1016/j.neuroimage.2021.118261

Wheeler, A.L., Teixeira, C.M., Wang, A.H., Xiong, X., Kovacevic, N., Lerch, J.P., McIntosh, A.R., Parkinson, J., Frankland, P.W., 2013. Identification of a Functional Connectome for Long-Term Fear Memory in Mice. Plos Comput Biol 9, e1002853. https://doi.org/10.1371/journal.pcbi.1002853

Whittle, N., Fadok, J., MacPherson, K.P., Nguyen, R., Botta, P., Wolff, S.B.E., Müller, C., Herry, C., Tovote, P., Holmes, A., Singewald, N., Lüthi, A., Ciocchi, S., 2021. Central amygdala micro-circuits mediate fear extinction. Nat Commun 12, 4156. https://doi.org/10.1038/s41467-021-24068-x

Witter, M.P., Groenewegen, H.J., Silva, F.H.L. da, Lohman, A.H.M., 1989. Functional organization of the extrinsic and intrinsic circuitry of the parahippocampal region. Prog Neurobiol 33, 161–253. https://doi.org/10.1016/0301-0082(89)90009-9

Wolff, A.R., Bygrave, A.M., Sanderson, D.J., Boyden, E.S., Bannerman, D.M., Kullmann, D.M., Kätzel, D., 2018. Optogenetic induction of the schizophrenia-related endophenotype of ventral hippocampal hyperactivity causes rodent correlates of positive and cognitive symptoms. Sci Rep-uk 8, 12871. https://doi.org/10.1038/s41598-018-31163-5

Yassa, M.A., Reagh, Z.M., 2013. Competitive Trace Theory: A Role for the Hippocampus in Contextual Interference during Retrieval. Front Behav Neurosci 7, 107. https://doi.org/10.3389/fnbeh.2013.00107

Yu, S.-B., 2012. Dexmedetomidine sedation in ICU. Korean J Anesthesiol 62, 405–411. https://doi.org/10.4097/kjae.2012.62.5.405

Yuen, N.H., Osachoff, N., Chen, J.J., 2019. Intrinsic Frequencies of the Resting-State fMRI Signal: The Frequency Dependence of Functional Connectivity and the Effect of Mode Mixing. Front Neurosci-switz 13, 900. https://doi.org/10.3389/fnins.2019.00900

Zerbi, V., Floriou-Servou, A., Markicevic, M., Vermeiren, Y., Sturman, O., Privitera, M., Ziegler, L. von, Ferrari, K.D., Weber, B., Deyn, P.P.D., Wenderoth, N., Bohacek, J., 2019. Rapid Reconfiguration of the Functional Connectome after Chemogenetic Locus Coeruleus Activation. Neuron 103, 702-718.e5. https://doi.org/10.1016/j.neuron.2019.05.034

Zhan, X., Yu, R., 2015. A Window into the Brain: Advances in Psychiatric fMRI. Biomed Res Int 2015, 542467. https://doi.org/10.1155/2015/542467

7. ACKNOWLEDGEMENTS

It is no surprise that there is a plethora of amazing people who have help me on this journey.

First and foremost, I profoundly thank Bastian Hengerer who took a chance on me twice (at least) and it is no exaggeration to say that he has completely changed my life. He showed me how exciting and rewarding neuroscience research is while I was a Manchester student and then gave me the opportunity to realize my dream of completing a PhD several years later. He has unwaveringly supported and guided me through every step of the way. His mentorship has given me the skills and confidence to pursue a career in science and feel confident that I will be able to figure out how to work through the obstacles and challenges that will undoubtedly come up in the future.

I must also wholeheartedly thank the other members of my TAC, Prof. Dr. Tobias Böckers and Dr. Dr. Francesco Roselli. They have always been forthcoming with sound advice and encouraged my enthusiasm for this project.

Many thanks to the members of BI CNS department who helped me find supplies and equipment, gave a critical ear during presentations, and taught and helped me with surgical procedures, especially to Susi Zach, Natalie Türk, and Caro Nolte. I also thank the wonderful veterinarians and animal care takers in the facility. It was reassuring to know that the animals were always closely monitored and very well taken care of and that I always has experts to turn to with questions and concerns. I cannot go without thanking some of my fellow compatriots throughout BI: Juliane Kuklik, Franzi Stoller, Raquel Rodriguez Perez, Patrick Latuske, Marzieh Funk, and Oana Dormann who were always available with advice or for a coffee and a sympathetic ear. I must thank the talented interns who worked with me along the way: Tabea Bieler, Ivana Flais, and most of all to Rebecca Smausz whose brilliant ideas, determination, and focus led to a top-notch project even in the face of adversity and a global pandemic. I am privileged to have worked alongside you.

I am also very grateful to my wonderful colleagues in Global Medical Writing, Marcin Teodorczyk and Julie Collins for their flexibility and encouragement as I completed my PhD work.

A very special thanks to the members of our fUS working group: Jeremy Ferrier, Artem Shatillo, Bruno Osmanski, and Marc Gesnik whose technical help and ideas have been crucial in working through problems to get results and interpret complex data.

My deepest gratitude to Hugo Cruces Solis, Olga Babaev, and Ester Nespoli for their friendship and for also sharing their unparalleled experience and expertise as well as their valuable time with me. Their professionalism, intelligence, resourcefulness, and focus are qualities that I continue to stive toward.

Thank you especially to my mom Julia and my brother Evan and the rest of my family who kept me going through the many obstacles I encountered and for also helping me work through a few coding errors! Thank you for your motivation and for believing in and supporting me through my entire academic career. Although I am not able to share the experience of this accomplishment with my father, I am thankful for the memory of his dedication and fortitude and for doing his best to impart these qualities onto myself.

Last, but certainly not least, from the bottom of my heart I thank my partner in every aspect of life, Baldu, for his emotional and intellectual support. You make everything worth the time and effort, and I can’t imagine going through this PhD or my life without you.

STATUTORY DECLARATION

I hereby declare that I wrote the present dissertation with the topic “characterization of neural networks in rodents using functional ultrasound imaging” independently and used no other aids than those cited. In each individual case, I have clearly identified the sources of the passages that are taken word for word or paraphrased from other works.

I also hereby declare that I have carried out my scientific work according to the principles of good scientific practice in accordance with the current “Satzung der Universität Ulm zur Sicherung gutter wissenschaftlicher Praxis” (Rules of the University of Ulm for Assuring Good Scientific Practice).

Ulm, 19.05.2022